Silicone Based Membranes for Organic Solvent Nanofiltration

(Silikonbasierte Membranen für die organophile Nanofiltration)

Von der Fakultät für Maschinenwesen

der Rheinisch-Westfälischen Technischen Hochschule Aachen

zur Erlangung des akademischen Grades

einer Doktorin der Ingenieurwissenschaften genehmigte Dissertation

vorgelegt von

Marina Lazar

Berichter: Univ.-Prof. Dr.-Ing. Matthias Wessling
Prof. Dr. Ir. Nieck E. Benes

Tag der mündlichen Prüfung: 07.12.2015

Danksagung

Die vorliegende Arbeit entstand im Rahmen meiner Tätigkeit als Doktorandin bei der Evonik Industries AG in der Abteilung Reaktionstechnik des Bereiches Verfahrenstechnik und Engineering.

Mein erster Dank gilt Herrn Prof. Dr.-Ing. Matthias Wessling für die wissenschaftliche Anleitung innerhalb dieser industriellen Doktorarbeit. Die interessanten und fordernden Diskussionen haben diese Arbeit sehr bereichert. Herrn Prof. Dr. Ir. Nieck Benes danke ich sehr herzlich für die Übernahme des Zweitgutachtens. Bei Herrn Prof. Roger A. Sauer, Ph.D. möchte ich mich für die Übernahme des Prüfungsvorsitzes ebenfalls herzlich bedanken.

Mein besonderer Dank geht an meinem ersten Betreuer bei der Evonik Industries AG Dr.-Ing. Goetz Baumgarten, der mir das Vertrauen gegeben hat, die Doktorarbeit anzufertigen. Für die Fortsetzung der ausgezeichneten Betreuung bei der Evonik Industries AG, die vielen Diskussionen und die Unterstützung beim Verfolgen neuer Ideen geht mein Dank an Dr.-Ing. Jörg Balster. Seine Begeisterung für die Forschung in diesem Gebiet war zugleich erfrischend wie inspirierend.

Bei den Kollegen und Kolleginnen der Fachgruppe der Membrantechnik möchte ich mich für die sehr gute und motivierende Zusammenarbeit bedanken. Mein Dank gilt auch den von mir betreuten Studenten, die mich bei der experimentellen Arbeit unterstützt haben. Zu guter Letzt bedanke ich mich aufs Herzlichste bei meinem Mann, meiner Familie und Freunden für die sowohl tatkräftige als auch emotionale Unterstützung in dieser Zeit.

Abstract

One of the polymers enabling successful application of organic solvent nanofiltration membranes is silicone or more precisely poly(organosiloxane). This thesis includes a study on silicone based membranes, as to their chemistry, their separation performance in organic solvents and influence of introduced functional groups.

The performance of a silicone based membrane was first compared to membranes based on polyimide and PIM-1 (polymers of intrinsic microporosity). The tests were made in heptane and acetone to emphasize the difference in the separation properties of the tested membrane materials. Further, the development of a predictive model for multicomponent mass transport through a silicone membrane was made. The applied modelling approach can be differentiated in a Flory-Rehner based model to estimate membrane swelling and a simplified Maxwell-Stefan mass transport model. The prediction accuracy of developed modelling approach was compared to the measured values for eleven pure solvents. The predicted values of styrene oligomer rejection curves in these solvents were also compared to the measured values.

Additionally, the production and performance of composite membranes made from acrylate-functional and epoxy-functional silicones in styrene oligomer/heptane mixture were also investigated. Next to this, a performance comparison in several solvents of acrylate-functional, epoxy-functional and a commercially available silicone based membrane was made. The measured results were used together with the modelling approach to determine membrane specific parameters and their relevance in accurate predicting of the measured data.

Zusammenfassung

Poly(Organosiloxan), kurz Silikon, ist eines der Polymere die eine besonders erfolgreiche Anwendung der organophilen Nanofiltrationsmembranen ermöglichen. Diese Doktorarbeit beinhaltet eine Studie silikonbasierter Membranen bezüglich deren chemischen Eigenschaften, sowie Trenneigenschaften in organischen Lösemitteln und dem Einfluss der zugefügten funktionellen Gruppen.

Die Trennleistung einer silikonbasierten Membran wurde zunächst mit polyimidbasierten und PIM-1 (Polymer mit intrinsischer Porosität) Membranen verglichen. Die Versuche wurden in Heptan und Aceton durchgeführt, um die Unterschiede der Membranmaterialien zu betonen. Des Weiteren, wurde ein prädiktives Model für den Stofftransport der Multikomponentenmischung für die Silikonmembran erstellt. Das angewandte Model beinhaltet einen Flory-Rehner-basierten Ansatz zur Beschreibung des Membranquellverhaltens und eine vereinfachte Form des Maxwell-Stefan Massentransportmodels. Die Vorhersagegenauigkeit des entwickelten Models wurde mit den Versuchsergebnissen für elf Lösemittel verglichen. Die vorhergesagten Werte für die Rückhaltekurven der Styrololigomere in diesen Lösemitteln wurden ebenfalls mit den Versuchsdaten verglichen.

Die Herstellung und die Trennleistung von Kompositmembranen auf Basis von acrylat- und epoxid-funktionalisierten Silikonen wurden zusätzlich in einem Styrololigomer/ Heptan Gemisch untersucht. Dazu wurde ein Vergleich der acrylat-, epoxid-funktionalisierten und einer kommerziell verfügbaren silikonbasierten Membran in mehreren Lösemitteln durchgeführt. Die Versuchsergebnisse wurden gemeinsam mit dem entwickelten Model angewandt um die spezifische Membranparameter und deren Bedeutung für eine möglichst genaue Wiedergabe der Versuchsdaten zu bestimmen.

Table of content

1 Introduction

In recent years membranes and membrane separations have stepped outside the well-established membrane applications, such as water desalination and dialysis. One of the polymers enabling this development is silicone or more precisely poly(organosiloxane). Silicone based membranes are already applied in gas separation, pervaporation, vapour permeation and organic solvent nanofiltration. These versatile applications of a silicone based separation layer are possible due to its excellent thermal, chemical and mechanical stability compared to other rubber polymers. Silicone has generally good permeabilities and selectivities for organic solvents, which mostly depends on the solubility and diffusivity [1].

In order to apply membrane separations in different process streams, the membrane development is shifting away from finding the “one-size-fits-all” membrane to “tailor-made” membranes. To achieve this, membrane development must become more feasible for the membrane producers. Membrane production processes with low development costs for membrane optimisation for a specific separation have to be considered.

In different branches of Evonik Industries AG know-how is already available on silicone chemistry, coating of polymers and application of silicone based membranes. Combining these competences can enable a fast and feasible development of silicone composite membranes for specific separation tasks. Industry can benefit from the gentle separation that a membrane separation offers. Also the reduced energy requirement, which membrane separation units enable, can play an important role in establishing sustainable production processes.

Future development of silicone based membranes needs better understanding

and prediction possibilities of silicone based membrane performance. This would enable a targeted silicone modification to achieve maximal performance in a specific separation task.

1.1 Scope of the thesis

This thesis includes a study on silicone based membranes, as to their chemistry, their separation performance in organic solvents and influence of introduced functional groups.

In Chapter 2 a general introduction on poly(organosiloxane) membranes and the chemistry which lies behind different reactive silicones is given. Also shown are the challenges of commercial production of silicone composite membranes. The chapter ends with examples of successful applications of silicone based membranes in industrially relevant separation processes.

In Chapter 3 the equipment, several experimental procedures and calibration of the analytics which were used in the experimental work are described. Also given are the correlations and the estimated coefficients for calculating concentration of the components on the membrane surface.

In Chapter 4 the results of comparative tests of three different membrane materials used for organic solvent nanofiltration are shown. The investigation was made in heptane and acetone to underlie the difference in the separation properties of the tested membrane materials.

In Chapter 5 the development of a predictive model for mass transport of pure solvent through a silicone membrane is shown. The applied modelling approach can be differentiated in a Flory-Rehner based model to estimate membrane swelling and

a simplified Maxwell-Stefan mass transport model. For the investigation of the developed Flory-Rehner based model swelling experiments with crosslinked RTV615 silicone were made in eleven solvents. For estimation and development of the Maxwell-Stefan mass transport model permeabilities of the same solvents were measured for the silicone membrane ONF-2 from GMT Membrantechnik.

In Chapter 6 the previously developed modelling approach for predicting solvent transport was applied to multicomponent mixtures of styrene oligomers with different molecular weights in the previously tested solvents. The predicted rejections of styrene oligomers and permeabilities were compared to the experimentally determined data measured with the silicone membrane ONF-2 (GMT Membrantechnik).

In Chapter 7 the production and performance of composite membranes made from acrylate-functional [2] and epoxy-functional silicones in styrene oligomer/heptane mixture are described. The separation performance of produced membranes was also compared to the silicone membrane ONF-2.

In Chapter 8 a performance comparison in several solvents of acrylate-functional silicone membrane, epoxy-functional silicone membrane and silicone based membrane ONF-2 was made. The measured results were used together with modelling approach given in Chapter 6 to determine membrane specific parameters and their relevance in accurate predicting of the measured data.

Conclusion and outlook are given in Chapter 9, which summarises the research results made in previous chapters.

1.2 References

[1] R. Baker, *Membrane Technology and Applications*, 3rd ed., Wiley 2012.

[2] R. Hänsel, H. Döhler, P. Schwab, P. Seidensticker, M. Ferenz, G. Baumgarten, M. Lazar, M. Ungerank, *Composite silicone membranes with high*

separating action, WO2011067054 A1, Evonik Goldschmidt GmbH, 2011.

2 Silicone based membrane separation layers

Establishing a membrane based separation process includes membrane and module development as well as process design and optimisation. However, each membrane process is based on the separation properties of the installed membrane [1]. To gain a better understanding of silicone based membranes, some basic insights in crosslinking reactions of the silicone chemistry are shown in this chapter. Further production of silicone based composite membranes including the challenges and possible solutions will be descibed. The final section will feature some successful commercial applications of silicone based membranes as well as future directions in the application of silicone based membranes in separation processes.

2.1 Chemistry of reactive silicones

Linear poly(dimethylsiloxane) (abbr. PDMS) as given in Figure 1 [2] are most often used silicones for coating purposes.

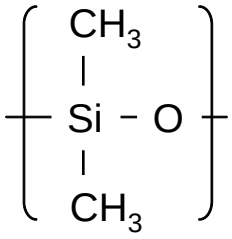

Figure 1: Dimethylsiloxane repetitive unit.

Attaching reactive groups to the dimethylsiloxane backbone enables crosslinking reactions, which result in a three-dimensional siloxane network. Based on the cross-

linking reactions the following groups of reactive silicones can be distinguished: peroxide induced free radical reactions, hydridosilane/silanol reactions, hydrosilylation addition reactions, modification of silicones with reactive organic functionalities and high energy radiation curing [2].

2.1.1 Peroxide induced free radical reaction

The peroxide induced crosslinking reaction of dimethylsiloxane is based on the radical abstraction of a hydrogen atom from the methyl group. The reaction does not introduce any additional organic functionality. A disadvantage of the peroxide induced free radical reaction is that strong peroxides must be used for the hydrogen atom abstraction from the methyl group. These peroxides reactions have an acidic by-product, which can cause corrosion of the substrate or even silicone decomposition. In the presence of vinyl modifications of silicones, the peroxides needed for the reaction are much milder and sufficient crosslinking degree is achieved even with a low content of vinyl modification [2]. The free radical reactions are summarised in Figure 2.

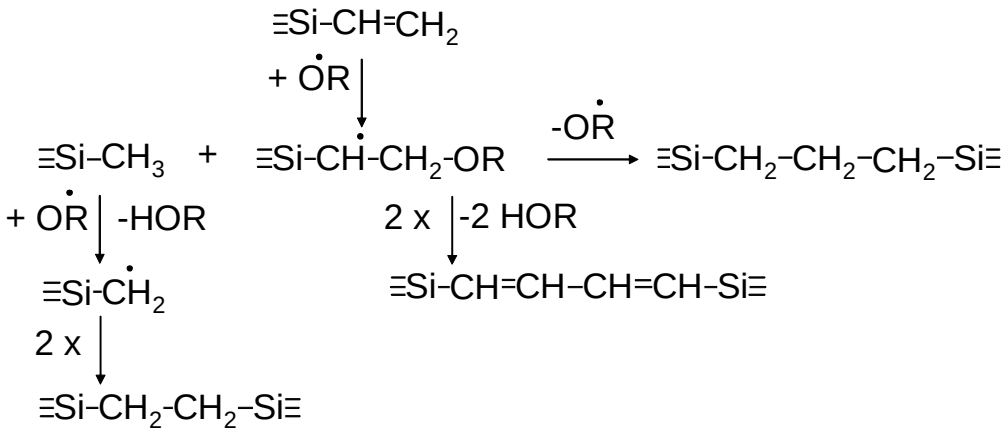

Figure 2: Chemistry of peroxide induced free radical reaction [2].

Depending on the peroxide used, next to prevailing three carbon bridges, side-

reactions occur that give two-carbon or four carbon bridges. It was also observed that the crosslinking degree of vinyl modified silicones was almost independent from the peroxide concentration and mostly dependent on the vinyl concentration [2].

2.1.2 Condensation reaction

The condensation polymerisation involves silicones modified with hydrolysable functionality, which gives silanol in a spontaneous reaction with atmospheric moisture. Silanol can further react releasing hydrolysed functionality [2].

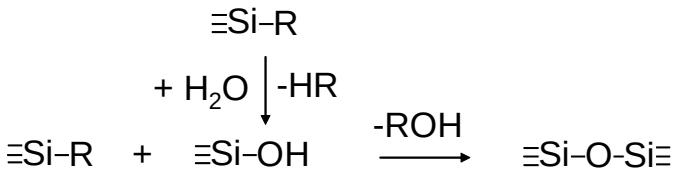

Figure 3: Chemistry of condensation reaction [2].

The rate of the condensation reaction given in Figure 3 strongly depends on the type of the used functionality. The fastest condensation curing siloxane is the acetoxy functionalised one (-OOCCH$_3$). The major limitation of the acetoxy functionality is the acetic acid by-product released during curing. In addition, the curing rate is limited by the transport of water vapour through the network, resulting in problems in the curing of thicker sections [2]. Crosslinking can be improved by the addition of tin catalyst. Concentrations in commercially available products are between 50 and 500 ppm [3]. Nevertheless, acetoxy functionalised silicones are widely used in households, because of their excellent adhesion to ceramic surfaces [2].

Neutral condensation curing silicones have an alkoxy (-OR) functionality. Because the alkoxy system has a low curing rate, a metal catalyst, titanate and/or tin based, are added to the system to accelerate the curing. Alkoxy functional silicones are mostly used for moulds, where a thick section curing is essential [2]. Tin levels

for these systems reach up to 5000 ppm. Condensation reaction systems can give sufficient polymerisation at low temperatures and are available as room temperature vulcanising (RTV) silicones. Next to acetoxy and alkoxy functionalised siloxanes, enoxy, oxime and amine systems are produced [3].

2.1.3 Hydridosilane/silanol reaction

Hydridosilane can react with silanol, or with water to form silanol, which can further polymerise as given in Figure 4. The reaction can be performed in presence of tin and platinum based catalyst [2].

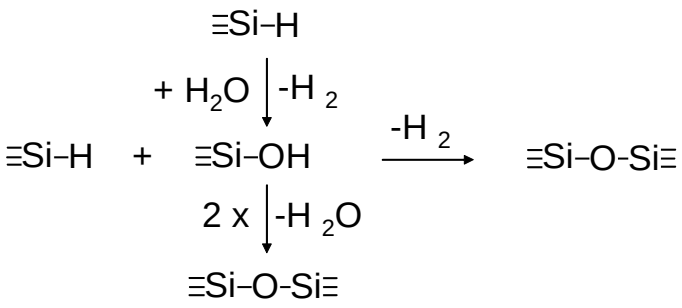

Figure 4: Chemistry of hydridosilane/silanol reaction [2].

The hydrogen gas evolution causes formation of foamed structures. Hence, industrial application of the hydridosilane/silanol reaction is in production of closed cell silicone foams. When a thin film of such silicone is coated, the evolved hydrogen can easily diffuse out of the layer. Hence, the hydridosilane/silanol systems are also used for the production of thin poly(dimethylsiloxane) coatings for certain release coating applications [2, 4].

2.1.4 Hydrosilylation addition reaction

Hydridosilane can crosslink with vinyl modified silicone in the presence of noble metal catalyst such as platinum or rhodium [2]. The hydrosilylation addition reaction

is often referred to as “addition” or “platinum cure” [3].

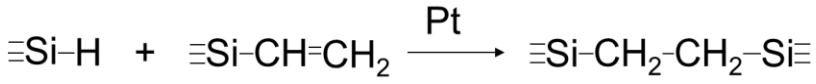

Figure 5: Chemistry of hydrosilylation addition reaction [2].

Crosslinking takes place exclusively between $SiCH=CH_2$ and SiH groups as given in Figure 5. Therefore the hydrosilylation addition reaction can be used to synthesise tailor-made poly(dimethylsiloxane) networks. Some side reactions occur in presence of O_2/H_2O, which promotes oxidation/hydrolysis of SiH to SiOH, which can also crosslink in condensation reactions as shown in Figure 4. This side reaction is nevertheless slower than hydrosilylation and has an effect in post-cure when SiH groups are in significant excess [2].

With ‘addition cure silicones’ it is possible to obtain versatile room temperature crosslinking systems with low viscosity, what is particularly useful for coating purposes [2]. Commercial ‘addition cured silicones’ systems are used in silicone release coating applications as solvent based, solvent-less or water emulsified formulations [4]. Concentration of the platinum in the silicone formulation is between 20 and 50 ppm [3]. Commercial hydrosilylation systems are available as two component formulation [2].

2.1.5 Modification of silicone with reactive organic functionalities

Silicone polymer with reactive organic functionalities can be synthetized directly from functionalised siloxane monomers, by reaction of silicone hydride with vinyl group and starting from chlorine functional silicone [2]. An example for the functionalisation of silicone through reaction of hydridosilane and organic modification (R) with vinyl group is presented in Figure 6.

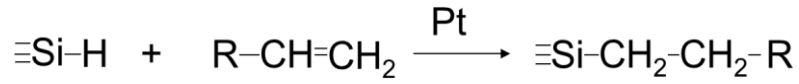

Figure 6: Reaction of hydridosilane and organic functionality with vinyl group.

Examples of reactive functionalities that are often introduced to silicones are given in Figure 7 [2].

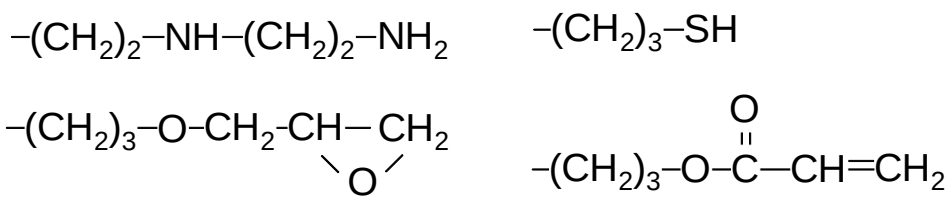

Figure 7: Examples of reactive functionalities of silicones [2].

The properties of functionalised silicone with less than 5 mol% of functional groups do not considerably differ from the properties of pure siloxanes. By attaching photopolymerisable functional groups to the poly(dimethylsiloxane) backbone (e.g. epoxy, acrylate, methyl acrylate group) different UV crosslinking systems were developed and are commercially available as release and protective coatings [5]. The crosslinking rate is usually increased by adding of a photoinitiator. The added amount of photoinitiator is limited by its solubility in the silicone prepolymer mixture [2].

Applications of functionalised silicones are versatile. Such functionalised silicones with nitrogen containing species and mercapto functional silicone modifications are used as adhesion promoters. These systems are used in cosmetic, textile and finishing metal polishes industry, because of their tuneable adsorption onto surfaces. Also, a wide area of applications have functional silicones with trifluoroalkyl modification for production of parts, where a low hydrocarbon solubility is required [2, 3].

2.1.6 High energy radiation curing

High energy radiation induces ionisation of poly(organosiloxanes), which leads to crosslinking or chain scission (i. e. degradation) [2, 6]. The two predominant free radical products are given in Figure 8.

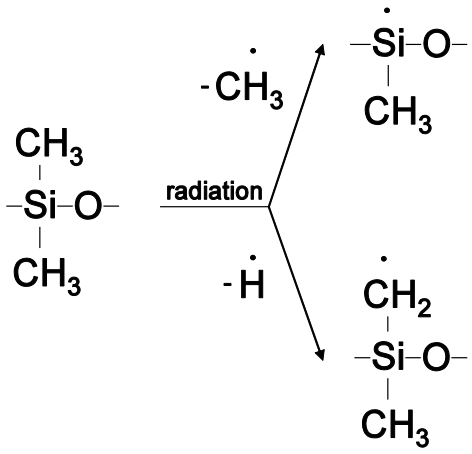

Figure 8: Free radical products after exposure of silicone to high energy radiation [2].

The crosslinking bonds are obtained by combination of radicals as shown in Figure 8, where the Si-CH_2-Si and Si-Si bridges predominate as a product [2]. Crosslinking yield relative to chain scissions depends on both, temperature and atmosphere in which the radiolysis is performed [7]. Until today no large scale application of high radiation crosslinking for silicone crosslinking has been realised [2].

2.2 Membrane production

2.2.1 Very first rubber membranes

The first systematic study of gas permeation through rubber was made by J. K. Mitchell in 1830 with balloons made from India rubber (caoutchouc) [8]. He inflated

rubber balloons with different gases and discovered that balloons deflated with different speed, depending on the nature of the gas. Mitchell also suggested that good permeability of carbon dioxide through the rubber film could be a consequence of large degree of sorption of carbon dioxide compared to other gases [9, 10].

Next to carbon dioxide various hydrocarbons are readily dissolved in the rubber phase; hence patents as early as 1939 claim the use of dense rubber diaphragm for separation and concentration of hydrocarbons in the gaseous state. The inventor explains that the separation of different hydrocarbons originates from the difference in permeation rates of components through the membrane, caused by differences in molecular weight, saturation and molecular structure of the hydrocarbon as well as solubility of the hydrocarbon in the rubber [11].

In 1960 Kammermeyer describes the use of a silicone membrane for separation of gases. The main advantage of the silicone is the unmatched permeability, compared to other available polymers at that time [12, 13].

2.3 Producing a rubber based membrane

After discovering the separation potential of rubber membranes, efforts were made to achieve higher permeability without losing the selectivity. Dip-coating is one of the oldest method to produce a very thin rubber layer [14]. Dip-coating techniques imply that an object is dipped and slowly withdrawn from a diluted polymer (monomer) solution. Adhesive forces between solution and the object's surface form a solution film, which covers the complete outer surface of the object. Subsequently, the solvent is evaporated, leaving a thin polymer skin on the surface. When macroporous structures, such as textile or wood, are coated adhesive forces cause a capillary effect, completely filling the pores of the coated substrate with polymer solution, and subsequently plugging the pores.

It was also observed that pore plugging during dip-coating can be used to increase the performance of gas separation membranes. The performance of gas separation membranes is significantly reduced, when defects are present in separation layer. Both, ultrathin polymer composites and thin skin phase inversion membranes can have defects, whether due to inhomogeneities or impurities in the preparation process. To plug these defects an overcoat of highly permeable polymer can be applied by dip-coating [15]. The final membrane achieves a selectivity which is only slightly less selective than the real selectivity of the original membrane, whereas the flux of the membrane is not changed [16, 17].

Earliest rubber membranes were produced as thin free standing homogeneous layers, to avoid the pore penetration of the support. During operation a thin rubber membrane was placed on a porous support (e.g. webs or sintered plates) to give additional mechanical strength. Nevertheless, when such thin film membranes were operated at high transmembrane pressures, the separation layer often ruptured. Hence, a dual film combination was suggested, where a very thin selective layer could be laminated to a highly permeable but mechanically stable membrane [18].

The biggest milestone in membrane development was made by Loeb and Sourirajan in 1960. They discovered the asymmetrical structure of phase inversion membranes and developed a phase inversion membrane for reverse osmosis applications [19, 20]. The Loeb and Sourirajan discovery was quickly adapted to other cellulosic polymers and then to a vast variety of polymers. Phase inversion membranes could offer for the first time an ideal support structure for rubber membranes with smooth surface, small pore radius combined with a high flux and good mechanical stability.

2.3.1 Optimisation of the dip-coating technique in silicone membrane production

In the 1960s Lonsdale, Riley and co-workers at General Atomic Co. started to develop a dip-coating technique for the production of composite membranes [21, 22]. As mentioned previously, the biggest challenge for dip-coating is intrusion of polymer into pores of the support layer, leading to a low permeability of the composite membrane. The effect of pore intrusion on the flux can be easily depicted by assuming a simple resistance in series model for mass transport through the membrane and neglecting the resistance of the porous support [16, 23].

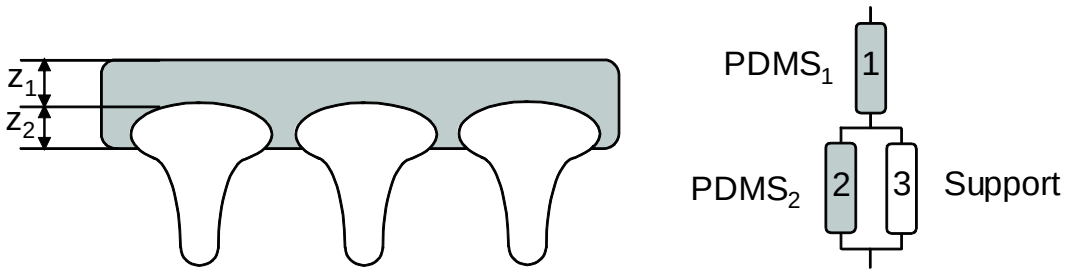

$$J = \left[\frac{z_1}{P_1} + \left(\frac{\varepsilon \cdot P_2}{z_2} + \frac{(1-\varepsilon) \cdot P_3}{z_2} \right)^{-1} \right]^{-1} \Delta p$$

Figure 9: Composite membrane with pore intrusion, taken from [16, 23].

In Figure 9 J is the solvent volume flux L $\cdot h^{-1} \cdot m^{-2}$, P_1 stands for the specific siloxane permeability of the free standing layer with unit L$\cdot \mu m \cdot h^{-1} \cdot m^{-2} \cdot bar^{-1}$ and z_1 is the thickness of free standing layer in μm. P_2 is the permeability of silicone layer confined in the pores and P_3 represents the permeability of the bulk polymer of the supporting membrane and z_2 is the thickness of intruded layer. The transmembrane pressure (Δp) is the driving force of permeation. Considering that the bulk phase of the support membrane has low permeability for most of the solvents and porosity of the ultrafiltration membrane (ε) is between 0.1 and 1 % [24], it is important that the separation takes place in the free standing layer and the pores serve only as

drainage as given in Figure 10.

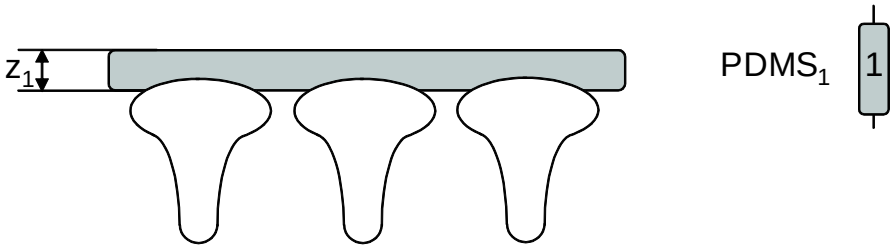

$$J_i = \left[\frac{z_1}{P_1}\right]^{-1} \Delta p$$

Figure 10: Composite membrane without pore intrusion, taken from [16, 23].

One way to reduce pore intrusion is filling the pores of the substrate prior to the coating step with non-solvent for the coating polymer [25]. Water was often used in the literature as “pore protector”. Wetting of the substrate was made by dipping it into water and removal of the water droplets by wiping the surface prior to coating [26, 27]. Otherwise, if continuous operation was needed, water could be partially evaporated [28]. Also suggested was passing the substrate through saturated water vapour atmosphere.

The pores of the substrate can also be filled by a non-volatile leachable component which mechanically holds the coated polymer on the surface. The non-volatile component used for impregnation of porous membrane can be inert to the coating polymer as described by Albrecht et al. [29].

Linder et. al. used reactive silanol terminated silicone oligomers as pore protecting agent [30]. In this way the layer of the impregnating solution that is in contact with reactive coating solution would crosslink, resulting in a better anchorage to the porous support.

For gas separation membranes was suggested to coat a highly permeable intermediate layer, between separation layer and porous support [31-33]. The advantage of this highly permeable intermediate layer is the enhancement of the flow in direction of the pores of the supporting membrane [34]. This approach is nevertheless hardly applicable to silicones because of their unmatched permeability. Likewise, in contact with organic solvents a highly permeable layer often swells extensively, which can lead to delamination of the separation layer [35].

Pore intrusion can be reduced by coating with diluted pre-polymer solution with a coil size larger than the pore size of the substrate [26, 36-40]. Coating with the high molecular weight polymer will likewise give a smoother and more uniform thickness of the selective layer of the composite membrane [38]. Also defects considerably larger than polymer coils will get sealed by coated polymer [41].

2.4 Silicones used for membrane production

In the following the literature overview of silicone composite membranes and their membrane production is subdivided as: membranes made out of hydrosilylation addition polymerised silicones; condensation reaction silicone membranes; membranes made out of functionalised silicones and silicone membranes additionally crosslinked by high energy radiation.

2.4.1 Membranes made out of hydrosilylation addition polymerised silicones

One of the most often used reactive silicone systems for membrane production according to literature is the commercially available two component RTV615 system, provided by General Electric [26, 27, 39, 42-44]. Stafie et al. analysed this

system and found that RTV615 A contains dimethylvinyl terminated silicone prepolymer (with a wide bimodal molar weight distribution of 4000 g·mol^{-1} and 67000 g·mol^{-1}) with Pt based catalyst and that RTV615 B contains silicone with hydridosilane components (also bimodal molar weight distribution of 1500 g·mol^{-1} and 60000 g·mol^{-1}) [45]. They obtained defect free silicone composite membranes using 7 w. % of prepolymerised silicone in hexane as coating solution on polyacrlyonitrile (PAN) support ultrafiltration membrane. The membranes were dip-coated by submersing a supporting membrane sheet glued to a glass plate into the coating solution. The produced silicone membrane was also compared to the MPF-50 membrane from Koch and a silicone based composite membrane provided by GKSS [27]. Dutzcak et al. developed a solvent stable silicone/ceramic composite membrane using the RTV615 silicone system. The silicone was dissolved in toluene and in a stepwise procedure prepolymerised prior to the dip-coating. This prepolymerisation enabled production of a stable separation layer with minimum pore penetration [40].

2.4.2 Condensation reaction membranes

Linder et al. [30] described a production procedure of composite membranes with improved solvent stability. As a support an ultrafiltration membrane made out of thermally crosslinked polyacrylonitrile was used. To prevent pore intrusion the highly solvent stable support was first coated with silanol terminated silicone (molar weight of 4200 g·mol^{-1}) without catalyst. The impregnated substructure was further coated with silanol terminated silicone (molar weight of 36000 g·mol^{-1}) with catalyst and then thermally crosslinked.

2.4.3 Membranes made out of silicone with reactive organic functionalities

Silicone with reactive organic functionalities can be crosslinked with different chemical reactions depending on the type of organic functionality introduced to the silicone chain. The added organic functionality can then reinforce the silicone network and/or tune the solubility of the final silicone separation layer.

2.4.4 Amino modified silicone for membrane production

An amine functional group can be effectively crosslinked with di- or poly- functional acid chlorides, acid anhydrides, isocyanate, thiocyanate, sulfonyl chloride, epoxides etc. [32, 46, 47]. Thin silicone separation layers can be produced out of amino-modified silicone by a two-step coating procedure. The membrane support is first impregnated with diluted amino-modified silicone solution and subsequently dried. The second coating follows with a crosslinker solution, after which the silicone is cured. Amino-modified silicone and crosslinker can also be dissolved in non-mixable solvents, from which a membrane can be produced by surface polycondensation [46].

2.4.5 Halogen functionalised silicones for membrane production

From the protective coating technology it is known that introduction of a fluorinated modification onto the poly(organosiloxane) backbone will reduce swelling of the silicone in hydrocarbons [3]. Halogen modified silicones usually have additional reactive groups, which can be crosslinked. Bitter et. al. [48] claimed such fluorinated silicones for production of membranes capable of permeating a mixture of aromatics and polar aliphatic components, while rejecting dissolved hydrocarbon oil. Abdellah et al. [49] investigated photocrosslinkable fluorinated silicone with acrylate and vinyl

urethane reactive groups for gas separation applications.

2.4.6 Radiation curable silicone for membrane production

Advantage of acrylate and epoxyde functionalities in silicone composite membrane production is the fast and complete cure of the coated separation layer [49-51]. These radiation curable silicones are available in the range from highly functional, which give hard glossy coatings, to low functionalised, linear chains of dimethylsiloxane groups [52]. Chiou et al. describes an epoxy-functional silicone composite membrane which has excellent solvent stability and a low level of leaching. Ebert [53] also claims the improved stability of composite membranes with an acrylate-functional silicone separation layer in separation of an edible oil and hexane mixture. The influence of different crosslinking densities of acrylate-functional silicones on membrane separation performance was investigated at Evonik Industries AG [54]. In this patent an example for the production of silicone acrylate based membranes with the desired properties was shown.

2.4.7 Membranes additionally crosslinked by high energy radiation

Schmidt et al. used high energy radiation crosslinking for post-treatment of already formed silicone layers. The radiation induced crosslinking of poly(dimethylsiloxane) improved anchorage of the separation layer onto the supporting membrane. The produced layer is claimed to swell less and to have a stable performance in organic solvents [55].

2.5 Applications of silicone based membranes

2.5.1 Recovery of volatile organic compounds

Separation of gases is determined by their sorption and diffusion in the membrane phase. Although volatile organic compounds have generally lower diffusion coefficients, they permeate preferentially through the silicone membrane [9]. The selectivity of commercial silicone membranes is for most organic compounds over nitrogen higher than 10 [56]. Hence, silicone membranes have been successfully used in chemical industry to recover hydrocarbons from plant off-gas streams. Silicone membranes were also investigated in the recovery of liquefied petroleum gas, such as the C_3+ hydrocarbons from methane or hydrogen [57]. Further applications include adjusting the dewpoint of natural gas and the methane number control of fuel gas for gas engines and gas turbines [58, 59].

One more distant industrial application of silicone membranes is biotreatment of large air streams for removal of traces of organic polluters. In this operation the membrane serves as a contactor between a contaminated air stream and a water solution containing bacteria which can decompose the permeated organic compounds [56].

2.5.2 Pervaporation

Pervaporation is a membrane separation process, where a feed liquid mixture is contacted with a membrane, vacuum is applied on the permeate side and permeate is removed as a vapour. A pervaporation process using a hydrophobic membrane is commercially applied for the removal of traces of volatile organic compounds from contaminated water. Good separation is achieved between nonpolar organic solvents and water, because of the large difference in their solubility in the membrane

phase [9]. Analogous applications have been studied for recovery of valuable aromas and flavours out of diluted solutions [60, 61]. Efforts were also made to obtain a robust and selective membrane for the recovery of ethanol. Potentially pervaporation of ethanol from fermentation broth/water could contribute to reduce the energy requirement for the production of fuel grade ethanol [44].

2.5.3 Application in food industry

In food industry no large scale application of hydrophobic membranes has been realised yet. Most promising applications of silicone membranes are partial concentration and de-acidification of hexane-extracted vegetable oils [62, 63]. Rama et al. studied a soybean oil extract and succeeded in 9-fold concentration with acceptable high flux, almost complete recovery of oil and significant reduction of the free fatty acids content [62].

2.5.4 Process for purifying a liquid hydrocarbon product

Removing a few percent of high molecular weight contaminants from a hydrocarbon stream is mostly achieved by distillation or precipitation of contaminants by refrigeration. Both distillation and refrigeration are energy intensive processes. The energy requirements of distillation increase considerably with higher boiling point of the hydrocarbon stream. It was very early recognised that silicone based membrane separations can be more efficient than conventional separation routes [64]. In the eighties The Shell Oil Company claimed halogenated silicone membranes for solvent recovery from a mixture with higher boiling hydrocarbons. The membrane was claimed for solvent dewaxing of hydrocarbon oils [48, 65]. Shell further broadened the patent to applications of hydrophobic membranes for purification of liquid hydrocarbons with up to 5% of high molecular weight components [65, 66].

2.5.5 Homogeneous catalyst recovery

The industrial application of homogeneous catalysts is strongly depending on the possibility to recover/remove the catalyst from the product. When noble metal based homogeneous catalysts are used, any improvement of catalyst recovery leads to a large economic benefit [67]. Hence, in the early development of the membranes the benefit of gentle separation of homogenous catalyst was investigated [68, 69]. Silicone based membranes have been tested and claimed for different homogeneous catalyst separations. Earliest applications of silicone based membranes involve continuously operated homogeneous catalysis [70] and recovery of homogeneous catalyst from a high boiling residue of a distillated hydroformylation reaction mixture [71]. Generally, since the seventies many homogeneous catalysed reactions in combination with membrane separation were investigated. More detailed information can be found in literature [72-75].

2.6 Conclusion

From the given chemical reactions of the silicone polymers one can recognise how versatile the silicone based polymers are. Each having slightly different properties depending on the modification, but continuing to be a robust and chemically stable material. Many of the reactive silicones were already used to produce silicone based membranes, but only few have been tested in organic solvent nanofiltration applications.

The chemical modification of the silicone has been further developed in many non-membrane related applications. Combining this knowledge with new achievements in membrane production technology could improve any of the already known application of silicone based membrane, as well as opening possibilities for novel membrane separations.

2.7 List of symbols

J	solvent volumetric flux	$L \cdot h^{-1} \cdot m^{-2}$
P	specific polymer permeability	$L \cdot \mu m \cdot h^{-1} \cdot m^{-2} \cdot bar^{-1}$
Δp	transmembrane pressure	bar
z	separation membrane thickness	μm
ε	porosity	-

2.8 References

[1] H. Strathmann, *Synthetic Membranes and Their Preparation* in: M.C. Porter (Ed.), *Handbook of Industrial Membrane Technology* Noyes Publications, 1990, p. 624.

[2] S.J. Clarson, J.A. Semlyen, *Siloxane Polymers*, Prentice Hall 1993.

[3] Gelest Inc., *Reactive silicones: Forging new polymer links*, 2007, Available at: www.gelest.com.

[4] Dow Corning Corporation, *Silicone Release Coatings for the Pressure Sensitive Industry – Overview & Trends*, 2003, Available at: www.dowcorning.com.

[5] Evonik Industries AG, *Radiation Curable Silicones - An Overview*, 2013, Available at: www.tego-rc.com.

[6] A.A. Miller, *Radiation Chemistry of Polydimethylsiloxane: I. Crosslinking and Gas Yields*, Journal of the American Chemical Society 82 (1960) 3519-3523.

[7] D.J.T. Hill, C.M.L. Preston, D.J. Salisbury, A.K. Whittaker, *Molecular weight changes and scission and crosslinking in poly(dimethyl siloxane) on gamma radiolysis*, Radiation Physics and Chemistry 62 (2001) 11-17.

[8] J.K. Mitchell, *On the penetrativeness of fluids*, American Journal of the Medical Sciences 13 (1930) 36-67.

[9] R. Baker, *Membrane Technology and Applications*, 3rd ed., Wiley 2012.

[10] R.M. Felder, G.S. Huvard, *Permeation, diffusion, and sorption of gases and vapors* in: R.A. Fava (Ed.), *Methods of Experimental Physics*, Academic Press, 1980.

[11] F.E. Frey, *Process for concentrating hydrocarbons*, US2159434, Philips Petroleum Company, 1939.

[12] K. Kammermeyer, *Separation of gases by diffusion through silicone rubber*, US2966235, Selas Corporation of America, 1960.

[13] R.M. Barrer, J.A. Barrie, N.K. Raman, *Solution and diffusion in silicone rubber I - A comparison with natural rubber*, Polymer 3 (1962) 595-603.

[14] T.A. Osswald, G. Menges, *Materials Science of Polymers for Engineers* Hanser Gardner 2002.

[15] W.R. Browall, *Method for sealing breaches in multi-layer ultrathin membrane composites*, US3980456, General Electric Company, 1976.

[16] J.M.S. Henis, M.K. Tripodi, *Composite hollow fiber membranes for gas separation: the resistance model approach*, Journal of Membrane Science 8 (1981) 233-246.

[17] J.M.S. Henis, M.K. Tripodi, *Multicomponent membranes for gas separations*, US4230463, Monsanto Company, 1980.

[18] R.J. Lee, J.F. Jennings, *Dual film combinations for membrane permeation*, US2960462, American Oil Company, 1960.

[19] S. Loeb, *The Loeb-Sourirajan Membrane: How It Came About* in: A.F. Turbak (Ed.), *Synthetic Membranes*, American Chemical Society, 1981, pp. 1-9.

[20] S. Loeb, S. Sourirajan, *High flow porous membranes for separating water from saline solutions*, US3133132, University of California, 1964.

[21] J.E. Cadotte, *Evolution of Composite Reverse Osmosis Membranes* in: D.R. Lloyd (Ed.), *Materials Science of Synthetic Membranes*, American Chemical Society, 1985, pp. 273-294.

[22] H.K. Lonsdale, *The evolution of ultrathin synthetic membranes*, Journal of Membrane Science 33 (1987) 121-136.

[23] K. Ebert, *Thin film composite membrane of glassy polymers for gas separation - Preparation and characterisation*, PhD Thesis, University of Twente, 1995.

[24] M. Mulder, *Basic Principles of Membrane Technology*, 2nd ed., Kluwer Academic Publisher 1996.

[25] S.C. Williams, B. Bikson, J.K. Nelson, R.D. Burchesky, *Supported semipermeable membranes and process for preparing same*, US3762566, Abcon Inc., 1973.

[26] I.F.J. Vankelecom, B. Moermans, G. Verschueren, P.A. Jacobs, *Intrusion of PDMS top layers in porous supports*, Journal of Membrane Science 158 (1999) 289-297.

[27] N. Stafie, *Poly (dimethyl siloxane) - based composite nanofiltration membranes for non-aqueous applications*, PhD Thesis, University of Twente, 2004.

[28] S.C. Williams, B. Bikson, J.K. Nelson, R.D. Burchesky, *Method for preparing composite membranes for enhanced gas separation*, US4840819, Union Carbide Corporation, 1989.

[29] W. Albrecht, T. Weigel, D. Paul, K. Kneifel, *Polyacrylonitrile membrane, especially capillary or base membrane* DE19546837, GKSS-Forschungszentrum Geesthacht GmbH, 1997.

[30] C. Linder, M. Nemas, M. Perry, R. Katraro, *Silicone-derived solvent stable membranes*, US5205934, Membrane Products Kiryat Weitzman Ltd., 1993.

[31] J. Shorr, *Composite membrane and process for making same*, US3556305, Amicon Corporation, 1971.

[32] I. Cabasso, K.A. Lundy, *Method of making membranes for gas separation and the composite membranes*, US4602922, Research Foundation of State University of New York 1986.

[33] W.R. Browall, R.M. Salemme, *Laminated porous/nonporous membranes*, US3874986, General Electric Company, 1975.

[34] R.P. Castro, R.W. Baker, J.G. Wijmans, *Multilayer interfacial composite membrane*, US5049167, Membrane Technology & Research Inc., 1991.

[35] C.R. Millington, A. Nijmeijer, J.P. Robinson, E.S. Tarleton, *The assessment of materials for crossflow nanofiltration of organic/organic liquids and the development of scale-up options*,9th World Filtration Congress New Orleans 18. - 22. April 2004.

[36] W.B. Mccormack, *Fluid separation*, US3246764, Pont DU., 1966.

[37] R.R. Ward, R.C. Chang, J.C. Danos, J.A. Carden Jr., *Processes for coating bundles of hollow fiber membranes*, US4214020, Monsanto Company, 1980.

[38] R.L. Riley, R.L. Grabowsky, *Preparation of gas separation membranes*, US4243701, UOP Inc., 1981.

[39] S.M. Dutczak, *Solvent resistant nanofiltation membranes*, PhD Thesis, University of Twente, 2011.

[40] S.M. Dutczak, M.W.J. Luiten-Olieman, H.J. Zwijnenberg, L.A.M. Bolhuis-Versteeg, L. Winnubst, M.A. Hempenius, N.E. Benes, M. Wessling, D. Stamatialis, *Composite capillary membrane for solvent resistant nanofiltration*, Journal of Membrane Science 372 (2011) 182-190.

[41] H. Strathman, C.-M. Bell, K. Kinnnerle, *Development of synthetic membranes for gas and vapor separation*, Pure and Applied Chemistry 58 (1986) 1663-1668.

[42] L.E.M. Gevers, G. Meyen, K. De Smet, P. Van De Velde, F. Du Prez, I.F.J. Vankelecom, P.A. Jacobs, *Physico-chemical interpretation of the SRNF transport mechanism for solutes through dense silicone membranes*, Journal of Membrane Science 274 (2006) 173-182.

[43] R.W. Baker, *Process for recovering organic vapors from air*, US4553983, Membrane Technology and Research Inc., 1985.

[44] L.M. Vane, V.V. Namboodiri, T.C. Bowen, *Hydrophobic zeolite-silicone rubber mixed matrix membranes for ethanol-water separation: Effect of zeolite and silicone component selection on pervaporation performance*, Journal of Membrane Science 308 (2008) 230-241.

[45] N. Stafie, D.F. Stamatialis, M. Wessling, *Effect of PDMS cross-linking degree on the permeation performance of PAN/PDMS composite nanofiltration membranes*, Separation and Purification Technology 45 (2005) 220-231.

[46] S. Hirose, Kurihara, Masaru, *Selective permeable membrane*, JP57105203, Toray Industry Inc., 1982.

[47] D. Ahn, C. Wong, J. Hrbal, *Method of preparing gas selective membrane using epoxy-functional siloxanes*, WO2012138755, Ahn Dongchan, Wong Christopher, Hrbal James 2012.

[48] J.G.A. Bitter, J.P. Haan, H.C. Rijkens, J.P. Haan, H.C. Rijkens, *Process for the separation of solvents from hydrocarbons dissolved in the solvents*, US4748288, Shell Oil Company, 1988.

[49] L. Abdellah, B. Boutevin, F. Guida-Pietrasanta, M. Smaihi, *Evaluation of photocrosslinkable fluorinated polydimethylsiloxanes as gas permeation membranes*, Journal of Membrane Science 217 (2003) 295-298.

[50] M.J. Steuck, *Porous membrane having hydrophilic surface and process*, US4618533, Millipore Corporation, 1986.

[51] R.W. Callahan, R.D. Johnson, *Membranes from UV-curable resins*, US5102552, Hoechst Celanese Corporation, 1992.

[52] J.J. Chiou, *Epoxysilicone coated membranes*, US6368382, UOP LLC, 2002.

[53] K. Ebert, J. Koll, J. Wind, *Composite membrane and process*, US7601263, GKSS-Forschungszentrum Geesthacht GmbH, 2009.

[54] R. Hänsel, H. Döhler, P. Schwab, P. Seidensticker, M. Ferenz, G. Baumgarten, M. Lazar, M. Ungerank, *Composite silicone membranes with high separating action*, WO2011067054 A1, Evonik Goldschmidt GmbH, 2011.

[55] M. Schmidt, K.-V. Peinemann, N. Scharnagel, K. Friese, R. Schubert, *Silicone composite membrane modified by radiation-chemical means and intended for use in ultrafiltration*, WO1996027430, GKSS-Forschungszentrum Geesthacht GmbH, 1996.

[56] S.P. Nunes, K.V. Peinemann, *Gas Separation with Membranes* in: S.P. Nunes, K.V. Peinemann (Eds.), *Membrane Technology*, Wiley-VCH Verlag GmbH & Co. KGaA, 2006, pp. 53-90.

[57] B.S. Minhas, D.W. Staubs, *Membrane process for LPG recovery*, US7799964, ExxonMobil Research and Engineering Company, 2010.

[58] K.G. Watler, *Process for separating higher hydrocarbons from natural or produced gas streams*, US4857078, Membrane Technology & Research, Inc., 1989.

[59] J. Schultz, K.V. Peinemann, *Membranes for separation of higher hydrocarbons from methane*, Journal of Membrane Science 110 (1996) 37-45.

[60] M. She, S.-T. Hwang, *Recovery of key components from real flavor concentrates by pervaporation*, Journal of Membrane Science 279 (2006) 86-93.

[61] F. Lipnizki, J. Olsson, G. Trägårdh, *Scale-up of pervaporation for the recovery of natural aroma compounds in the food industry. Part 1: simulation and performance*, Journal of Food Engineering 54 (2002) 183-195.

[62] L.P. Rama, M. Cheryan, N. Rajagopalan, *Solvent recovery and partial deacidification of vegetable oils by membrane technology*, Lipid / Fett 98 (1996) 10-14.

[63] P. Vandezande, L.E.M. Gevers, I.F.J. Vankelecom, *Solvent resistant nanofiltration: separating on a molecular level*, Chemical Society Reviews 37 (2008) 365-405.

[64] D.E. McVannel, *Fractionation of organic compounds of high molecular weight*, US34402641969.

[65] J.G.A. Bitter, J.P. Haan, *Process for separating a fluid feed mixture containing hydrocarbon oil and an organic solvent*, US4810366, Shell Oil Company, 1989.

[66] R.P. Cossee, E.R. Geus, H.E.J. Van Den, C.E. Weber, *Process for purifying a liquid hydrocarbon product*, US6488856, Shell Oil Company, 2002.

[67] Sumit Bhaduri, D. Mukesh, *Homogeneous Catalysis: Mechanisms and Industrial Applications*, Wiley-Interscience 2000.

[68] M.T. Westaway, G. Walker, *Catalyst ultrafiltration process*, US3617553, The British Petroleum Company Ltd., 1971.

[69] R.C. Binning, J.T. Kelly, *Hydrocarbon conversion with dialytic separation of the catalyst from the hydrocarbon products*, US2913507, American Oil Company, 1959.

[70] A. Goldup, M.T. Westaway, G. Walker, *Separation of metal compounds*, US3645891, British Petroleum Company Ltd., 1972.

[71] F. William, C. Terence, *Hydroformylation of olefines*, GB1432561 A Imperial Chemical Industries LTD, 1976.

[72] H.P. Dijkstra, G.P.M. van Klink, G. van Koten, *The Use of Ultra- and Nanofiltration Techniques in Homogeneous Catalyst Recycling*, Accounts of Chemical Research 35 (2002) 798-810.

[73] I.F.J. Vankelecom, *Polymeric Membranes in Catalytic Reactors*, Chemical Reviews 102 (2002) 3779-3810.

[74] M. Priske, K.-D. Wiese, A. Drews, M. Kraume, G. Baumgarten, *Reaction integrated separation of homogenous catalysts in the hydroformylation of higher olefins by means of organophilic nanofiltration*, Journal of Membrane Science 360 (2010) 77-83.

[75] M. Janssen, C. Müller, D. Vogt, *Recent advances in the recycling of homogeneous catalysts using membrane separation*, Green Chemistry 13 (2011) 2247-2257.

3 General theoretical and experimental part

3.1 Basic membrane concepts

A membrane is in general a physical barrier separating two phases. Membrane separation processes are based on the difference in transport velocities of components through this barrier. The driving force for component transport is the difference in their chemical potential between the two phases.

Organic solvent nanofiltration (OSN) is a pressure driven membrane separation process. The feed solution with a certain solute concentration is pressurised and subsequently a portion of the feed solution starts to permeate through the membrane. If the permeation rate of the solute is lower than the permeation rate of the solvent a positive difference between solute feed concentration and solute permeate concentration is observed. During the filtration the solute concentration in the feed is increased compared to the beginning of the filtration process. This stream is referred to as retentate or concentrate. The different streams in membrane filtration are shown in Figure 11.

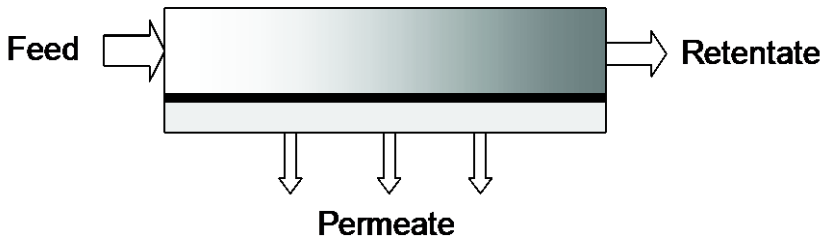

Figure 11: Feed, retentate and permeate streams in membrane filtration.

The solute with the lower permeation rate is transported with the permeate stream to the membrane surface, where it can accumulate. The back flow diffusion counteracts the developed concentration difference of the solute between the boundary

layer on the membrane and the bulk feed phase. This phenomena is referred to as concentration polarisation and is shown in Figure 12 under steady state conditions (taken from [1]).

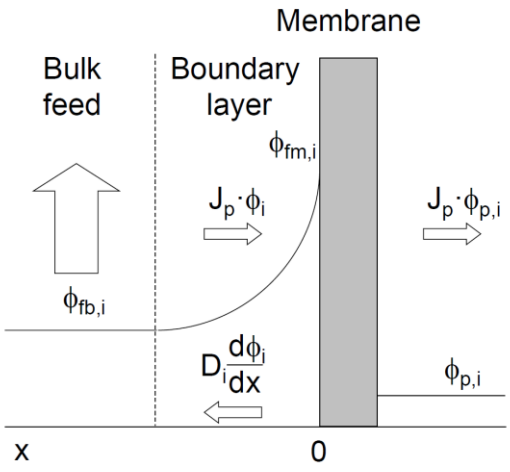

Figure 12: Concentration polarisation phenomena under steady state conditions, taken from [1].

Where J_p is the total volume flux equivalent to permeate velocity through the membrane in m·s^{-1}, $\phi_{fm,i}$, $\phi_{fb,i}$ and $\phi_{p,i}$ are the volume fractions of component i in the bulk feed phase, in the feed phase near the membrane surface and in permeate, respectively. D_i is the Fickian's diffusion coefficient of the highly diluted component i in the boundary layer and x is the distance to the membrane surface. Hence two rejections can be defined, the measured or observed membrane rejection according to

$$Rejection_{fb,i} = 1 - \frac{\phi_{p,i}}{\phi_{fb,i}}, \qquad 1$$

and the real membrane rejection given by equation 2, which is in general higher than the measured rejection.

$$Rejection_{fm,i} = 1 - \frac{\phi_{p,i}}{\phi_{fm,i}} \qquad 2$$

The value of real membrane rejection can be calculated from value of measured rejection by correcting it for the effect of concentration polarisation. The concentration polarisation phenomenon in filtration experiments can be mathematically described by the Sherwood's stagnant film approach [2]. Taking the volume fraction as solute concentration, the concentration polarisation can be described by equation 3.

$$\frac{J_p}{k_{sf,i}} = \ln\left(\frac{\phi_{fm,i} - \phi_{p,i}}{\phi_{fb,i} - \phi_{p,i}}\right) \qquad 3$$

Where $k_{sf,i}$ is the mass transfer coefficient of component i in the feed boundary layer in $m \cdot s^{-1}$. Equation 3 can also be defined in the form of characteristic dimensionless Peclet (Pe) and Sherwood (Sh) numbers given by equation 4 [3].

$$\frac{Pe}{Sh} = \ln\left(\frac{\phi_{fm,i} - \phi_{p,i}}{\phi_{fb,i} - \phi_{p,i}}\right) \text{ with}$$

$$Pe = \frac{M \cdot d_{hyd}}{\rho \cdot D_i} = \frac{J_p \cdot d_{hyd}}{D_i} \qquad 4$$

$$Sh_i = \frac{k_{sf,i} \cdot d_{hyd}}{D_i}$$

Where M is the total permeate mass flux, ρ is the mass density in $kg \cdot m^3$ and d_{hyd} is the hydrodynamic diameter in m.

Substituting equations 1 and 2 into equation 3, the following relation between measured and real membrane rejection is derived (see equation 5).

$$\frac{1 - Rejection_{fb,i}}{Rejection_{fb,i}} = \frac{1 - Rejection_{fm,i}}{Rejection_{fm,i}} \exp\left(\frac{J_p}{k_{sf,i}}\right) \qquad 5$$

3.2 Cross-flow filtration rig

The cross-flow filtration setup has three flat rectangular membrane cells connected in parallel. The filtration cells have 20 cm length, 4 cm width and 0.1 cm channel height. The process flow diagram of the setup is given in Figure 13 .

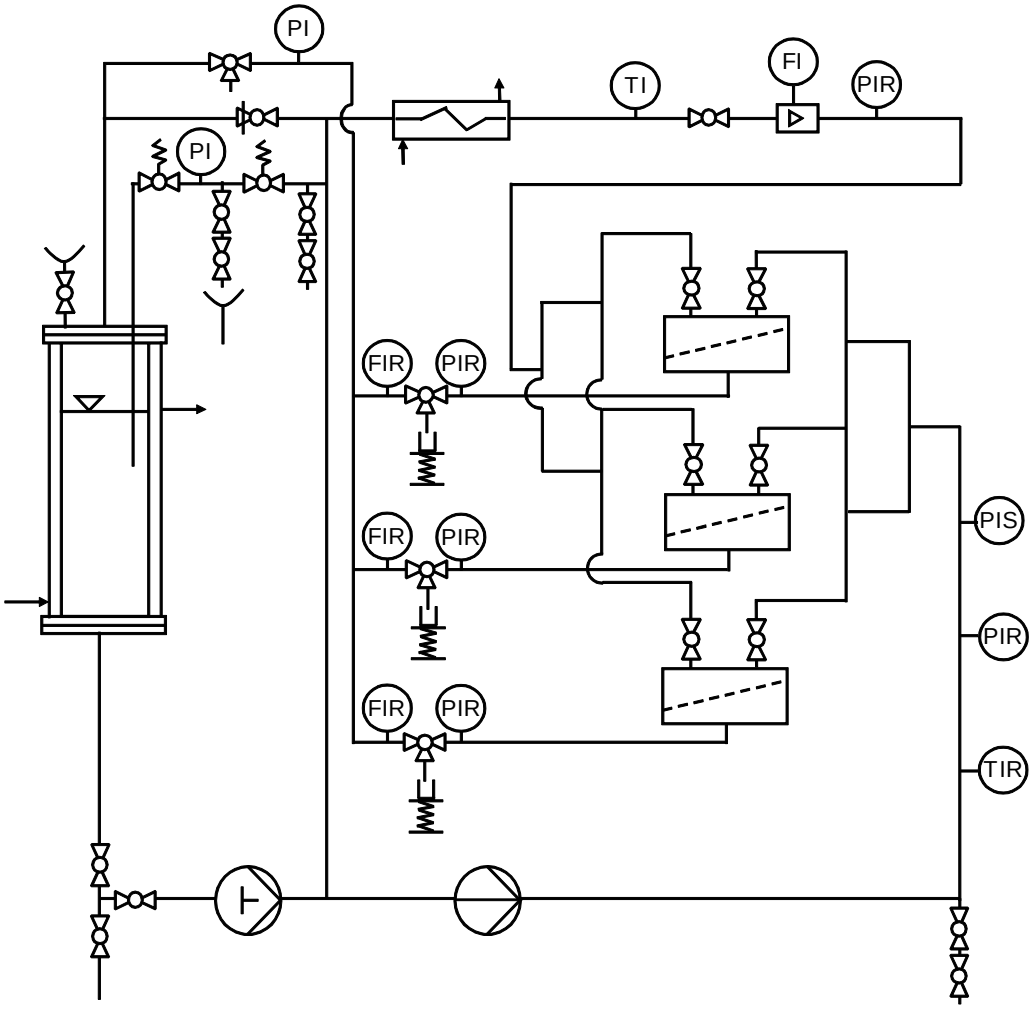

Figure 13: Process flow diagram of the cross-flow filtration set-up.

At the start of operation approximately 2 L of feed mixture is poured into the closed jacked tank equipped with a mechanical stirrer. Then the feed is directed into a recirculation loop by a high pressure pump (12 $kg \cdot h^{-1}$). In the recirculation loop a pump with capacity of approximately 700 $L \cdot h^{-1}$, temperature and pressure indicators and a low/high pressure security switch are installed. Further on, the recirculated

stream separates into three membrane modules. After the modules pressure, flow rate and temperature are measured. A heat exchanger and jacketed feed tank are used for tempering via external temperature control by an additional cryostat.

Permeate streams can be directed to the feed tank over coriolis flow meters or for sampling. The permeate pressures are monitored on all permeate streams. Permeability was calculated from the measured mass flow ($\dot{m}$), mass density at experiment temperature (ρ), transmembrane pressure (Δp) and active membrane area (A_m) as given by equation 6.

$$Permeability = \frac{\dot{m}}{A_m \cdot \rho \cdot \Delta p} \qquad 6$$

The rejection was calculated using measured volume fraction of styrene oligomers in permeate and retentate (see equation 1).

3.3 Concentration polarisation in rectangular cross-flow filtration cells

The Sherwood correlation derived by Lyster and Cohen was taken for evaluation of an axially averaged mass transfer coefficient in a rectangular channel [4]. The Reynolds number (Re) is in this case defined by equation 7.

$$Re = \frac{v \cdot H \cdot \rho}{\eta} \qquad 7$$

Where v is the average feed cross-flow velocity in $m \cdot s^{-1}$, H is the feed channel height in m, ρ is the mass density in $kg \cdot m^3$ and η is the viscosity in Pa·s.

The Schmidt number Sc is given by equation 8.

$$Sc_i = \frac{\eta}{\rho \cdot D_i} \qquad 8$$

Where diffusion coefficient (D_i) is given in $m^2 \cdot s^{-1}$. The effect of permeate flux is included by the average Reynolds number for permeate ($\overline{Re_p}$) given by equation 9 which contains the axial average permeation velocity, which is equal to the permeate volume flux.

$$\overline{Re_p} = \frac{J_p \cdot H \cdot \rho}{\eta} \qquad 9$$

The Sherwood number of a rectangular filtration channel with height H and length L is given by equation 10 [4].

$$Sh_i = \frac{k_{sf,i} \cdot H}{D_i} = A_1 \left(1 + A_2 \cdot Re^{A_3} \cdot Sc^{A_4} \left(\frac{H}{L}\right)^{A_5} \overline{Re_p}\right)\left(Re \cdot Sc \cdot \frac{H}{L}\right)^{1/3} \qquad 10$$

$A_1 = 1.72$
$A_2 = 1.25$
$A_3 = -0.31$
$A_4 = 0.50$
$A_5 = -0.28$

3.4 EMET stirred filtration cell

The Evonik Membrane Extraction Technology (EMET) stirred cell is a high pressure Hastelloy filtration unit. The total volume of the cell is approximately 250 ml and the active membrane surface is 51.4 cm^2. The Teflon coated magnetic stirrer is fixed on a guiding axis on the top of the cell and enables stirring of the feed close to the membrane surface. A sketch of the EMET stirred cell is given in Figure 14.

At the beginning of the filtration experiments the dry membrane sheet is installed. After filling the cell with the feed, it is closed and pressurised using external high

pressure nitrogen supply. The collected permeate is measured by an analytical scale and recorded over time. The mass flux in $kg \cdot h^{-1} \cdot m^{-2}$ is calculated using equation 11.

$$M = \frac{\Delta m}{\Delta t \cdot A_m} \qquad 11$$

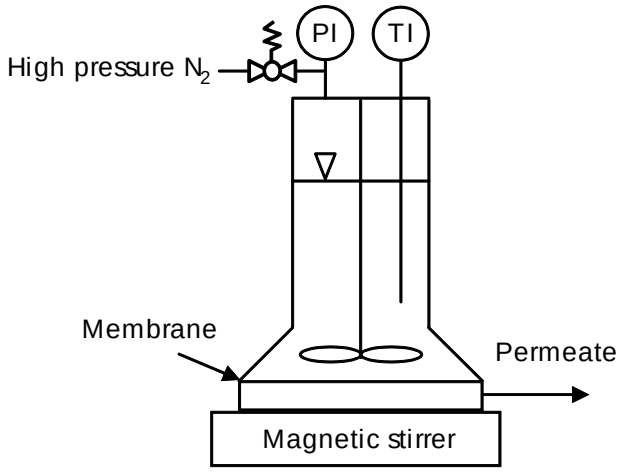

Figure 14: Scheme of EMET stirred filtration cell.

The measured membrane flux at room temperature is transformed to the value at 23 °C using the following viscosity correlation

$$M(23°C) = M(T) \frac{\eta(T)}{\eta(23°C)}. \qquad 12$$

3.5 Concentration polarisation in EMET stirred cell

The Sherwood correlation given by equation 13 can be used to predict the mass transfer coefficient in the boundary layer of a stirred filtration cell [5].

$$Sh_i = \frac{k_{sf,i} \cdot r}{D_i} = A \cdot Re^B \cdot Sc_i^C \qquad 13$$

Where r is the radius of the membrane cell in m. The corresponding Reynolds and Schmidt numbers are defined by equations 14 and 15.

$$Re = \frac{\omega \cdot r^2 \cdot \rho}{\eta} \qquad 14$$

$$Sc_i = \frac{\eta}{\rho \cdot D_i} \qquad 15$$

Where ω is the average radial velocity of the feed in rad·s^{-1}. The average radial velocity of the feed is smaller than the radial velocity of a stirrer ω_S or in this case the radial velocity of a magnetic stirrer ω_{mb}. Hence, by using the radial velocity of a magnetic stirrer instead of the feed radial velocity, the Reynolds number for the stirrer (Re_S) can be defined (see equation 16).

$$Re_S = \frac{\omega_{mb} \cdot r^2 \cdot \rho}{\eta} \qquad 16$$

The modified Sherwood correlation is shown in equation 17.

$$Sh = A \cdot Re_S^B \cdot Sc^C \qquad 17$$

The average radial velocity is strongly influenced by cell geometry, thus coefficients A, B and C are different for each type of stirred cell. Hence, determination of coefficients A, B and C for the EMET stirred cell has been done from experimental data.

3.5.1 Estimation of Sherwood correlation parameters for EMET stirred cell

The measured rejection defined in equation 1, changes with the intensity of the concentration polarisation, hence measured rejection is a function on radial stirrer

velocity (see equation 18).

$$Rejection_{fb,i}(\omega_{mS}) = 1 - \frac{\phi_{p,i}}{\phi_{fb,i}} \qquad 18$$

When no concentration polarisation occurs, which would be the case of infinitely fast stirring $\omega_S \to \infty$, the concentration of component i on the membrane approaches the concentration in the bulk feed $\phi_{fm,i} \to \phi_{fb,i}$ and the measured rejection approaches (real) membrane rejection. The expression for membrane rejection is defined by

$$Rejection_{fm,i} = \lim_{\omega \to \infty} Rejection_{fb,i}(\omega_S) \qquad 19$$

Assuming that the membrane rejection is constant for the investigated concentration range of component i in one solvent; at the applied transmembrane pressure and temperature the Sherwood correlation coefficients (A, B, C) can be estimated from experimental data by applying equations 5 and 20.

$$\frac{k_{sf,i}(\omega_{mS}) \cdot r}{D_i} = A \cdot (Re_S(\omega_{mS}))^B \cdot Sc^C \qquad 20$$

3.5.2 Experimental results for estimation of coefficients of the Sherwood correlation for the EMET stirred cell

Filtration experiments with ONF-2 membrane from GMT Membrantechnik were performed with docosane/heptane and docosane/toluene mixtures at two pressures at different magnetic stirrer velocities, hence at different intensities of the concentration polarization phenomenon.

The investigated EMET stirred cell given in Figure 10, was equipped with a high pressure pump (1.1 kg·h^{-1}) and an external feed tank. Both retentate and permeate stream were redirected into the feed tank. With this modification, it was possible to

run longer experiments with fast permeating solvents and make the estimation of coefficients A, B and C in a steady-state operation. The scheme of the modified set-up is given in Figure 15.

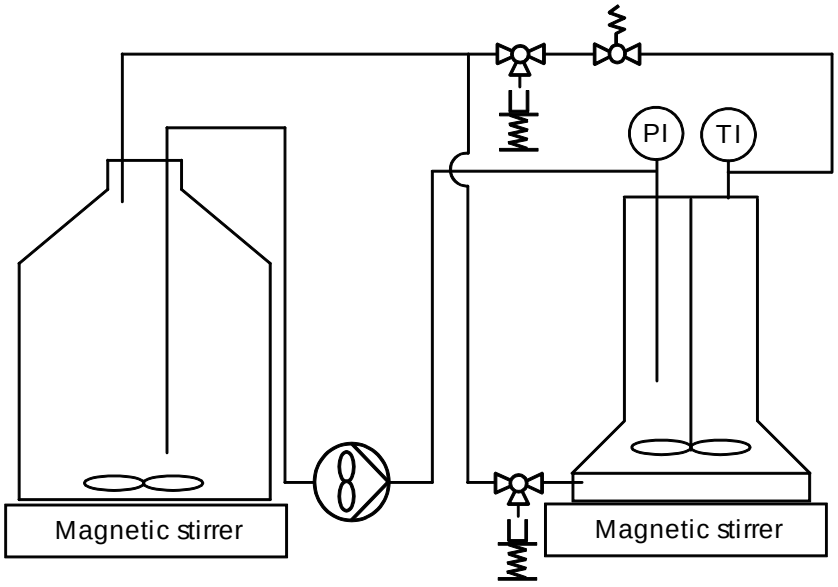

Figure 15: Scheme of EMET stirred filtration cell equipped with pump and external feed tank.

The concentration of docosane in heptane and toluene was 1.1 ± 0.1 g·L^{-1}. The experiments were made at 20 bar and 30 bar for each mixture at room temperature. The stirrer of the used setup was driven by a magnetic stirrer plate. The experiments were performed at a magnetic stirrer rotational speed between 0 and 625 rounds per minute.

The estimation of coefficients A, B and C was done for experimental data with a stirrer rotational speed between 100 and 625 rounds per minute assuming that above 100 rounds per minute the effect of the turbulence of the introduced pump can be neglected. The measured rejection without stirring was very low (see Figure 16 and Figure 17), indicating that the formed concentration polarisation layer was not affected by the feed pump flow.

For the evaluation of the experimental results, the diffusion coefficient of docosane was required. For the calculation of the diffusion coefficient of docosane in heptane the Hayduk and Minhas correlation for normal paraffin solutions [6, 7] was chosen (see equations 21 and 22).

$$D_{i,j} = 13.3 \cdot 10^{-8} \frac{T^{1.47} \cdot \eta_j{}^{\kappa}}{V_i^{mol\ 0.71}} \qquad 21$$

$$\kappa = \frac{10.2}{V_i^{mol}} - 0.791 \qquad 22$$

Where $D_{i,j}$ is diffusion coefficient in $cm^2 \cdot s^{-1}$, T is temperature in K, η_j is solvent viscosity in cP and V_i^{mol} is the molar volume of the solute in $cm^3 \cdot mol^{-1}$.

For the diffusion coefficient of docosane in toluene the Hayduk and Minhas correlation for nonaqueous solutions was applied [7] as shown by equation 23.

$$D_{i,j} = 1.55 \cdot 10^{-8} \frac{\left(V_j^{mol}\right)^{0.27}}{\left(V_i^{mol}\right)^{0.42}} \frac{T^{1.29}}{\eta_j{}^{0.92}} \frac{\gamma_j{}^{0.125}}{\gamma_i{}^{0.105}} \qquad 23$$

The diffusion coefficient ($D_{i,j}$) is given in $cm^2 \cdot s^{-1}$, the temperature (T) is given in K, the solvent viscosity (η_j) in cP. Molar volumes (V_i^{mol} and V_j^{mol}) are given in $cm^3 \cdot mol^{-1}$ and surface tension values (γ_i and γ_j) in $mN \cdot m^{-1}$.

The estimation of Sherwood coefficients was made by applying Microsoft Excel Solver function and minimising the average absolute difference between measured and rejection values calculated by the mathematical model. The variables set in the solver function are model coefficients A, B and C, and four specific membrane separation properties: real membrane rejection of docosane in heptane at 20 bar and 30 bar and real membrane rejection of docosane in toluene at 20 bar and 30 bar. The resulting Sherwood expression for the EMET stirred cell is presented in

equation 24.

$$Sh_i = \frac{k_{sf,i} \cdot r}{D_i} = A \cdot Re_s^B \cdot Sc^C \qquad 24$$

$A=0.0117$

$B=0.845$

$C=0.349$

The calculated docosane concentration range on the membrane surface was between 1.2 $g \cdot L^{-1}$ to 2.1 $g \cdot L^{-1}$, thus supporting the hypothesis of constant membrane rejection for a highly diluted mixtures.

Figure 16 and Figure 17 show measured rejections, real membrane rejection given and rejection values calculated by the mathematical model with the estimated parameters.

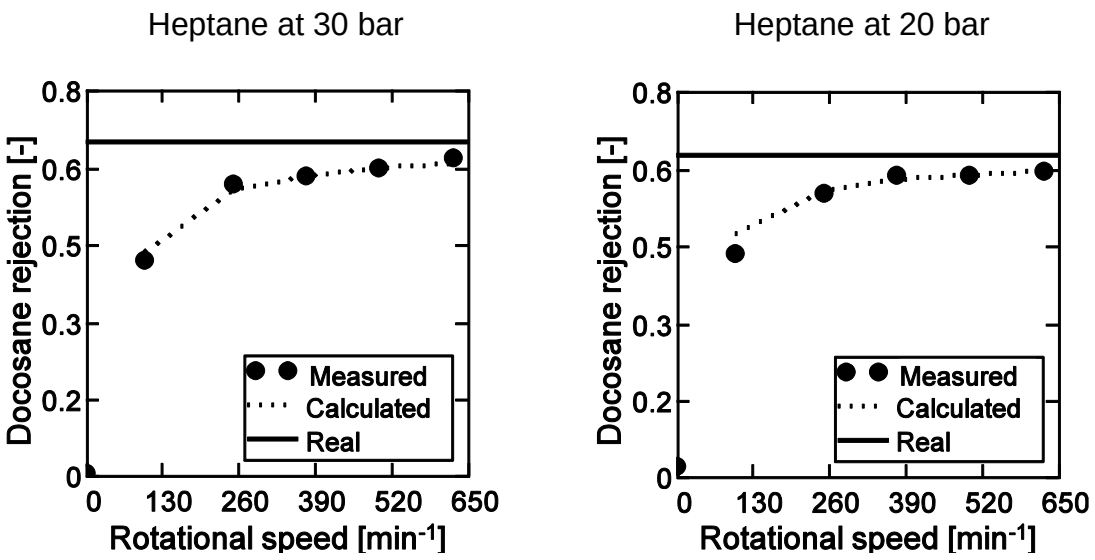

Figure 16: Measured rejections (●), estimated real membrane rejection (-) and rejections calculated by the Sherwood correlation with estimated parameters (···) of docosane in heptane at different magnetic stirrer velocities.

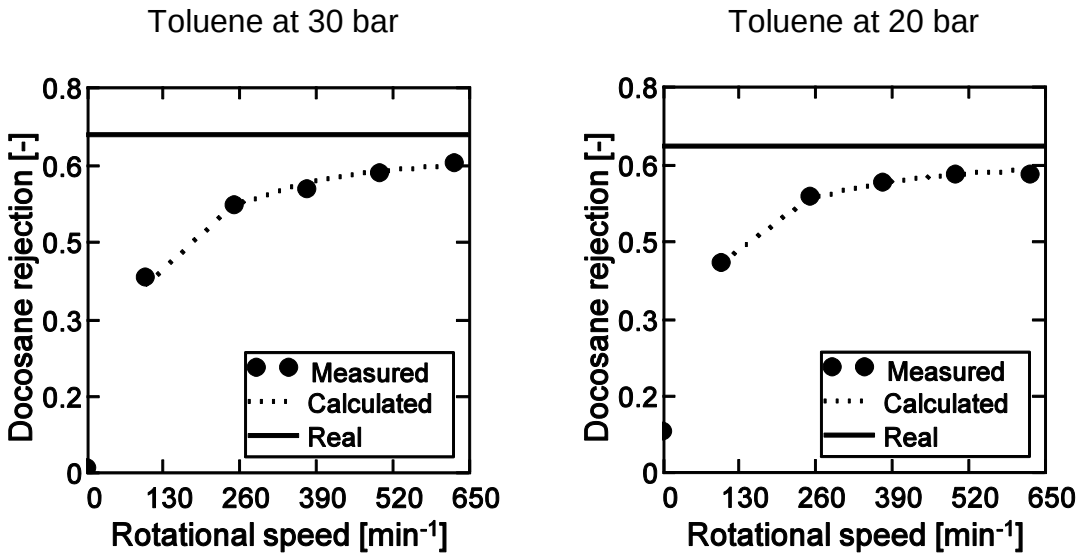

Figure 17: Measured rejections (●), estimated real membrane rejection (-) and rejections calculated by the Sherwood correlation with estimated parameters (···) of docosane in toluene at different magnetic stirrer velocities.

The derived Sherwood correlation with estimated parameters specific for the EMET stirred cell could accurately represent the measured rejections at different stirrer velocities of docosane in heptane and in toluene at 20 bar and 30 bar with

the assumption of constant membrane rejection in a solvent at a defined filtration pressure and temperature.

In the following, the obtained Sherwood correlation for EMET stirred cell was further applied to correct the measured rejections in diluted styrene oligomer/solvent mixtures which were used to investigate the mass transport through the silicone based membrane.

3.6 Styrene oligomer series

Styrene oligomer series were obtained by mixing of 2,4-diphenyl-4-methyl-1-pentene (α-methylstyrene dimer) with 97% purity (Aldrich Chemistry), polymer standard polystyrene PS580 and polystyrene standard PS1000 (Varian). According to supplier information for polystyrene standards, styrene oligomers have n-butyl end groups. Therefore, the molecular weight of individual oligomers was calculated using the structural formula given in Figure 18.

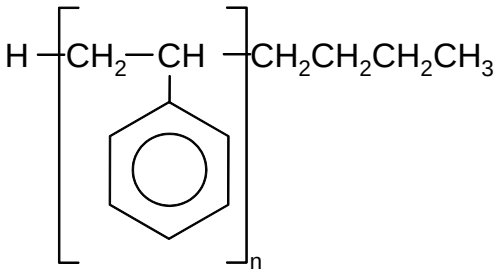

Figure 18: Structural formula of polystyrene standard from Varian.

The α-methylstyrene dimer has the following structural formula:

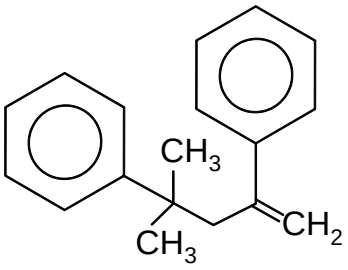

Figure 19: Structural formula of α-methylstyrene dimer from Aldrich Chemistry.

The density of α-methylstyrene dimer was given by Aldrich specification as 0.99 $kg \cdot dm^{-3}$ at 25 °C.

3.6.1 HPLC analytics of styrene oligomer series

As suggested in literature [8], for all styrene oligomer samples a solvent swap was performed and the samples consequently analysed using HPLC (Shimadzu Corporation) with a diode array detector.

Separation of styrene oligomers was achieved with a reverse phase column Nucleodur C18 Pyramid, 5 µm (250 x 4 mm) and eluent tetrahydrofuran/water (THF:H2O 65:35 vol.%) and additional 0.1 vol.% trifluoroacetic acid (TFA) on top. HPLC operation parameters used are 1 mL/min flow rate, 50 µL injection volume, 45 °C oven temperature and UV chromatogram output at 264 nm.

3.6.2 Calibration of styrene oligomer analytics

Using relative peak surfaces of a HPLC chromatogram of pure polystyrene standard PS580 a weight averaged molecular weight of approximately 580 $g \cdot mol^{-1}$ was calculated. This confirmed that the measured peak surface is directly proportional to the mass concentration of each oligomer.

The developed HPLC method was calibrated using dilution series of polystyrene

standard PS580 and peak surfaces of each oligomers (“Since the UV detector is sensitive to the number of light-absorbing phenyl rings units in the oligomer” [9]). The obtained calibration curve based on peak surface and mass concentration is identical for all oligomers as given in Figure 20.

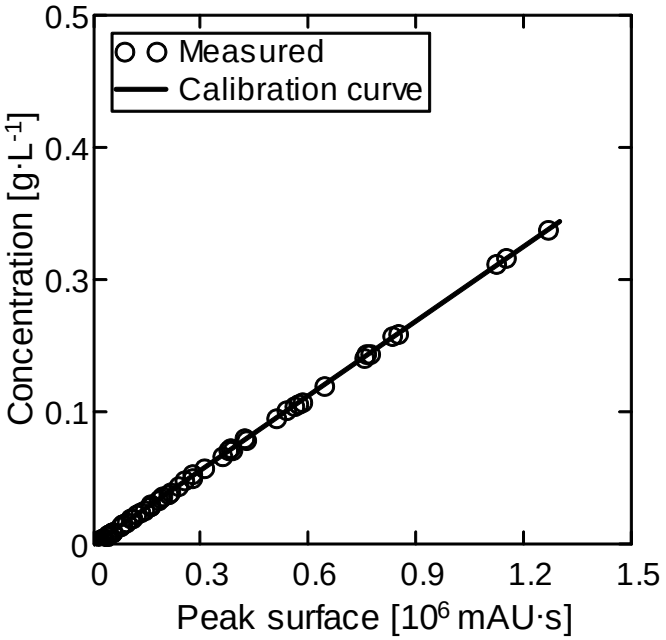

Figure 20: HPLC calibration line of styrene oligomers.

Since the absolute peak surface is used (Absorption Units in time - mAU·s), the obtained calibration curve is fixed to the injection volume of 50 µL. The concentration in $g \cdot L^{-1}$ can be obtained by equation 25.

$$c_i = 2.35 \cdot 10^{-7} \cdot \textit{Peak surface} \qquad 25$$

The calibration of α-methylstyrene dimer could be made with the pure substance (see Figure 21).

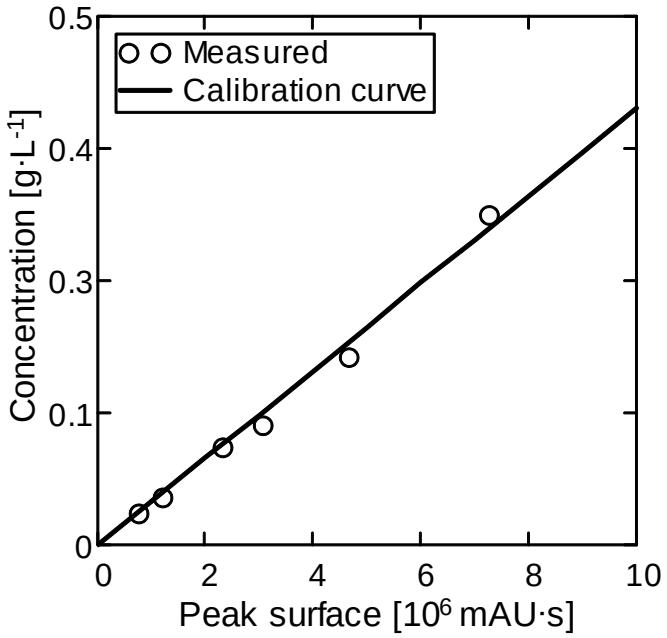

Figure 21: HPLC calibration line of styrene oligomers.

The α-methylstyrene dimer calibration curve for injection volume of 50 µL and absolute peak surface is given in equation 26.

$$c_i = 4.12 \cdot 10^{-8} \cdot \textit{Peak surface} \qquad 26$$

3.6.3 Density and volume fraction of styrene oligomers

For evaluation of concentration polarisation in the performed filtration experiments, molar volumes and diffusion coefficients of all oligomers are needed. The liquid molar volumes at 298 K of styrene oligomers were estimated by using the Constantinou and Gani group contribution method [10]. The estimated liquid mass densities of styrene oligomers were compared to density data of crystalline polystyrene ($n \to \infty$) and hexylbenzene ($n = 1$) as shown in Figure 22.

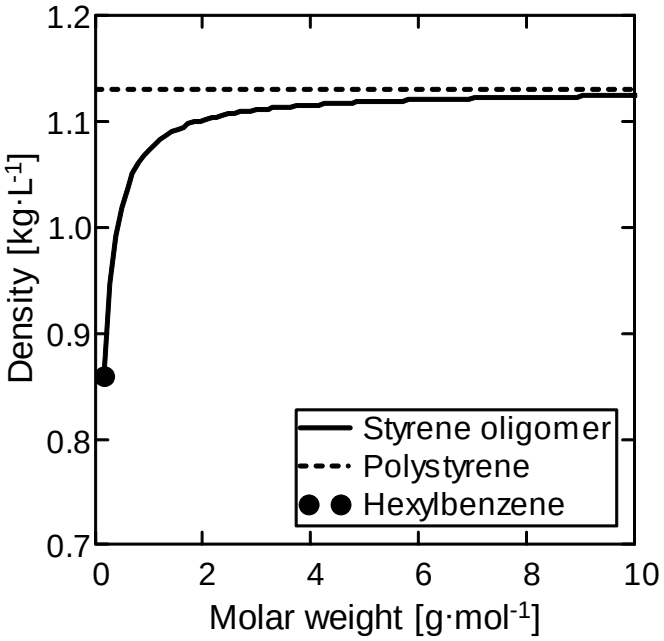

Figure 22: Predicted densities of styrene oligomers in comparison with the densities of crystalline polystyrene and hexylbenzene.

If additivity of molar volume is assumed, the volume fraction of the styrene oligomer in the mixture can be calculated using equation 27.

$$\phi_i = c_i \frac{V_i^{mol}}{Mw_i} \qquad 27$$

Where c_i is the measured mass concentration of the styrene oligomer in g·L^{-1}, Mw_i is the molar weight of styrene oligomer in g·mol^{-1} according to the formula given in Figure 18 and V_i^{mol} are the estimated liquid molar volumes of styrene oligomer in dm^3·mol^{-1}.

3.6.4 Diffusion coefficients of styrene oligomers

The Nakanishi correlation given by equation 28 was chosen for the prediction of the styrene oligomer diffusion coefficients ($D_{i,j}$) in liquids at infinite dilution in cm^2·s^{-1}. The Nakanishi correlation has a good predictive accuracy for solvents used in this

work and requires unlike other correlations the styrene oligomer molar volume at 298 K.

$$D_{i,j} = \left(\frac{9.97 \cdot 10^{-8}}{\left(I_i \cdot V_i^{mol} \right)^{1/3}} + \frac{2.40 \cdot 10^{-8} \cdot A_j \cdot S_j \cdot V_j^{mol}}{I_i \cdot S_i \cdot V_i^{mol}} \right) \frac{T}{\eta_j} \qquad 28$$

Where factors I_i, S_i, S_j and A_j are corrections for nonidealities and V_i^{mol} and V_j^{mol} are molar volumes in $cm^3 \cdot mol^{-1}$, for solute and solvent, respectively. The solvent viscosity (η_j) is given in cP at system temperature T in K [7]. Taking the estimated liquid molar volumes at 298 K of styrene oligomers and assuming Nakanishi factors for the styrene oligomers to be equal to 1, diffusion coefficients of styrene oligomers at infinite dilution in toluene and cyclohexane could be calculated. The predicted diffusivities for styrene oligomers at infinite dilution at 25 °C and measured literature data in toluene at 20 °C and cyclohexane at 34.5 °C [11] are given in Figure 23.

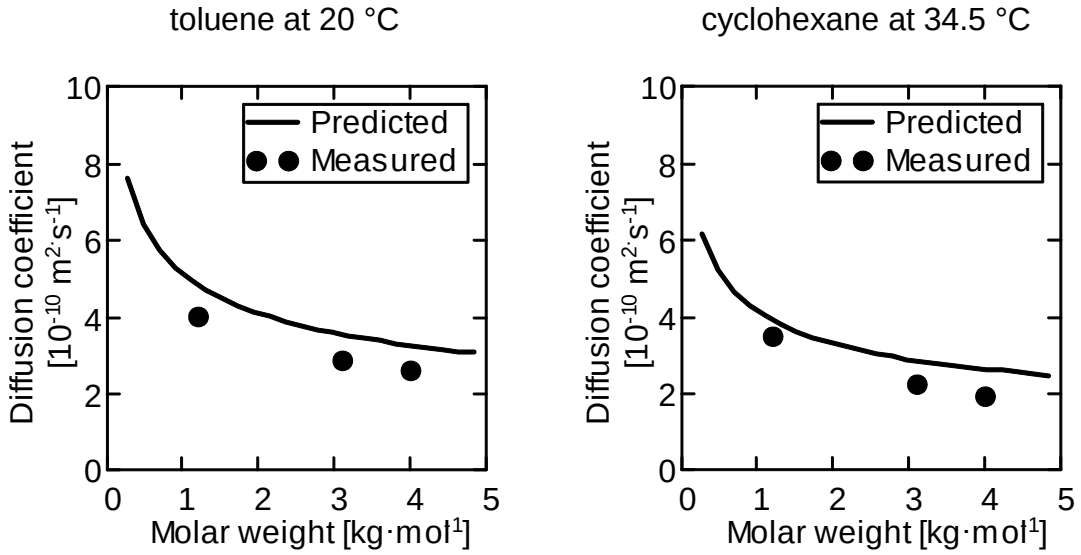

Figure 23: Diffusion coefficients of styrene oligomers: predicted by Nakanishi correlation and measured literature data in toluene at 20 °C and cyclohexane at 34.5°C (taken from [11]).

3.7 List of symbols

A_m	active membrane surface	m^2
c_i	mass concentration	$g \cdot L^{-1}$
D_i	diffusion coefficient of component i	$m^2 \cdot s^{-1}$, $cm^2 \cdot s^{-1}$
$D_{i,j}$	diffusion coefficient of component i in component j	$m^2 \cdot s^{-1}$, $cm^2 \cdot s^{-1}$
d_{hyd}	hydrodynamic diameter	m
H	feed channel height	m
I_i, S_i, S_j, A_j	Nakanishi nonlinearity factors for component i in component j	-
J_p	permeate volumetric flux	$m \cdot s^{-1}$
$k_{sf,i}$	mass transfer coefficient of component i in the boundary layer	$m \cdot s^{-1}$
L	feed channel length	m
M	permeate mass flux	$kg \cdot s^{-1} \cdot m^{-2}$, $kg \cdot h^{-1} \cdot m^{-2}$
m	mass	kg
$\dot{m}$	mass flow	$kg \cdot h^{-1}$
Mw_i	molar weight of component i	$g \cdot mol^{-1}$
n	number of monomer units	-
Pe	Peclet number	-
Δp	transmembrane pressure	Pa, bar
r	radius of membrane cell	m
Re	Reynolds number	-

Re_s	stirrer Reynolds number	-
$\overline{Re_p}$	average Reynolds number for permeate	-
Sc	Schmidt number	-
Sh	Sherwood number	-
T	absolute temperature	K
t	time	s, h
v	average feed cross-flow velocity	$m \cdot s^{-1}$
V_i^{mol}	liquid molar volume of component i	$cm^3 \cdot mol^{-1}$
w_i	mass fraction of solvent i	-
x	distance to membrane surface	m

Greek symbols

γ_i	surface tension of component i	$mN \cdot m^{-1}$
η_i	dynamic viscosity of component i	Pa·s
ρ	mass density	$kg \cdot m^{-3}$, $kg \cdot dm^{-3}$
ρ_i	solvent mass density	$kg \cdot m^{-3}$
ρ_{PDMS}	PDMS mass density	$kg \cdot m^{-3}$
$\phi_{fb,i}$	volume fraction of component i in the bulk feed	-
$\phi_{fm,i}$	volume fraction of component i in the bulk feed in the feed near the membrane surface	-
$\phi_{p,i}$	volume fraction of component i in the permeate	-

ω	average radial velocity of feed	rad·s^{-1}
ω_s	radial velocity of a stirrer	rad·s^{-1}
ω_{ms}	radial velocity of a magnetic stirrer	rad·s^{-1}

3.8 References

[1] M. Mulder, *Basic Principles of Membrane Technology*, 2nd ed., Kluwer Academic Publisher 1996.

[2] T.K. Sherwood, P.L.T. Brian, R.E. Fisher, L. Dresner, *Salt Concentration at Phase Boundaries in Desalination by Reverse Osmosis*, Industrial & Engineering Chemistry Fundamentals 4 (1965) 113-118.

[3] T. Melin, R. Rautenbach, *Membranverfahren: Grundlagen der Modul- und Anlagenauslegung*, 3rd ed., Springer 2010.

[4] E. Lyster, Y. Cohen, *Numerical study of concentration polarization in a rectangular reverse osmosis membrane channel: Permeate flux variation and hydrodynamic end effects*, Journal of Membrane Science 303 (2007) 140-153.

[5] S.T. Johnston, K.A. Smith, W.M. Deen, *Concentration polarization in stirred ultrafiltration cells*, AIChE Journal 47 (2001) 1115-1125.

[6] W. Hayduk, B.S. Minhas, *Correlations for prediction of molecular diffusivities in liquids*, The Canadian Journal of Chemical Engineering 60 (1982) 295-299.

[7] B.E. Poling, J.M. Prausnitz, J.P. O'Connell, *The Properties of Gases and Liquids* 5th Edition ed., McGraw-Hill 2000.

[8] Y.H. See Toh, X.X. Loh, K. Li, A. Bismarck, A.G. Livingston, *In search of a standard method for the characterisation of organic solvent nanofiltration membranes*, Journal of Membrane Science 291 (2007) 120-125.

[9] M.C. Piton, R.G. Gilbert, B.E. Chapman, P.W. Kuchel, *Diffusion of oligomeric species in polymer solutions*, Macromolecules 26 (1993) 4472-4477.

[10] L. Constantinou, R. Gani, *New group contribution method for estimating properties of pure compounds*, AIChE Journal 40 (1994) 1697-1710.

[11] K. Huber, S. Bantle, P. Lutz, W. Burchard, *Hydrodynamic and thermodynamic behavior of short-chain polystyrene in toluene and cyclohexane at 34.5.degree.C*, Macromolecules 18 (1985) 1461-1467.

4 Comparison of different OSN membranes

Polymeric membranes produced for organic solvent nanofiltration (OSN) applications, similar to nanofiltration membranes for water applications, can be divided into composite and integrally skinned asymmetric membranes. For composite asymmetric membranes the separation layer is a homogenous polymer layer which is supported by a porous structure of a second polymer matrix, whereas an integrally skinned asymmetric membranes separation layer and porous support are made out of one polymer. Both types of membranes are backed by a non-woven fabric to give additional mechanical stability to the final membrane structure. The schematic structures of composite and asymmetric nanofiltration membranes are given in Figure 24.

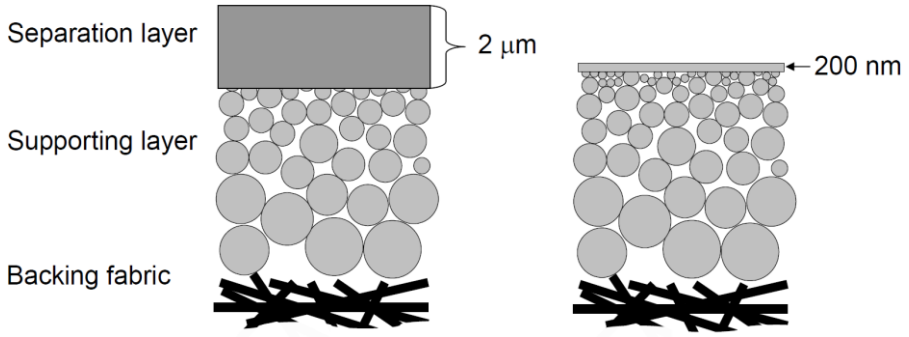

Figure 24: Schematic structures of composite and integrally skinned asymmetric OSN membranes.

The membrane separation of two components is achieved by the difference in transport velocities caused by difference in sorption of the two components and/or difference in diffusion coefficients of the components in the separation layer. Consequently, different polymers and polymer morphologies result in different separation performance. Due to this reason an experimental comparison of a silicone based composite membrane, a PIM (polymers of intrinsic microporosity) composite

membrane and integrally skinned polyimide based membrane is given.

4.1 Polymers for OSN membranes

A highly crosslinked poly(dimethylsiloxane), a rubbery state polymer at room temperature, was often reported in the literature for the production of silicone based membranes for OSN applications [1, 2]. It was assumed that the separation layer of the commercial silicone membrane ONF-2 provided by GMT Membrantechnik is also a highly crosslinked poly(dimethylsiloxane) [3]. The structural formula of a dimethylsiloxane monomer unit is shown in Figure 25.

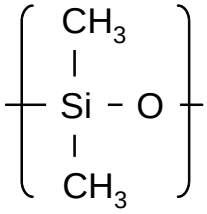

Figure 25: Structural formula of a dimethylsiloxane monomer unit.

The composite membranes based on a PIM separation layer for organic solvent nanofiltration are in general in an academic stage of development [4, 5]. The structural formula of a PIM-1 monomer unit is given in Figure 26. The PIM material, an amorphous glassy state polymer at room temperature, consists of a rigid molecular structure which cannot efficiently pack in the solid state, resulting in very high free volume of this glassy polymer [6].

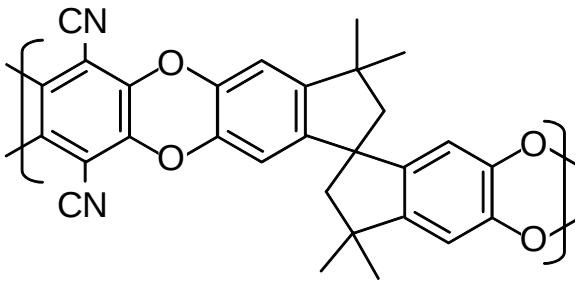

Figure 26: Structural formula of PIM-1 monomer unit, taken from [4].

The integrally skinned asymmetric membranes made by phase inversion process, have been first developed by Loeb and Sourirajan [7]. For the production of integrally skinned OSN membranes, both, solvent stability and polymer processability are important properties [8].

Commercial solvent stable polyimides: P84® and Matrimid® are amorphous glassy polymers at room temperature and have been used to produce membranes for OSN applications [9]. To increase the polymer stability the polyimide membranes made by phase inversion can also be additionally crosslinked [10-13]. Such highly solvent stable membranes are the DuraMem® membrane series provided by EMET [14]. The DuraMem® membranes are formed out of polyimide P84® dope solutions by phase inversion process and are then treated by amine crosslinking agent [13].

The general formula of monomers of P84® polyimide are shown in Figure 27 [15].

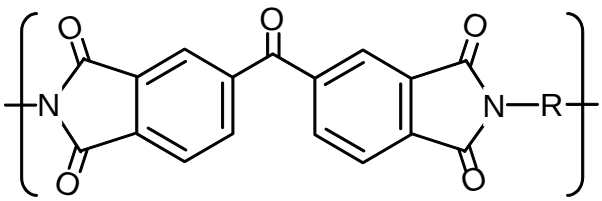

R=

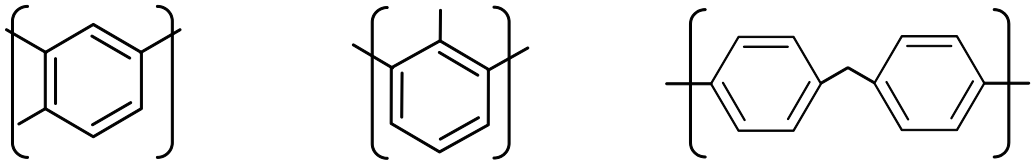

Figure 27: Structural formula of polyimide P84® monomer units, taken from [15].

4.2 Experimental

4.2.1 Swelling experiments

The preferential sorption of a component in the membrane polymer influences the membrane separation properties. Acetone and heptane were chosen because of their difference in polarities and similar viscosities. Dispersion, polar and hydrogen bonding Hansen solubility parameters (see definition in Chapter 5) are given together with other solvent properties in Table 1 [16, 17].

Table 1: Hansen solubility parameters, molar volume, surface tension and viscosity of acetone and heptane at 25 °C.

	δ^d	δ^p	δ^h	V_i^{mol}	γ_i	η_i
		[(MPa)$^{0.5}$]		[cm^3·mol^{-1}]	[mN·m^{-1}]	[mPa·s]
Acetone	15.5	10.4	7.0	74.0	22.72	0.308
Heptane	15.3	0	0	147.4	20.01	0.388

The poly(dimethylsiloxane) swelling experiments were made with eleven solvents. The experimental work with PDMS sheets is described in detail in Chapter 5.

The swelling experiments of P84 polymer sheets were made in heptane and acetone. The P84 polymer was provided by Evonik Industries AG. In order to have short diffusion paths for the solvent in the polymer sheet, 300 μm thick layers of 27 w. % of P84 in dimethylformamide were cast on a glass plate. The solvent was evaporated at 100 °C over night. The rest solvent was extracted in water, after which the polymer sheets were dried at 120 °C for 3 h. The produced polymer sheets with length l were further soaked in solvents (over 90 days) and the elongation of the polymer sheets was measured (Δl). Assuming isotropic swelling, the solvent volume fraction in the swollen polymer sheets was calculated using equation 29.

$$\phi_i = 1 - \left(\frac{l}{l + \Delta l} \right)^3 \qquad 29$$

The swelling results for PIM-1 in heptane and acetone were taken from literature [18].

The summarised values of volume fraction of acetone and heptane in PDMS, PIM-1 and P84 sheets are given in Table 2.

4.2.2 Filtration experiments

Filtration experiments were performed with ONF-2 (GMT Membrantechnik), PIM-1 and DuraMem500 (EMET) flat sheet membranes. For filtration experiments heptane and acetone in technical purity were used. Filtration experiments were performed in the cross-flow filtration rig at a pressure of 30 bar and a temperature of 30 °C. Previous to the styrene oligomer mixture the membranes were operated at given conditions with pure solvent for approximately 3 days. The styrene oligomer solution was made from solvent and approximately 2.1 $g \cdot L^{-1}$ of styrene oligomers (0.1 $g \cdot L^{-1}$ α- methyl styrene dimer, 1 $g \cdot L^{-1}$ polystyrene standard PS580, and 1 $g \cdot L^{-1}$ polystyrene standard PS1000). After the solvent was replaced by the styrene oligomer/solvent mixture the filtration was run for another 24 h, after which the samples of permeate and retentate were taken for analysis. The conditioning and sampling procedure were similar for all membrane samples.

From the measured styrene oligomer rejection results the membrane (real) styrene oligomer rejections were calculated by applying the Sherwood correlation for concentration polarisation for a rectangular channel [19]. The process flow diagram of the used filtration rig, the used analytical tools and complete set of concentration polarisation equations are given in Chapter 3.

4.3 Results and discussion

The measured solvent volume fractions for PDMS and P84 homogeneous polymer sheets, together with the literature data of PIM-1 [18] swelling are given in Table 2 together with the measured solvent permeabilities of the membranes produced from these materials.

The permeabilities of the rubbery silicone composite membrane ONF-2 (GMT Membrantechnik) and the glassy composite membrane PIM-1 are consistent with

the swelling degree of these polymers in solvents. Likewise, for the P84 polyimide the swelling behaviour has the same trend as the permeability of integrally skinned membrane DuraMem500 (EMET), made out of crosslinked P84.

Table 2: Acetone and heptane permeabilities of ONF-2, PIM-1 and DuraMem500 membranes and the solvent volume fractions in the sheets of corresponding polymers.

Membrane	Material	Geometry	Volume fraction [-]		Permeability [$L \cdot h^{-1} \cdot m^{-2} \cdot bar^{-1}$]	
			Acetone	Heptane	Acetone	Heptane
ONF-2	PDMS	composite	0.253	0.624	2.05	4.40
PIM-1	PIM-1	composite	0.394	0.353	18.24	3.06
DuraMem500	P84	asymmetric	0.143	0.012	1.72	0.08

The measured styrene rejection in acetone and heptane for the rubbery silicone composite membrane ONF-2 (GMT Membrantechnik), the glassy composite membrane PIM-1 and the integrally skinned DuraMem500 (EMET) are given as symbols, while the real membrane rejections corrected for a concentration polarisation are given as lines in Figure 28, Figure 29 and Figure 30, respectively.

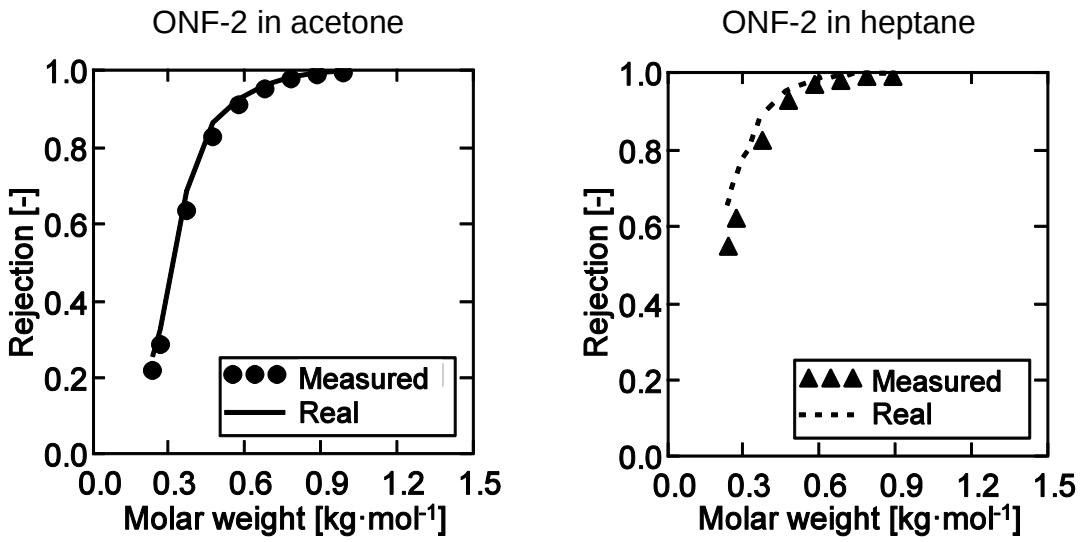

Figure 28: Measured rejection (●,▲) and real membrane rejection corrected for concentration polarisation effects (-, ···) of styrene oligomers for ONF-2 membrane in heptane and acetone.

For the rubbery silicone composite membrane ONF-2 a lower rejection of styrene oligomers in acetone compared to rejection of styrene oligomers in heptane can be observed in Figure 28. This can be explained by the reduced acetone permeability while the styrene oligomer transport is similar compared to the heptane mixture, resulting in the lower difference in the transport velocities between solvent and solute, hence in a lower rejection.

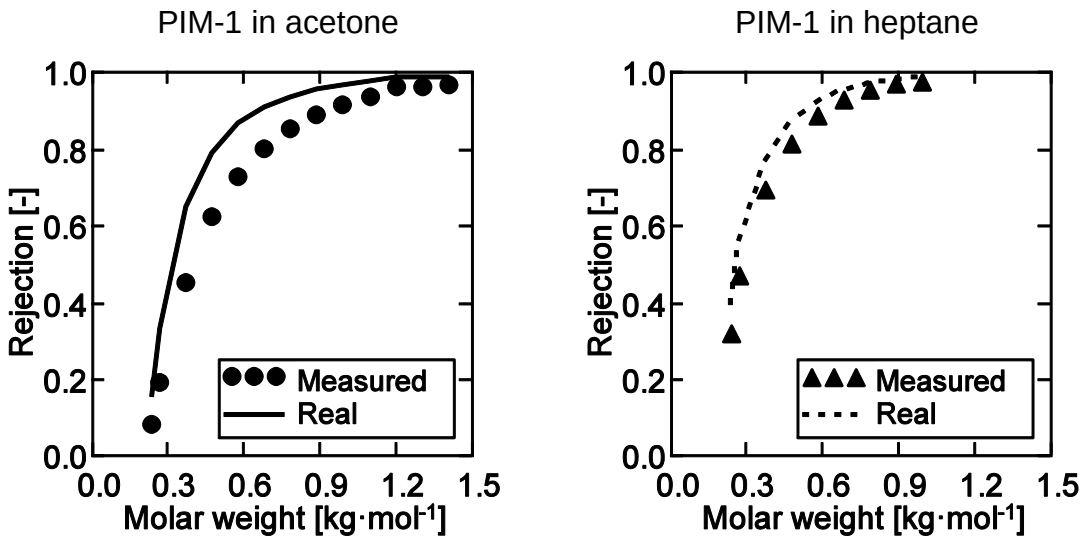

Figure 29: Measured rejection (●,▲) and real membrane rejection corrected for concentration polarisation effects (-, ···) of styrene oligomers for PIM-1 membrane in heptane and acetone.

In the case of the glassy composite membrane PIM-1 the measured rejection in acetone is much lower than for heptane (see Figure 29). Once the measured rejections in acetone were corrected for the concentration polarisation effects it can be observed that the real membrane rejection of PIM-1 in acetone is similar to the PIM-1 membrane rejection in heptane.

The styrene oligomer rejections in heptane and acetone for integrally skinned DuraMem500 are given in Figure 30.

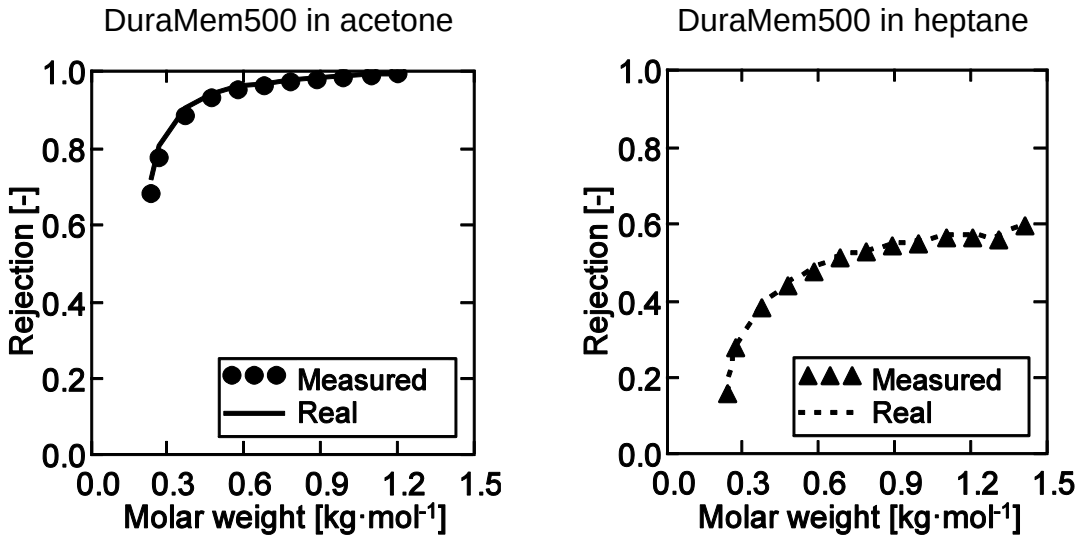

Figure 30: Measured rejection (●,▲) and real membrane rejection corrected for concentration polarisation effects (-, ···) of styrene oligomers for DuraMem500 membrane in heptane and acetone.

For the DuraMem500, crosslinked integrally skinned membrane made by phase inversion process, the rejection in acetone reaches the expected 95% for the styrene oligomer with 500 g/mol. When the same membrane sheet was tested in heptane as solvent, the flux was much lower and a maximal rejection of 58% was recorded. Concerning the morphology of this nanofiltration membrane it is not clear if the separation layer can be considered as homogeneous or as a porous structure.

If assumed that the separation layer of DuraMem500 is a dense layer, the low swelling of the membrane separation layer in heptane leads to low solvent permeability and no separation performance between styrene oligomers and heptane. The low rejection of larger styrene oligomers could then be explained by the existence of imperfections in the membrane separation layer.

Otherwise, if a fine porous structure of the membrane separation layer is assumed the adsorbed liquid film on the pore wall will influence the separation performance. Guizard et. al. discussed for ceramic membranes that the capillary pressure

is mostly defining penetration of a liquid in the membrane pores. But “In the presence of a meso- or microporous network, the disjoining pressure of wetting films cannot be neglected. Repulsive forces with aqueous or polar solvents yield in a positive contribution to the driving force whereas attractive (adhesive) forces encountered with non-polar solvents have a negative contribution.”[20] Expanding the discussion given by Guizard et. al. to the relatively polar surface of a crosslinked P84 integrally skinned membrane [11, 21] can lead to the interpretation, that the low heptane flux of DuraMem500 can be explained by low surface tension and the low polarity of heptane. Hence, heptane permeates mostly through the fractions of the pores which are larger than the average. For larger pores the sieving effect for styrene oligomer is lower, resulting in a low rejection.

4.4 Conclusion

From the presented data on styrene oligomer rejections by the rubbery silicone composite ONF-2, glassy composite PIM-1 and crosslinked integrally skinned P84 based membranes it can be seen that the PDMS combines both chemical stability and good performance in nonpolar and moderately polar organic solvents. The composite structure of the ONF-2 and PIM-1 membranes underlines the homogeneous polymer separation layer and gives the possibility to develop thermodynamic models to predict the membrane separation performance.

The glassy composite PIM-1 membrane has both, high fluxes and a good performance in heptane and acetone. The very large flux of the PIM-1 layer can lead to reduced system performance because of the concentration polarisation. The PIM-1 layer is not crosslinked. Hence it has limited stability in several industrially important organic solvents [18]. As reported, additional crosslinking of PIM-1 would simultaneously increase the chemical stability and reduce membrane permeability [4].

The crosslinked integrally skinned DuraMem500 has, as given in the recommendation of EMET, excellent performance in acetone as a polar organic solvent. Hence, DuraMem membranes have directly opposite application fields compared to PDMS based membranes [14]. The performance in nonpolar solvents, in this case heptane, resulted in a very low flux and rejection. The integrally skinned structure of the membrane makes it difficult to differentiate the separation layer and the supporting porous structure. Hence, the separation layer and its morphology cannot be easily described or modelled.

Because of the versatility of available PDMS materials, its good chemical stability and the successful application of this polymer material in organic solvent nanofiltration, PDMS still remains one of the most promising materials in the development of new optimised solvent stable membranes.

4.5 List of symbols

l	polymer sheet length	m
Δl	elongation of polymer sheet	m
V_i^{mol}	molar volume of component i	$cm^3 \cdot mol^{-1}$

Greek symbols

γ_i	surface tension of component i	$mN \cdot m^{-1}$
δ^d	dispersion Hansen solubility parameter	$(MPa)^{0.5}$
δ^p	dipole-dipole Hansen solubility parameter	$(MPa)^{0.5}$
δ^h	hydrogen bonding Hansen solubility parameter	$(MPa)^{0.5}$

ϕ_i	solvent volume fraction	-
η_i	solvent dynamic viscosity	mPa·s

4.6 References

[1] M. Schmidt, K.-V. Peinemann, N. Scharnagel, K. Friese, R. Schubert, *Silicone composite membrane modified by radiation-chemical means and intended for use in ultrafiltration*, WO1996027430, GKSS-Forschungszentrum Geesthacht GmbH, 1996.

[2] C. Linder, M. Nemas, M. Perry, R. Katraro, *Silicone-derived solvent stable membranes*, US5205934, Membrane Products Kiryat Weitzman Ltd., 1993.

[3] S. Zeidler, U. Kätzel, P. Kreis, *Systematic investigation on the influence of solutes on the separation behavior of a PDMS membrane in organic solvent nanofiltration*, Journal of Membrane Science 429 (2013) 295-303.

[4] D. Fritsch, P. Merten, K. Heinrich, M. Lazar, M. Priske, *High performance organic solvent nanofiltration membranes: Development and thorough testing of thin film composite membranes made of polymers of intrinsic microporosity (PIMs)*, Journal of Membrane Science 401–402 (2012) 222-231.

[5] P.M. Budd, B.S. Ghanem, S. Makhseed, N.B. McKeown, K.J. Msayib, C.E. Tattershall, *Polymers of intrinsic microporosity (PIMs): robust, solution-processable, organic nanoporous materials*, Chemical Communications (2004) 230-231.

[6] P.M. Budd, E.S. Elabas, B.S. Ghanem, S. Makhseed, N.B. McKeown, K.J. Msayib, C.E. Tattershall, D. Wang, *Solution-Processed, Organophilic Membrane Derived from a Polymer of Intrinsic Microporosity*, Advanced Materials 16 (2004) 456-459.

[7] S. Loeb, S. Sourirajan, *High flow porous membranes for separating water from saline solutions*, US3133132, University of California, 1964.

[8] M. Mulder, *Basic Principles of Membrane Technology*, 2nd ed., Kluwer Academic Publisher 1996.

[9] P. Vandezande, L.E.M. Gevers, I.F.J. Vankelecom, *Solvent resistant*

nanofiltration: separating on a molecular level, Chemical Society Reviews 37 (2008) 365-405.

[10] P. Vandesande, K. Vanherck, I.F.J. Vankelecom, *Crosslinked polyimide membranes*, WO2008138078, Katholieke Universiteit Leuven, Vandezande Pieter, Vanherck Katrien, Vankelecom Ivo, 2008.

[11] K. Vanherck, G. Koeckelberghs, I.F.J. Vankelecom, *Crosslinking polyimides for membrane applications: A review*, Progress in Polymer Science Article in press (2012).

[12] A.T. Boam, A.M.M. Miranda, A.G. Livingston, *Polyimide membrane*, EP2440314, Membrane Extraction Technology Ltd., 2012.

[13] A.G. Livingston, Y.H. See-Toh, *Asymmetric membranes for use in nanofiltration*, US20100038306 A1, Imperial Innovations Limited, 2010.

[14] Evonik Industries AG, *Membrane Properties - DuraMem® and PuraMem®*, (2008).

[15] H. Harms, M. Schobesberger, H. Sollradl, K. Weinrotter, *Process for providing a high-temperature resistant polyimide film*, US4871500, Lenzing AG, 1989.

[16] C.M. Hansen, *Hansen Solubility Parameters: A Users Handbook*, 2nd ed., CRC Press 2007.

[17] DECHEMA e.V., *DETHERM-Thermophysical Properties of Pure Substances & Mixtures* 2012, http://i-systems.dechema.de/detherm.

[18] K. Heinrich, *Polymere mit intrinsischer Mikroporosität – Membranmaterialien mit Zukunft?*, PhD Thesis, GKSS-Forschungszentrum Geesthacht GmbH, 2009.

[19] E. Lyster, Y. Cohen, *Numerical study of concentration polarization in a rectangular reverse osmosis membrane channel: Permeate flux variation and hydrodynamic end effects*, Journal of Membrane Science 303 (2007) 140-153.

[20] C. Guizard, A. Ayral, A. Julbe, *Potentiality of organic solvents filtration with ceramic membranes. A comparison with polymer membranes*, Desalination 147 (2002) 275-280.

[21] S.M. Dutczak, *Solvent resistant nanofiltation membranes*, PhD Thesis, University of Twente, 2011.

5 Solvent permeation through silicone-based membranes

As the industrial interest rises for the application of organic solvent nanofiltration (OSN) in production plants, the academic effort to develop predictive tools for solvent and solute transport gain on importance [1-4]. The membrane flux and the separation behaviour of OSN membranes are mostly determined experimentally with limited success in predicting these results. In the literature a large variety of models were formulated to correlate the permeability of the membrane with different solvent and membrane properties. Most of them use a solution-diffusion model in which the permeability depends on the ability of the solvent to sorb into the polymer and the solvent diffusion through the membrane in direction of the lower chemical potential at the permeate side. The deviations between the experimental data and values predicted by the solution diffusion models are regularly attributed to imperfections in the membrane and non-selective convective contributions to the membrane [1, 4-13].

Since, the chemical potential difference in the membrane is the driving force for membrane separation, an accurate prediction of solvent concentration in the membrane is crucial for the evaluation of mass transport through the membrane [14-16]. Here we start with a rigorous description using a predictive Flory-Rehner based approach to quantify the membrane swelling. To quantify the diffusive contribution to the permeation through the membrane a Maxwell-Stefan description is used and different methods to estimate the diffusion coefficient were compared.

5.1 Theoretical background

5.1.1 Solubility parameters

Hansen solubility parameters (HSP) have been successfully used to predict polymer-solvent compatibility [17]. A good solubility is expected when two substances have similar values of HSP. The three dimensional HSP are based on the assumption that cohesive intermolecular forces consist of dispersion, dipole-dipole and hydrogen-bonding forces (see equation 30).

$$\frac{E_i}{V_i^{mol}} = \left(\delta_i^d\right)^2 + \left(\delta_i^p\right)^2 + \left(\delta_i^h\right)^2 \qquad 30$$

Where E_i is the total cohesive energy density, V_i^{mol} is the molar volume, δ_i^d, δ_i^p and δ_i^h are dispersion, polar and hydrogen bonding Hansen solubility parameter, respectively. Even though HSP have a thermodynamic meaning for most substances, the HSP are determined empirically with only limited accuracy [17, 18]. The HSP are obtained by plotting a large number of experimental solubility data for one component into a three dimensional plot and determining the centre of the solubility sphere as HSP values of the investigated component.

Additional to HSP, the molar volume of a solvent influences the solubility behaviour. It was observed that smaller molecules have better solubility power than comparable larger molecules. Zellers et. al. [18] investigated alternative approaches in determining HSP for polymers, by weighting the HSP of solvents, for example with the volume factions of solvent (ϕ_i) in the polymer/solvent mixture. The equation of volume averaged HSP is given by equation 31.

$$\delta = \frac{\sum\left(\frac{\phi_i}{1-\phi_i} V_i^{mol} \cdot \delta_i\right)}{\sum\left(\frac{\phi_i}{1-\phi_i} V_i^{mol}\right)} \qquad 31$$

The Zellers et. al. expression is valid for dispersion as well as polar and hydrogen bonding HSP. Next to the weight averaged HSP, Zellers et. al. estimated the HSP using a modified Flory-Rehner equation for the calculation of the activity coefficient of a solvent in a polymer. In the case of two butyl and natural rubber materials, negative values of partial HSP were obtained [18]. Beerbower and Dickey [19] and Zellers et. al. [18] discussed that the HSP can be regarded as empirical parameters, which helps to predict the thermodynamic behaviour of polymers. Likewise, Hansen states that it would be more appropriate to consider HSP as free energy parameters, which represent all free energy effects other than the combinatorial entropy of solution [17]. Hence, HSP include other effects than enthalpy and can also have negative values. For example, the negative values have been reported in the literature for several polyolefines, a polyamide, an amino resin and an acrylic compound [17].

Efforts have been made in expanding the HSP approach to predict membrane performance [20-24]. Additionally, HSP are used in combination with the Flory-Huggins equation to predict polymer swelling in multicomponent mixtures [25]. Following up on Flory-Huggins/HSP approach to predict membrane separation, we first present a short discussion on the Flory-Rehner (Huggins) model, in particular the assumptions made within and the applicability of this model to predict PDMS swelling will be given.

Then we extend the Flory-Huggins theory to incorporate elastic strain corrections (Flory-Rehner) to the free energy together with HSP estimations of the enthalpy interaction parameter. This Flory-Rehner/HSP model is formulated in such way that

the swelling of a free standing polymer film as well as a polymer film attached to the surface can be described. The Flory-Rehner/HSP model is further used with a Maxwell-Stefan diffusion model to predict membrane permeability. The detailed derivation of Flory-Rehner/HSP model and Maxwell-Stefan diffusion model models is given in Appendix.

5.1.2 Consideration on Flory-Rehners' approach

The Flory-Rehner equation has been long used to predict the concentration of the solvents inside polymer networks. It comprises three free energy terms: entropy, enthalpy and elasticity as given by equation 32 [26-28]. The Flory-Huggins equation can be obtained from Flory-Rehner equation by neglecting the elastic chemical potential contribution term.

$$\frac{\mu_i}{R\cdot T}=\frac{\mu_i^{mix,entropy}}{R\cdot T}+\frac{\mu_i^{mix,enthalpy}}{R\cdot T}+\frac{\mu_i^{elastic}}{R\cdot T} \quad with$$

$$\frac{\mu_i^{mix,entropy}}{R\cdot T}=\ln(\phi_i)+1-\phi_i$$

$$\frac{\mu_i^{mix,enthalpy}}{R\cdot T}=\chi_{i,m}(1-\phi_i)^2 \qquad 32$$

$$\frac{\mu_i^{elastic}}{R\cdot T}=\frac{V_i^{mol}}{V_{m,monomer}^{mol}}\frac{Mw_{monomer}}{Mw_c}\left(1-\frac{2\cdot Mw_c}{Mw_o}\right)\left(\phi_m{}^{1/3}-\frac{\phi_m}{2}\right)$$

Where μ_i is the total chemical potential of component i in the mixture, R is the universal gas constant and T the absolute temperature of the mixture. $\mu_i^{mix,entropy}$, $\mu_i^{mix,enthalpy}$ and $\mu_i^{elastic}$ are the chemical potential contribution terms of mixing entropy, mixing enthalpy and elastic contribution due to swelling of the polymer network, respectively. In the chemical potential contribution of mixing enthalpy figures

the Flory-Huggins interaction parameter $\chi_{i,m}$. The elastic chemical potential contribution includes the molar weight of monomer unit ($Mw_{monomer}$), monomer molar volume ($V_{m,monomer}^{mol}$), the molar weight of subchains between two crosslinks (Mw_c), the molar weight of oligomer before crosslinking (Mw_o) and ϕ_m the volume fraction of the membrane polymer in the mixture.

In the Flory-Huggins theory the interaction parameter ($\chi_{i,m}$) determines an energetic interaction between solvent molecule and monomer and it is assumed to be constant. In the model derivation, the Flory-Huggins interaction parameter contains several parameters as given by

$$\chi_{i,m} = \frac{1}{Z'}\left(1 - \frac{V_i^{mol}}{V_{m,monomer}^{mol}}\right) + \frac{V_i^{mol}}{R \cdot T}\left(\delta_i^t - \delta_m^t\right)^2$$

$$Z' = \frac{Z_{polymer}}{\left(\frac{V_{m,monomer}^{mol}}{V_i^{mol}} - 1\right)(1 - f_0)} - \frac{2 \cdot f_0}{1 - f_0} \quad , \qquad 33$$

where $Z_{polymer}$ is the polymer lattice coordination number, $V_{m,monomer}^{mol}$ monomer molar volume and δ_m^t and δ_i^t are Hildebrand solubility parameters of the monomer unit and of the solvent, respectively. The f_0 ($f_0 << 1$) parameter is the probability "that the site is occupied by a polymer segment of a chain being placed [15]" [26-28].

The thermodynamic foundation and this simple mathematical form of the Flory-Huggins equation are the biggest advantages of the model. Even though it has been successfully applied for many polymer systems it had only limited success in describing systems with higher non-ideality. The assumptions made in the derivation of this theory are often analysed to explain the failure of the Flory-Huggins or Flory-Rehner expressions in predicting concentration of weak solvents in the PDMS network [29] and are stated as follows:

- Does not account for the probability of overlapping chains.
- Does not account for volume change upon mixing.
- Does not account for local composition variations (e.g. cluster formation) caused by differences in intermolecular forces.
- Assumes that all of the lattice sites are filled.
- Does not account for free volume differences between polymer and solvent molecules.

Further developments on the Flory-Huggins theory which included the influence of the free volume difference between polymer and solvent resulted in a group of the free volume activity coefficient models [29]. PDMS is an exceptionally loose polymer structure, where its free volume percentage ranges the free volume of the organic solvents. Therefore the free volume consideration had a low impact on predicting PDMS swelling [30].

Other thermodynamic descriptions such as UNIFAC models can only predict with difficulty PDMS swelling in weak solvents [31] or solvent mixtures [32]. A comparison between Flory-Huggins (Rehner) and other methods to predict PDMS swelling can be found elsewhere [31, 33-35].

5.1.3 Application of Flory-Huggins theory on membrane separation layer

Flory-Huggins theory has been applied to many solvent/PDMS mixtures, hence a large number of interaction parameters are available in the literature [36]. A more accurate prediction of PDMS swelling with Flory-Huggins model was made by including a concentration dependence of the solvent/PDMS interaction parameters [37-41]. The correlations describing the concentration dependence of the interaction

parameters are mostly empirical expressions of second order polynomial functions of solvent volume fraction [37, 42], potential functions of volume fraction [42] or simple power law approaches [43]. Further optimisation in this direction was made in postulating a more thermodynamically based correlation for the interaction parameter dependence on the solvent concentrations [44].

Bitter [15] addressed the non-ideality of a polymer lattice when different shaped molecules are introduced. He added a correction for the coordination number Z, which only effects the entropy contribution of the original Flory-Huggins expression. He could find correlations for different solvent groups and polyolefins, which could predict the change of the coordination number of the lattice. In a multicomponent mixture Bitter suggested to use a ratio of the pure solvent coordination number and the volume averaged coordination number of the whole mixture. With the changes introduced to the Flory-Huggins expression, Bitter showed only moderate success in predicting the swelling of polypropylene in a certain range of solvents [15].

Favre et. al. focused on the application of the Flory-Huggins theory to solvent swelling of PDMS [45]. He reports some success of the Flory-Huggins equation in describing PDMS/solvent mixtures for good and moderate solvents, but the model fails in the case of weak solvents [46]. Favre et. al. identified the two most sensitive parameters of the Flory-Huggins equation: the interaction parameter of weak solvent/good solvent and the interaction parameter of weak solvent/membrane. The authors discussed the phenomena of solvent cluster formation inside the PDMS network [47]. Solvent clustering is expected when a large interaction energy difference between solvent-solvent and solvent-polymer segment molecules occurs. The bulk phase of several solvents inside the PDMS network could also be experimentally proven by differential scanning calorimetry [48-50]. The cluster formation influences both, entropy and enthalpy contributions of the Flory-Huggins expression [45]. Likewise, the presence of solvent clusters influences the mass transport of the

solvent through the polymer network. Favre et. al. further developed an empirical two parameter correlation for the polymer swelling in a single solvent [46]. The possibility to predict the swelling in multicomponent systems was not further investigated.

5.2 Predictive Flory-Rehner/Hansen solubility parameters model

Only a few thermodynamic models can be used in a purely predictive manner. These can be distinguished into two groups: the group-contribution based models and the solubility parameter based models [25]. Lindvig et. al. [51] suggested to use HSP to predict the Flory-Huggins interaction parameters as given by

$$\frac{\mu_i}{R\cdot T} = \frac{\mu_i^{mix,entropy}}{R\cdot T} + \frac{\mu_i^{mix,enthalpy}}{R\cdot T} \quad with$$

$$\frac{\mu_i^{mix,entropy}}{R\cdot T} = \ln(\phi_i) + \sum_j \phi_j \left(1 - \frac{V_i^{mol}}{V_j^{mol}}\right)$$

$$\frac{\mu_i^{mix,enthalpy}}{R\cdot T} = 2\cdot V_i^{mol} \sum_j (\phi_j \cdot a_{i,j}) - V_i^{mol} \sum_j \sum_k (\phi_j \cdot \phi_k \cdot a_{j,k}) \qquad 34$$

$$a_{i,j} = \frac{0.3}{R\cdot T}\left(\left(\delta_i^d - \delta_j^d\right)^2 + 0.25\left(\delta_i^p - \delta_j^p\right)^2 + 0.25\left(\delta_i^h - \delta_j^h\right)^2\right)$$

where the $a_{i,j}$ is the symmetrical interaction parameter between two components. Hence, the Flory-Huggins interaction parameters can be calculated by equation 35.

$$\chi_{,i,j} = 2\cdot V_i^{mol} \cdot a_{i,j} \qquad 35$$

Lindvig et. al. have shown that the prediction accuracy of the derived Flory-Huggins/Hansen solubility parameters model for multicomponent polymer mixtures is

comparable to other predictive thermodynamic models [25]. Nevertheless, the general limitations in the prediction of the Flory-Huggins interaction parameters from solubility parameters remain: the solubility parameter approach neglects the concentration dependence of the interaction parameters and only positive values of interaction parameters can be predicted whereas for some systems negative values are found [36].

To describe the crosslinking effect on the swelling of polymer sheets and further on the swelling of free standing and surface attached films, elastic free energy terms were introduced to the Flory-Huggins/HSP model [25, 52, 53].

In the case of a free standing polymer film it was assumed that the network can swell in all three dimensions when contacted with solvent. Whereas, the surface attached network can deform in only in one dimension when contacted with a solvent, because one plane of the film is immobilised by the surface attachment. The Flory-Rehner/HSP model for multicomponent mixtures for free standing polymer or surface attached polymer sheet is shown by equation 36.

$$\frac{\mu_i}{R \cdot T} = \frac{\mu_i^{mix,entropy}}{R \cdot T} + \frac{\mu_i^{mix,enthalpy}}{R \cdot T} + \frac{\mu_i^{elastic}}{R \cdot T} \quad with$$

$$\frac{\mu_i^{mix,entropy}}{R \cdot T} = \ln(\phi_i) + \sum_j \phi_j \left(1 - \frac{V_i^{mol}}{V_j^{mol}}\right)$$

$$\frac{\mu_i^{mix,enthalpy}}{R \cdot T} = 2 \cdot V_i^{mol} \sum_j (\phi_j \cdot a_{i,j}) - V_i^{mol} \sum_j \sum_k (\phi_j \cdot \phi_k \cdot a_{j,k})$$

For free standing polymer swelling (three-dimensional):

$$\frac{\mu_i^{elastic}}{R \cdot T} = \frac{V_i^{mol}}{V_{m,monomer}^{mol}} \frac{Mw_{monomer}}{Mw_c} \left(1 - \frac{2 \cdot Mw_c}{Mw_o}\right)\left(\phi_m^{1/3} - \frac{\phi_m}{2}\right) \qquad 36$$

For surface attached polymer swelling (one-dimensional):

$$\frac{\mu_i^{elastic}}{R \cdot T} = \frac{V_i^{mol}}{V_{m,monomer}^{mol}} \frac{Mw_{monomer}}{Mw_c} \left(1 - \frac{2 \cdot Mw_c}{Mw_o}\right)\left(\frac{1}{\phi_m} - \frac{\phi_m}{2}\right)$$

$$a_{i,j} = \frac{0.3}{R \cdot T}\left(\left(\delta_i^d - \delta_j^d\right)^2 + 0.25\left(\delta_i^p - \delta_j^p\right)^2 + 0.25\left(\delta_i^h - \delta_j^h\right)^2\right)$$

From equations 36 it is evident that the elastic term has a positive value only when the molar weight of subchains between two crosslinks is smaller than half of the molar weight of the oligomer. The models for free standing and surface attached films have a value of zero for the elastic term when molar weight of subchains between two crosslinks is equal half of the molar weight of the initial oligomer. Hence, the predicted solvent volume fraction for $Mw_c = Mw_o / 2$ is same for the free standing film and the surface attached one. Figure 31 shows a comparison of predicted swelling of PDMS network in toluene as a free standing polymer film and a surface attached polymer film with different crosslinking degrees. The used model parameters are given in Table 3.

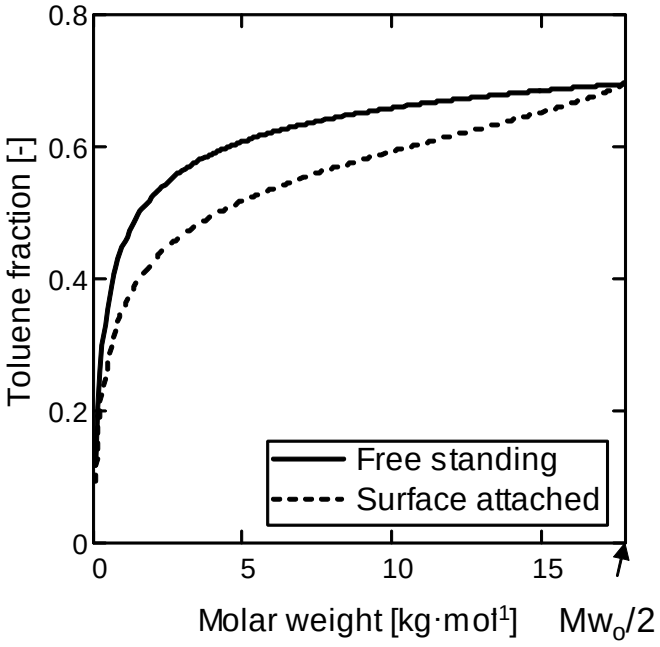

Figure 31: Comparison of free swelling and swelling of a surface attached PDMS sheet in toluene for different values of polymer molar weight between two crosslinks.

In Figure 31 it can be observed that attachment of the polymer sheet to a surface will suppress the swelling of polymer film. The relative difference in swelling of a free and surface attached polymer film is decreasing with increasing molecular weight of subchains between two crosslinks [54].

5.3 Experimental

5.3.1 Swelling experiments

It was assumed that the two-part silicone RTV615 from GE cured at high temperature has a similar composition and final crosslinking degree as the separation layer of the PDMS based membrane ONF-2 from GMT Membrantechnik which was used in filtration experiments.

The cured RTV615 silicone has been often used as material in producing laboratory made PDMS membranes [10, 54, 55]. PDMS sheets were prepared by dissolving two RTV615 silicone parts in toluene (10 w. %) with the recommended ratio of 1 part hydridosiloxane crosslinker with catalyst and 10 parts vinylsiloxane oligomer. The PDMS solution was then poured into a flat dish. The toluene was left to completely evaporate at room temperature. Afterwards the PDMS sheet was cured at 120 °C for 24 h. An approximately 3 mm thick sheet was obtained and was cut in two pieces. The leachable components of the produced sheet were removed previous to the swelling experiments by several extraction cycles with fresh toluene. The prepared PDMS sheets were then used for swelling experiments and density measuring. The PDMS density (ρ_{PDMS}) was determined using a pycnometer and toluene as the reference liquid. The density was measured as 1.014 kg·dm^{-3}. The molar volume of monomer unit was calculated by

$$V_{m,monomer}^{mol} = \frac{Mw_{monomer}}{\rho_{PDMS}} . \qquad 37$$

For the determination of equilibrium solvent swelling, the samples were placed in the solvents at room temperature and left to swell for a day at minimum. The excess solvent from the sheets was removed by paper tissue, after which the samples were weighted with an analytical scale. The measurement was made for two sheets and repeated to confirm the equilibrium swelling of the sheets. Between each solvent, the sheets were dried at elevated temperature. Volume fraction of the solvent ϕ_i was calculated from the solvent weight fraction w_i by

$$\phi_i = \frac{w_i / \rho_i}{w_i / \rho_i + (1 - w_i) / \rho_{PDMS}} , \qquad 38$$

where ρ_i is the solvent mass density at room temperature. The measured solvent volume fractions are given in Table 4.

5.3.2 Permeation experiments

The ONF-2 membrane was installed and operated in an Evonik Membrane Extraction Technology (EMET) stirred cell (see Chapter 3 [56]) at approximately 23 °C and 10 bar transmembrane pressure. The measured volume permeabilities of the ONF-2 membrane at 23 °C and 10 bar are given in Table 5.

5.4 Results and discussion

5.4.1 Determining HSP of silicone membrane

For the application of the Flory-Rehner/HSP equation the molar mass of starting PDMS oligomer and the crosslinked polymer networks are needed. Molar mass of the RTV615 oligomer was taken from the literature [54] and the molar mass of the polymer network was assumed to be very large. The HSP and the molar volume of solvents were taken from the literature [17].

For a parameter sensitivity study of the derived model, the molar mass of the polymer chains between two crosslinks was calculated using elastic theory given by equation 39 [57].

$$Mw_c = \frac{3 \cdot \rho_{PDMS} \cdot R \cdot T}{E_{PDMS}} \qquad 39$$

Where E_{PDMS} is the Young's modulus of elasticity, which can be found in the literature for RTV615 silicone cured at high temperature [58].

The predicted values of polymer swelling were also compared to the model predicted polymer swelling using literature values of HSP for PDMS material [18, 59]. The estimation of the parameters was made using MathCad software. The average absolute (AAD) and relative deviations (ARD) of predicted solvent volume fraction in the membrane using different sets of values for HSP and crosslinking parameter are given in Table 3.

Table 3: Flory-Rehner/HSP prediction of PDMS swelling for different values of HSP and crosslinking parameter with corresponding averaged absolute (AAD) and averaged relative deviations (ARD).

	δ_m^d	δ_m^p	δ_m^h	Mw_c	AAD	ARD
		[(MPa)$^{0.5}$]		[kg·mol^{-1}]	[-]	[-]
Literature [58, 59]	17.0	2.9	2.4	3.9	0.240	0.842
Volume averaged HSP [18, 58]	15.6	1.7	2.5	3.9	0.243	0.833
HSP estimated	14.8	-5.6	5.4	3.9	0.025	0.083
All estimated	14.8	-5.4	5.2	3.0	0.022	0.078

From the values given in Table 3 it can be observed that the crosslinking parameter has only a low influence on the prediction accuracy of the PDMS swelling. In the following modelling studies estimated HSP and Mw_c parameters were used for the description of membrane separation layer properties. The comparison between experimental and predicted solvent volume fraction is given in Table 4.

Table 4: Comparison between experimental and predicted volume fractions of the solvent in solvent/PDMS mixtures.

Solvent	Measured solvent fraction [-]	Predicted solvent fraction [-]
Toluene	0.574	0.565
Dichloromethane	0.545	0.513
Hexane	0.627	0.677
Heptane	0.624	0.625
Octane	0.595	0.568
Ethyl acetate	0.491	0.476
Acetone	0.253	0.228
1-Butanol	0.189	0.171
1-Hexanol	0.154	0.155
1-Octanol	0.099	0.128
Isopropanol	0.236	0.205

5.4.2 Membrane permeability

In the next step a volume fraction based Maxwell-Stefan equation and the Flory-Rehner/HSP model for surface attached polymer films were combined. For the prediction of the Maxwell-Stefan diffusion coefficients the interpolation approach given by Bitter [15] and the Free Volume theory by Wesslingh and Bollen [60] were investigated. The predicted permeabilities are compared with the measured solvent volume permeabilities given in Table 5.

Table 5: Measured solvent permeabilities of ONF-2 at 23 °C and 10 bar.

Solvent	ONF-2 solvent permeability [$L \cdot h^{-1} \cdot m^{-2} \cdot bar^{-1}$]
Toluene	2.25
Dichloromethane	5.31
Hexane	4.14
Heptane	2.72
Octane	2.62
Ethyl acetate	2.48
Acetone	1.18
1-Butanol	0.24
1-Hexanol	0.21
1-Octanol	0.14
Isopropanol	0.18

5.5 Maxwell-Stefan mass transport model

5.5.1 Maxwell-Stefan equation based on volume fraction

The solvent volume fractions on the boundaries of the membrane separation layer were calculated assuming no mechanical pressure loss over the membrane – a prerequisite of the solution-diffusion mechanism [8, 53, 61].

The assumptions used for the calculation of the average volume fraction of the solvent in the membrane separation layer are given by

$$\frac{\mu_{i,\alpha}}{R \cdot T} = 0 \qquad \text{feed side}$$

$$\frac{\mu_{i,\beta}}{R \cdot T} = -\frac{\Delta p \cdot V_i^{mol}}{R \cdot T} \qquad \text{permeate side} \qquad 40$$

$$\overline{\phi_i} = \frac{\phi_{i,\alpha} - \phi_{i,\beta}}{\ln\left(\frac{\phi_{i,\alpha}}{\phi_{i,\beta}}\right)} \qquad \text{logarithmic average volume fraction,}$$

where $\mu_{i,\alpha}$ and $\mu_{i,\beta}$ are the chemical potential of component i in membrane at feed and permeate side, respectively. Analogous, $\phi_{i,\alpha}$ and $\phi_{i,\beta}$ are volume fraction of component i in membrane at feed and permeate side, respectively. The Δp stands for the transmembrane pressure ($\Delta p > 0$). For the prediction of the average volume fraction of the solvent in the membrane ($\overline{\phi_i}$) several mathematical expressions were tested. The logarithmic average which is between the geometrical and arithmetic mean value was applied [61]. The general Maxwell-Stefan equation is given by

$$\frac{x_i}{R \cdot T} \nabla_{T,P} \mu_i = -\sum_{j=1}^{n} \frac{x_i \cdot x_j \cdot \left(\mathbf{u}_i - \mathbf{u}_j\right)}{Đ_{i,j}} \qquad 41$$

.

Where x_i is mole fraction of component i, $\mathbf{u}_i$ the component velocity and $Đ_{i,j}$ are the molar Maxwell-Stefan diffusion coefficients. For describing the mass transfer over a polymer film, it is more practical to use volume or mass fraction [16, 62, 63]. In the case of pure solvent the difference form of the volume fraction based Maxwell-Stefan model [16] results in equation 42.

$$\frac{1}{R \cdot T} \frac{\Delta \mu_i}{z_m} = -\frac{\overline{\phi_m}}{\overline{Đ_{i,m}}} \left(\frac{J_i}{\overline{\phi_i}}\right) \frac{\overline{V_{mix}^{mol}}}{V_m^{mol}} \qquad 42$$

Where z_m is the total membrane separation layer thickness, $\overline{\phi_m}$ is the average volume fraction of membrane polymer, $\overline{Đ_{i,m}}$ is the average molar Maxwell-Stefan diffusion coefficients of component i and the membrane, J_i is the component volumetric flux and V_m^{mol} is the molar volume of membrane polymer and $\overline{V_{mix}^{mol}}$ is the average molar volume of the mixture. The detailed derivation of this volume fraction base Maxwell-Stefan model can be found in Appendix.

Since one-dimensional swelling of the film attached to the surface in pure solvent is assumed, the membrane thickness can be defined as

$$z_m = \frac{z_{m,dry}}{\overline{\phi_m}} \quad . \qquad 43$$

The thickness of the dry membrane separation layer ($z_{m,dry}$) was estimated from a SEM image of the membrane as 2.75 μm.

Assuming the existence of an effective molar volume of the membrane $V_{m,eff}^{mol}$ which is not infinitely large, the average molar volume becomes

$$\overline{V_{mix}^{mol}} = \left(\frac{\overline{\phi_i}}{V_i^{mol}} + \frac{\left(1-\overline{\phi_i}\right)}{V_{m,eff}^{mol}} \right)^{-1} \quad . \qquad 44$$

The average molar fraction ($\overline{x_i}$) is then calculated by

$$\overline{x_i} = \frac{\overline{\phi_i} / V_i^{mol}}{\left(\overline{\phi_i} / V_i^{mol} + \left(1-\overline{\phi_i}\right) / V_{m,eff}^{mol}\right)} \quad . \qquad 45$$

The expression for volumetric permeability is finally derived as

$$\frac{J_i}{\Delta p} = \overline{Đ_{i,m}} \frac{\overline{\phi_i} \cdot V_i^{mol} \cdot V_{m,eff}^{mol}}{z_{m,dry} \cdot R \cdot T} \left(\frac{\overline{\phi_i}}{V_i^{mol}} + \frac{\left(1-\overline{\phi_i}\right)}{V_{m,eff}^{mol}} \right) \quad . \qquad 46$$

Now, only the value for the Maxwell-Stefan diffusion coefficient remains unknown. It can be estimated using two different methods: (a) the Vignes and Darken estimation and (b) based on the Free Volume theory.

5.5.2 Darken and Vignes interpolation rules for the prediction of Maxwell-Stefan diffusion coefficients

For ideal mixtures and mixtures of similar components it was suggested in literature [15, 16] to predict the Maxwell-Stefan diffusion coefficient at intermediate compositions by interpolation of the binary diffusivities at infinite dilution. The different interpolation rules for the prediction of the Maxwell-Stefan diffusion coefficient have been intensively studied for liquid mixtures [64]. In this case the binary diffusivities at infinite dilution refer to solvent/solvent diffusivity coefficient and solvent/membrane diffusivity coefficient. Bitter has applied the logarithmic interpolation to predict the diffusion coefficient of components through the membrane [15]. He suggested introduction of an additional constant in the Vignes interpolation rule to compensate the non-ideality of the mixture. In this work such parameters were not included. We focus on the membrane parameters, which determine the solvent/membrane diffusivity at infinite dilution in a combination of different interpolation rules. The interpolation rules for predicting the Maxwell-Stefan diffusion coefficient used here are based on the Vignes and Darken equation [64] combined with volumetric fraction and molar fraction (see Table 7).

The diffusivity coefficient at infinite dilution of the solvent/solvent ($Đ_{i,i}$) and solvent/membrane ($Đ_{i,m}^{m\to\infty}$) was assumed to follow the Nakanishi correlation given in equation 47, which unlike other correlations requires the room temperature molar volume and viscosity [65].

$$Đ_{i,j}^{j\to\infty} = \left(\frac{9.97\cdot 10^{-8}}{(I_i \cdot V_i)^{1/3}} + \frac{2.40\cdot 10^{-8}\cdot A_j \cdot S_j \cdot V_j}{I_i \cdot S_i \cdot V_i} \right) \frac{T}{\eta_j} \qquad 47$$

Where $Đ_{i,j}^{j\to\infty}$ is given in $cm^2 \cdot s^{-1}$, molar volumes V_i^{mol} and V_j^{mol}, for solute and solvent, respectively, are given in $cm^3 \cdot mol^{-1}$ and η_j is the solvent viscosity in cP at system temperature T in K [65]. The Nakanishi correlation includes parameters I_i, S_i, S_j and A_j, which reflect the influence of polarity of the molecules.

The diffusivity coefficient at infinite dilution of the solvent/solvent has been predicted using the Nakanishi correlation with both, solvent and solute, having the same molar volume and viscosity. The Nakanishi parameters used for solvents and the membrane are given in Table 6 [65].

Finally, the effective membrane molar volume and effective membrane viscosity were estimated from measured permeability data given in Table 5 using interpolations rules given in Table 7 using MathCad software. Additional constraints were imposed in the estimation of the effective membrane molar volume ($V_{m,eff}^{mol}$) and the effective membrane viscosity ($\eta_{m,eff}$): The solvent/solvent diffusion coefficient must be larger than binary diffusivity of the solvent in the membrane at infinite dilution and the effective membrane molar volume must be larger than the molar volume of the monomer.

The estimated parameters and corresponding averaged absolute and averaged relative deviations of the solvent volume permeability calculated using the estimated values of effective membrane molar volume and effective membrane viscosity are given in Table 7.

Table 6: Solvent and solute parameters in the Nakanishi diffusion correlation.

Solvent	Solute parameters		Solvent parameters	
	I_i	S_i	A_j	S_j
Toluene	1.00	1.00	1.00	1.00
Dichloromethane	1.00	1.00	1.00	1.00
Hexane	1.00	0.70	1.00	0.70
Heptane	1.00	0.70	1.00	0.70
Octane	1.00	0.70	1.00	0.70
Ethyl acetate	1.00	1.00	1.00	1.00
Acetone	1.50	1.00	1.80	1.00
1-Butanol	1.50	1.00	1.80	1.00
1-Hexanol	1.50	1.00	1.80	1.00
1-Octanol	1.25	1.00	1.50	1.00
Isopropanol	2.30	1.00	2.30	1.00
PDSM	1.00	1.00	1.00	1.00

Considering the averaged absolute and relative deviation within Table 7, the Vignes equation with molar fractions gives the best representation of the measured permeability data. The applied Vignes interpolation rule requires two estimated parameters for describing mass transport of the solvent through the membrane: the effective molar volume of the membrane and the membrane viscosity. To apply such a logarithmic interpolation rule to a multicomponent mixture, Bitter suggested to expand the expression with terms of binary diffusion coefficients at infinite dilution for other components in the mixture [15].

Table 7: The estimated parameters of Vignes and Darken interpolation rules and corresponding averaged absolute and averaged relative deviations of the predicted solvent volume permeability.

Interpolation rule	$\eta_{m,eff}$ [mPa·s]	$V_{m,eff}^{mol}$ [cm^3 · mol^{-1}]	*AAD* [L·h^{-1}·m^{-2} ·bar^{--1}]	*ARD* [-]
$\overline{Đ_{i,m}} = \left(Đ_{i,i}\right)^{\overline{\phi_i}} \cdot \left(Đ_{i,m}^{m\to\infty}\right)^{\left(1-\overline{\phi_i}\right)}$	17.3	330.5	0.447	0.221
$\overline{Đ_{i,m}} = \overline{\phi_i} \cdot Đ_{i,i} + \left(1-\overline{\phi_i}\right) \cdot Đ_{i,m}^{m\to\infty}$	6.5	73.1	0.656	0.261
$\overline{Đ_{i,m}} = \left(Đ_{i,i}\right)^{\overline{x_i}} \cdot \left(Đ_{i,m}^{m\to\infty}\right)^{\left(1-\overline{x_i}\right)}$	5.5	136.1	0.272	0.181
$\overline{Đ_{i,m}} = \overline{x_i} \cdot Đ_{i,i} + \left(1-\overline{x_i}\right) \cdot Đ_{i,m}^{m\to\infty}$	4.2	73.1	0.340	0.158

The parity plot in Figure 32 shows the measured over the predicted solvent volume permeabilities using Vignes interpolation rule based on molar fraction.

For the Darken interpolation rule based on molar fraction it could be observed from Table 7 that the effective membrane molar volume has the value of the molar volume of the monomer. Hence, only the effective membrane viscosity needs to be estimated. The parity plot of predicted volume permeabilities using the Darken interpolation rule is given Figure 33. The application of the Darken interpolation rule on multicomponent mixtures has already been reported in literature [64].

The Darken and Vignes interpolation rules have good prediction accuracy for the solvent volume permeation except for dichloromethane. This discrepancy contributed most to the averaged absolute and relative deviation of these models.

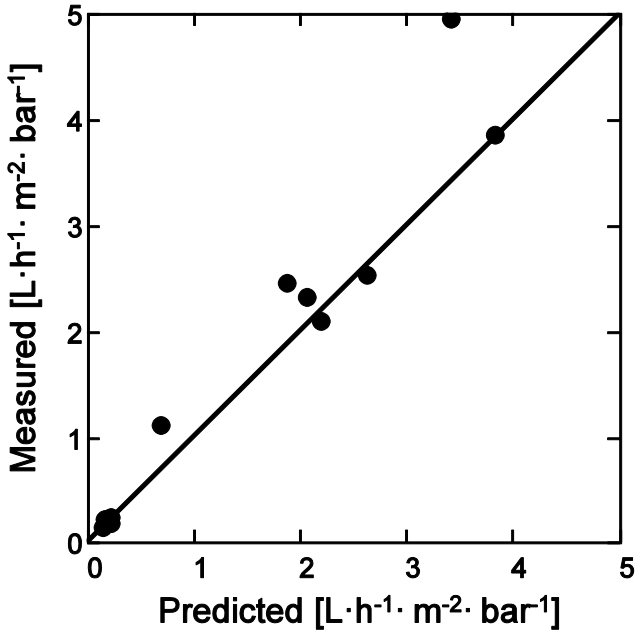

Figure 32: Pure solvent permeability compared to predicted values using the Vignes interpolation rule with estimated effective membrane molar volume and viscosity.

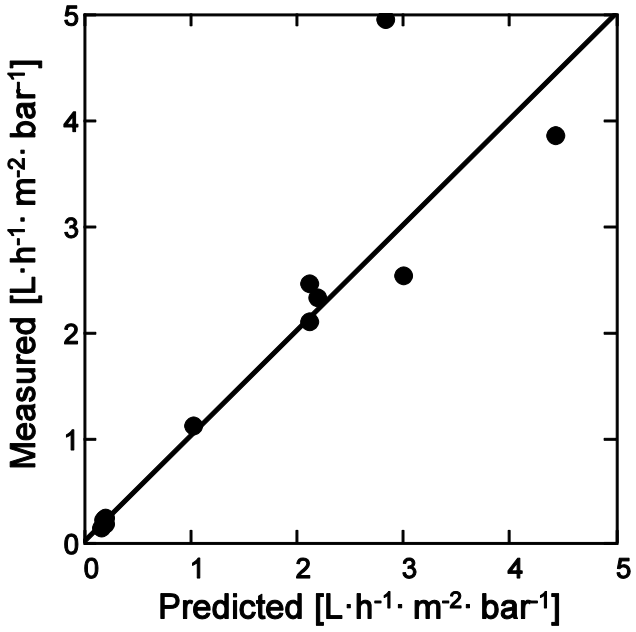

Figure 33: Pure solvent permeability compared to predicted values using the Darken interpolation rule with estimated effective membrane viscosity.

5.5.3 Free Volume theory for the prediction of the Maxwell-Stefan diffusion coefficient

The Free Volume theory dates its first application at the beginning of the twentieth century [60]. The application of the Free Volume theory on organic solvent transport through silicone membranes can be found in literature [6, 7, 66].

The basic assumption made in the Free Volume theory is that a molecule only migrates through the mixture when a “hole”, large enough for the molecule to fit in, opens in its vicinity. Such migration of the molecules can be found under diffusive and viscous flow conditions. The latest development in this theory has been contributed by Wesselingh and Bollen [60]. Different to the previous Free Volume theories, Wesselingh and Bollen define the free volume accessible for a component using surface fraction of the component in the mixture.

In the Free Volume theory, the molar free volume of a pure component ($V_{F,i}^{*}$) is defined as the difference between actual molar volume and the minimal (compressed) molar volume of the component ($V_i^{\bullet}$) and is given by equation 48.

$$V_{F,i}^{*} = V_i^{mol} - V_i^{\bullet} \qquad 48$$

The minimal molecule diameters (d_i) can be calculated using the minimal molar volume, the Avogadro constant (N_A) and assuming a spherical molecule by

$$d_i = 2\left(\frac{3 \cdot V_i^{\bullet}}{4 \cdot \pi \cdot N_A}\right)^{1/3} . \qquad 49$$

The compressed pure solvent mass density ($\rho_i^{\bullet}$) relates to minimal (compressed) molar volume and molar weight (Mw_i) as

$$\rho_i^{\bullet} = \frac{Mw_i}{V_i^{\bullet}} . \qquad 50$$

Using the Aspen Properties and the UNQUAC properties method solvent molar volumes and viscosities at temperatures between 0 °C and 40 °C at 30 bar were estimated. Further, the minimal molar volume and overlap factor (λ_i) for each solvent can estimated from the free volume definition of the viscosity as given by equation 51 [60].

$$\eta_i(T) = \frac{3}{\pi}\sqrt{\frac{\rho_i^{\bullet}\cdot k\cdot T}{3\cdot d_i}}\exp\left(\lambda_i \frac{V_i^{\bullet}}{V_i^{mol}(T) - V_i^{\bullet}}\right) \qquad 51$$

The estimated values of free volume overlap factor and minimal molar volume for the used solvents are given in Table 8.

The minimal molar volume of the monomer ($V_{m,monomer}^{\bullet}$) was calculated using the expression of Bondi and a group contribution method for the Van der Waals molar volume ($V_{m,monomer}^{VdW}$) as shown in equation 52 [67].

$$V_{m,monomer}^{\bullet} = 1.3 \cdot V_{m,monomer}^{VdW} \qquad 52$$

Further equations used to predict mutual Maxwell-Stefan diffusivities are molar fractions based on the monomer unit molar volume ($V_{m,monomer}^{mol}$) as given by

$$\overline{x_i} = \frac{\overline{\phi_i}/V_i^{mol}}{\left(\overline{\phi_i}/V_i^{mol} + \left(1-\overline{\phi_i}\right)/V_{m,monomer}^{mol}\right)}. \qquad 53$$

The total free volume of the solvent/polymer mixture (V_F), which is assumed to be the molar averaged free volume of the pure components, is given by

$$V_F = \sum\left(\overline{x_i}\cdot V_{F,i}^{*}\right). \qquad 54$$

Table 8: Estimated values of free volume overlap factor and minimal molar volume for the tested solvents.

Solvent	λ_i [-]	$V_i^\bullet$ [$cm^3 \cdot mol^{-1}$]
Toluene	0.609	85.6
Dichloromethane	0.593	48.8
Hexane	0.645	99.0
Heptane	0.616	116.2
Octane	0.720	126.7
Ethyl acetate	0.651	75.8
Acetone	0.574	56.2
1-Butanol	0.764	77.5
1-Hexanol	0.702	108.9
1-Octanol	0.792	136.8
Isopropanol	0.717	64.7

The free molar volume of the monomer unit can be directly calculated from the measured polymer density and minimal molar volume using equations 48 and 52. The surface fraction (σ_i) of solvent and polymer are defined as

$$\overline{\sigma_i} = \frac{\overline{x_i} \cdot \left(V_i^{mol}\right)^{2/3}}{\sum\left(\overline{x_i} \cdot (V_i^{mol})^{2/3}\right)}. \qquad 55$$

The surface weighed free volume ($V_{F,i}$) is given by

$$V_{F,i} = \frac{\overline{\sigma_i}}{\overline{x_i}} V_F \quad . \qquad 56$$

The compressed mixture density ($\rho^\bullet$) is given by

$$\rho^\bullet = \sum \left(\overline{x_i} \frac{Mw_i}{V_i^\bullet} \right) . \qquad 57$$

The pre-exponential friction factors ($\zeta^0_{i\#,j}$) are derived from the Einstein-Stokes equation and are for both, solvent and monomer, defined as

$$\zeta^0_{i\#,j} = 2 \cdot N_A \sqrt{3 \cdot k \cdot T \cdot \rho^\bullet \cdot d_i} \quad . \qquad 58$$

The effective tracer friction coefficient ($\zeta_{i\#,eff}$) is given by

$$\zeta_{i\#,eff} = \zeta^0_{i\#,j} \exp\left(\lambda_i \frac{V_i^\bullet}{V_{F,i}} \right) . \qquad 59$$

Mutual friction coefficients ($\zeta_{i,j}$) are calculated by

$$\zeta_{i,j} = \frac{\zeta_{i\#,eff} \cdot \zeta_{j\#,eff}}{\sum \left(\overline{x_k} \cdot \zeta_{k\#,eff} \right)} \quad i \neq j \quad . \qquad 60$$

For pure solvent permeation experiments, a binary mixture solvent/membrane is considered. The Maxwell-Stefan diffusion coefficient of the solvent in the membrane is then defined by equation 61.

$$\overline{Đ_{i,m}} = \frac{R \cdot T}{\zeta_{i,m}} \quad . \qquad 61$$

The above defined Maxwell-Stefan diffusion coefficient was included in the expression for the volumetric permeability of the solvents (see equation 46).

The free volume of the monomer is influenced by the density of the polymer [31], the minimal molar volume and the overlap factor [7] and has a large influence on the predicted volumetric permeabilities [16]. The influence of the free volume overlap factor (λ_m) and the minimal molar volume of the monomer ($V^{\bullet}_{m,monomer}$) on the averaged absolute and relative deviation are given in Table 9.

Table 9: Overview of estimated values of coefficients in the Free Volume theory model and the corresponding averaged absolute and relative deviation of the predicted permeabilities.

	λ_m	$V^{\bullet}_{m,monomer}$	*AAD*	*ARD*
	[-]	[$cm^3 \cdot mol^{-1}$]	[$L \cdot h^{-1} \cdot m^{-2} \cdot bar^{-1}$]	[-]
Literature data	0.700	62.0	0.372	0.246
Both estimated	0.694	62.0	0.370	0.244

The accuracy of the Free Volume approach [60] could not be significantly improved by parameter estimation for the monomer from pure solvent permeability data. The parity plot of measured permeabilities and predicted permeability values using the Free Volume theory and model parameters found in literature is shown in Figure 4.

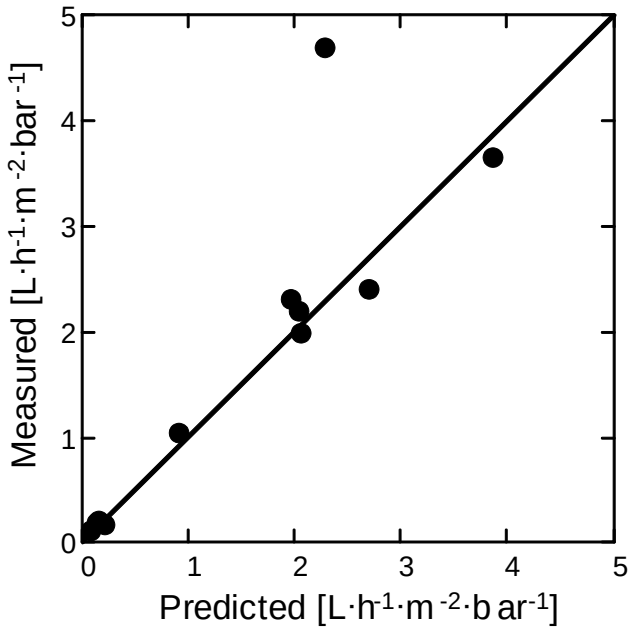

Figure 34: Pure solvent permeability compared to the model prediction using the Free Volume theory and model parameters found in literature.

It can be observed in Figure 34 that dichloromethane has a considerably larger error compared to other solvents, similar to the previously investigated models based on Darken and Vignes interpolation rules. This deviation, could be a result of excessive swelling of supporting membrane layers such as poly(acrylonitrile) and non-woven. But further research would be required to finally explain the experimental data. The rest of the predicted permeability values have a remarkably small error.

The biggest advantage of the Free Volume approach is the relatively high prediction accuracy of the permeability without any estimated parameter from the permeability measurements being required. The Free Volume theory can be applied to predict the Maxwell-Stefan diffusion coefficients of multicomponent mixtures through the membrane as found in the literature [4, 6, 16, 60].

5.6 Conclusion

The modelling approach reported here focuses on the prediction of the swelling behaviour of PDMS using Flory-Huggins (Rehner) based model equations and the derivation of diffusion correlations, together predicting the solvent permeability through PDMS membranes.

The Flory-Huggins/Hansen solubility parameters equation suggested by Lindvig et. al. was expanded for the elastic contribution term for the case of free swelling as well as confined swelling when the polymer film is attached to the surface [52]. The Hansen solubility parameters of PDMS and the crosslinking degree were estimated from experimental data made with a PDMS sheet. The derived Flory-Huggins/Hansen solubility parameters model and the estimated parameters gave a good prediction accuracy of the swelling behaviour of PDMS sheet for the whole range of polar to nonpolar solvents.

Combining the swelling of the membrane separation layer with different approaches to estimate the diffusional properties of the solvent allows a prediction of the solvent permeability through PDMS membranes. The investigated diffusion models included the Maxwell-Stefan diffusion coefficient approach with different diffusion interpolation rules and the Free Volume theory. The Vignes interpolation rule was found to best correlate the Maxwell-Stefan diffusion coefficients with binary diffusion coefficients at infinite dilution. The Vignes interpolation rule was based on the Nakanishi diffusion correlation with two estimated parameters, which describe effective membrane molar volume and effective membrane viscosity.

The Free Volume theory involves a larger set of equations, but these can be easily programmed [60]. The accuracy of the Free Volume model in combination with the Flory-Rehner/Hansen solubility parameters expression was good, even if litera-

ture values for the polymer free volume parameters were applied. The large influence of the free volume parameters of the solvent on the overlap factor and the minimal molar volume of the solvent leave possibilities to refine the Free Volume theory.

5.7 List of symbols

AAD	average absolute deviation	$L \cdot h^{-1} \cdot m^{-2} \cdot bar^{-1}$
ARD	average relative deviation	-
$a_{i,j}$	symmetrical interaction parameter between components i and j	$mol \cdot m^{-3}$
d_i	minimal molecule diameters	m
E_i	total cohesive energy density of component i	$J \cdot mol^{-1}$
E_{PDMS}	Young's modulus of elasticity for PDMS sheet	Pa
f_0	probability "that the site is occupied by a polymer segment of a chain being placed [15]"	-
I_i, S_i, S_j, A_j,	Nakanishi correlation parameters	-
J_i	volumetric flux of component i	$m \cdot s^{-1}$
k	Boltzmann constant	$J \cdot K^{-1}$
Mw_i	molar weight	$kg \cdot m^{-3}$
Mw_c	molar weight of subchains between two crosslinks	$kg \cdot m^{-3}$
Mw_o	molar weight of oligomer before crosslinking	$kg \cdot m^{-3}$
$Mw_{monomer}$	molar weight of oligomer unit	$kg \cdot m^{-3}$

N_A	Avogadro constant	-
Δp	transmembrane pressure	Pa
R	the universal gas constant	$J \cdot mol^{-1} \cdot K^{-1}$
T	absolute temperature	K
$\mathbf{u}_i$	velocity component i in the membrane	$m \cdot s^{-1}$
V_F	total free volume of mixture	m^3
$V_{F,i}^*$	molar free volume of a pure component i	$m^3 \cdot mol^{-1}$
$V_{F,i}$	surface weighed free volume of component i	$m^3 \cdot mol^{-1}$
$V_i^\bullet$	minimal (compressed) molar volume of the component i	$m^3 \cdot mol^{-1}$
V_i^{mol}	molar volume of component i	$m^3 \cdot mol^{-1}$
V_m^{mol}	molar volume of membrane polymer	$m^3 \cdot mol^{-1}$
$V_{m,eff}^{mol}$	effective molar volume of the membrane	$m^3 \cdot mol^{-1}$
$\overline{V_{mix}^{mol}}$	average molar volume of the mixture	$m^3 \cdot mol^{-1}$
$V_{m,monomer}^{mol}$	monomer molar volume	$m^3 \cdot mol^{-1}$
$V_{m,monomer}^\bullet$	minimal molar volume of monomer	$m^3 \cdot mol^{-1}$
$V_{m,monomer}^{VdW}$	Van der Waals molar volume of monomer	$m^3 \cdot mol^{-1}$
w_i	solvent weight fraction	-
x_i	mole fraction of component i	-
$\overline{x_i}$	molar fraction of component i	-
$Z_{polymer}$	polymer lattice coordination number	-

z_m	total membrane separation layer thickness	m
$z_{m,dry}$	thickness of the dry membrane separation layer	m
$Đ_{i,j}$	molar Maxwell-Stefan diffusion coefficient	$m^2 \cdot s^{-1}$
$Đ_{i,j}^{j\to\infty}$	diffusivity coefficient of component i in component j at infinite dilution	$m^2 \cdot s^{-1}$
$\overline{Đ_{i,m}}$	average molar Maxwell-Stefan diffusion coefficients of component i and the membrane	$m^2 \cdot s^{-1}$
$Đ_{i,m}^{m\to\infty}$	solvent/membrane diffusivity coefficient at infinite dilution	$m^2 \cdot s^{-1}$

Greek symbols

δ_i^d	dispersion Hansen solubility parameter of component i	$(Pa)^{0.5}$
δ_i^p	dipole Hansen solubility parameter of component i	$(Pa)^{0.5}$
δ_i^h	hydrogen bonding Hansen solubility parameter of component i	$(Pa)^{0.5}$
δ_m^t	Hildebrand solubility parameters of the monomer unit	$(Pa)^{0.5}$
δ_i^t	Hildebrand solubility parameters of component i	$(Pa)^{0.5}$
$\zeta_{i\#,j}^0$	pre-exponential friction factors	$kg \cdot mol^{-1} \cdot s^{-1}$
$\zeta_{i\#,eff}$	effective tracer friction coefficient	$kg \cdot mol^{-1} \cdot s^{-1}$
$\zeta_{i,j}$	mutual friction coefficients	$kg \cdot mol^{-1} \cdot s^{-1}$

η_j	dynamic viscosity of component j	Pa·s
$\eta_{m,eff}$	effective membrane viscosity	Pa·s
λ_i	overlap factor	-
μ_i	total chemical potential of component i in the mixture	J·mol^{-1}
$\mu_i^{mix,entropy}$	chemical potential contribution term of mixing entropy	J·mol^{-1}
$\mu_i^{mix,enthalpy}$	chemical potential contribution term of mixing enthalpy	J·mol^{-1}
$\mu_i^{elastic}$	elastic chemical potential contribution term of mixing enthalpy	J·mol^{-1}
$\rho^{\bullet}$	compressed mixture density	kg·m^{-3}
ρ_i	mass density	kg·m^{-3}
$\rho_i^{\bullet}$	compressed mass density of component i	kg·m^{-3}
ρ_{PDMS}	PDMS mass density	kg·m^{-3}
$\overline{\sigma_i}$	average surface fraction	-
ϕ_i	the volume factions of component i	-
$\overline{\phi_i}$	average volume fraction of component i in the membrane	-
$\chi_{i,j}$	Flory-Huggins interaction parameter	-

Indices

m	membrane polymer

PDMS	poly(dimethylsiloxane)
α	membrane polymer near feed surface
β	membrane polymer near permeate surface

5.8 References

[1] L. Hesse, J. Mićović, P. Schmidt, A. Górak, G. Sadowski, *Modelling of organic-solvent flux through a polyimide membrane*, Journal of Membrane Science 428 (2013) 554-561.

[2] S. Zeidler, U. Kätzel, P. Kreis, *Systematic investigation on the influence of solutes on the separation behavior of a PDMS membrane in organic solvent nanofiltration*, Journal of Membrane Science 429 (2013) 295-303.

[3] P. Schmidt, T. Köse, P. Lutze, *Characterisation of organic solvent nanofiltration membranes in multi-component mixtures: Membrane rejection maps and membrane selectivity maps for conceptual process design*, Journal of Membrane Science 429 (2013) 103-120.

[4] D. Fierro, A. Boschetti-de-Fierro, V. Abetz, *The solution-diffusion with imperfections model as a method to understand organic solvent nanofiltration of multicomponent systems*, Journal of Membrane Science 413–414 (2012) 91-101.

[5] J.P. Robinson, E.S. Tarleton, K. Ebert, C.R. Millington, A. Nijmeijer, *Influence of Cross-Linking and Process Parameters on the Separation Performance of Poly(dimethylsiloxane) Nanofiltration Membranes*, Industrial & Engineering Chemistry Research 44 (2005) 3238-3248.

[6] M.F.J. Dijkstra, S. Bach, K. Ebert, *A transport model for organophilic nanofiltration*, Journal of Membrane Science 286 (2006) 60-68.

[7] D. Fierro, N. Scharnagl, T. Emmler, A. Boschetti-de-Fierro, V. Abetz, *Experimental determination of self-diffusivities through a polymer network for single components in a mixture*, Journal of Membrane Science 384 (2011) 63-71.

[8] J.G. Wijmans, R.W. Baker, *The solution-diffusion model: a review*, Journal of Membrane Science 107 (1995) 1-21.

[9] D. Bhanushali, S. Kloos, C. Kurth, D. Bhattacharyya, *Performance of solvent-resistant membranes for non-aqueous systems: solvent permeation results and modeling*, Journal of Membrane Science 189 (2001) 1-21.

[10] D.F. Stamatialis, N. Stafie, K. Buadu, M. Hempenius, M. Wessling, *Observations on the permeation performance of solvent resistant nanofiltration membranes*, Journal of Membrane Science 279 (2006) 424-433.

[11] J.L.C. Santos, A.M. Hidalgo, R. Oliveira, S. Velizarov, J.G. Crespo, *Analysis of solvent flux through nanofiltration membranes by mechanistic, chemometric and hybrid modelling*, Journal of Membrane Science 300 (2007) 191-204.

[12] S. Darvishmanesh, A. Buekenhoudt, J. Degrève, B. Van der Bruggen, *General model for prediction of solvent permeation through organic and inorganic solvent resistant nanofiltration membranes*, Journal of Membrane Science 334 (2009) 43-49.

[13] A. Miyagi, H. Nabetani, M. Nakajima, *Analysis of transport mechanism of binary organic solvent system through a PDMS-based dense membrane using a regular solution model combined with a solution-diffusion model*, Separation and Purification Technology 88 (2012) 216-226.

[14] E. Favre, P. Schaetzel, Q.T. Nguygen, R. Clément, J. Néel, *Sorption, diffusion and vapor permeation of various penetrants through dense poly(dimethylsiloxane) membranes: a transport analysis*, Journal of Membrane Science 92 (1994) 169-184.

[15] J.G. Bitter, *Transport mechanisms in membrane separation processes*, Plenum Press 1991.

[16] J.A. Wesselingh, R. Krishna, *Mass transfer in multicomponent mixtures*, Delft University Press 2000.

[17] C.M. Hansen, *Hansen Solubility Parameters: A Users Handbook*, 2nd ed., CRC Press 2007.

[18] E.T. Zellers, D.H. Anna, R. Sulewski, X. Wei, *Improved methods for the determination of Hansen's solubility parameters and the estimation of solvent uptake for lightly crosslinked polymers*, Journal of Applied Polymer Science 62 (1996) 2081-2096.

[19] A. Beerbower, J.R. Dickey, *Advanced methods for mredicting elastomer/fluids interactions*, A S L E Transactions 12 (1969) 1-20.

[20] O.M. Farid, *Investigating membrane selectivity based on polymer swelling*, PhD Thesis, University of Nottingham, 2010.

[21] R. Anim-Mensah Alexander, E. Mark James, B. Krantz William, *Use of solubility parameters for predicting the separation characteristics of poly(dimethylsiloxane) and siloxane-containing membranes*, Science and Technology of Silicones and Silicone-Modified Materials 964 (2007) 203-219.

[22] M.K. Buckley-Smith, *The Use of Solubility Parameters to Select Membrane Materials for Pervaporation of Organic Mixtures*, PhD Thesis, The University of Waikato 2006.

[23] S.K. Ray, S.B. Sawant, J.B. Joshi, V.G. Pangarkar, *Development of new synthetic membranes for separation of benzene−cyclohexane mixtures by pervaporation: A solubility parameter approach*, Industrial & Engineering Chemistry Research 36 (1997) 5265-5276.

[24] S. Mandal, V.G. Pangarkar, *Development of co-polymer membranes for pervaporative separation of methanol from methanol–benzene mixture—a solubility parameter approach*, Separation and Purification Technology 30 (2003) 147-168.

[25] T. Lindvig, I.G. Economou, R.P. Danner, M.L. Michelsen, G.M. Kontogeorgis, *Modeling of multicomponent vapor–liquid equilibria for polymer–solvent systems*, Fluid Phase Equilibria 220 (2004) 11-20.

[26] P.J. Flory, *Thermodynamics of High Polymer Solutions*, The Journal of Chemical Physics 10 (1942) 51-61.

[27] P.J. Flory, J. John Rehner, *Statistical Mechanics of Cross-Linked Polymer Networks I. Rubberlike Elasticity*, The Journal of Chemical Physics 11 (1943) 512-520.

[28] P.J. Flory, J.J. Rehner, *Statistical Mechanics of Cross-Linked Polymer Networks II. Swelling*, The Journal of Chemical Physics 11 (1943) 521-526.

[29] R.P. Danner, M.S. High, *Handbook of Polymer Solution Thermodynamics*, Wiley 1993.

[30] M. Gottlieb, M. Herskowitz, *Estimation of the η parameter for poly(dimethylsiloxane) solutions by the UNIFAC group contribution method*, Macromolecules 14 (1981) 1468-1471.

[31] H.-K. Oh, K.-H. Song, K.-R. Lee, J.-M. Rim, *Prediction of sorption and flux of solvents through PDMS membrane*, Polymer 42 (2001) 6305-6312.

[32] S.J. Lue, J.S. Ou, C.H. Kuo, H.Y. Chen, T.-H. Yang, *Pervaporative separation of azeotropic methanol/toluene mixtures in polyurethane–poly(dimethylsiloxane) (PU–PDMS) blend membranes: Correlation with sorption and diffusion behaviors in a binary solution system*, Journal of Membrane Science 347 (2010) 108-115.

[33] S.J. Lue, S.Y. Wu, S.F. Wang, L.D. Wang, C.L. Tsai, *Modeling multi-component vapor sorption in a poly(dimethyl siloxane) membrane*, Desalination 233 (2008) 286-294.

[34] G.M.N. Costa, T. Dias, M. Cardoso, Y. Guerrieri, F.L.P. Pessoa, S.A.B.V. de Melo, M. Embiruçu, *Prediction of vapor–liquid and liquid–liquid equilibria for polymer systems: Comparison of activity coefficient models*, Fluid Phase Equilibria 267 (2008) 140-149.

[35] N. Pedrosa, J. Gao, I.M. Marrucho, J.A.P. Coutinho, *Correlation of solvent activities in polymer solutions: a comparison of models*, Fluid Phase Equilibria 219 (2004) 129-138.

[36] J.E. Mark, *Physical Properties of Polymers Handbook*, 2nd ed., Springer 2007.

[37] T.C. Merkel, V.I. Bondar, K. Nagai, B.D. Freeman, I. Pinnau, *Gas sorption, diffusion, and permeation in poly(dimethylsiloxane)*, Journal of Polymer Science Part B: Polymer Physics 38 (2000) 415-434.

[38] B. Neff, A. Heintz, R.N. Lichtenthaler, *Thermodynamics of Polydimethylsiloxane Solutions. I. Calorimetric Results of the Enthalpy of Dilution with Seven Organic Solvents*, Berichte der Bunsengesellschaft für physikalische Chemie 87 (1983) 1165-1169.

[39] A. Heintz, B. Neff, R.N. Lichtenthaler, *Thermodynamics of Polydimethylsiloxane Solutions. II. Application of an Extended Flory-Theory*, Berichte der Bunsengesellschaft für physikalische Chemie 87 (1983) 1169-1176.

[40] E. Dolch, M. Glaser, A. Heintz, H. Wagner, R.N. Lichtenthaler, *Thermodynamics of Polydimethylsiloxane-Solutions III. Experimental Results and Theoretical Calculations of Solvent Activities*, Berichte der Bunsengesellschaft für physikalische Chemie 88 (1984) 479-484.

[41] J.S. Yoo, S.J. Kim, J.S. Choi, *Swelling equilibria of mixed solvent/poly(dimethylsiloxane) systems*, Journal of Chemical & Engineering Data 44 (1998) 16-22.

[42] R. Koningsveld, L.A. Kleintjens, *Liquid-Liquid Phase Separation in Multicomponent Polymer Systems. X. Concentration Dependence of the Pair-Interaction Parameter in the System Cyclohexane-Polystyrene*, Macromolecules 4 (1971) 637-641.

[43] A. Jonquières, L. Perrin, A. Durand, S. Arnold, P. Lochon, *Modelling of vapour sorption in polar materials: Comparison of Flory–Huggins and related models with the ENSIC mechanistic approach*, Journal of Membrane Science 147 (1998) 59-71.

[44] C. Etxabarren, M. Iriarte, C. Uriarte, A. Etxeberría, J.J. Iruin, *Polymer–solvent interaction parameters in polymer solutions at high polymer concentrations*, Journal of Chromatography A 969 (2002) 245-254.

[45] Q.T. Nguyen, E. Favre, Z.H. Ping, J. Néel, *Clustering of solvents in membranes and its influence on membrane transport properties*, Journal of Membrane Science 113 (1996) 137-150.

[46] E. Favre, Q.T. Nguyen, D. Sacco, A. Moncuy, R. Clement, *Multicomponent polymer/solvents equilibria: An evaluation of Flory-Huggins theory for crosslinked PDMS networks swelled by binary mixtures*, Chemical Engineering Communications 140 (1995) 193-205.

[47] J.L. Lundberg, *Molecular clustering and segregation in sorption systems*, Pure and Applied Chemistry 31 (1972) 261-281.

[48] L.E.M. Gevers, G. Meyen, K. De Smet, P. Van De Velde, F. Du Prez, I.F.J. Vankelecom, P.A. Jacobs, *Physico-chemical interpretation of the SRNF transport mechanism for solutes through dense silicone membranes*, Journal of Membrane Science 274 (2006) 173-182.

[49] H. Yang, Q.T. Nguyen, Y. Ding, Y. Long, Z. Ping, *Investigation of poly(dimethyl siloxane) (PDMS)–solvent interactions by DSC*, Journal of Membrane Science 164 (2000) 37-43.

[50] E. Favre, Q.T. Nguyen, P. Schaetzel, R. Clement, J. Neel, *Sorption of organic solvents into dense silicone membranes. Part 1.-Validity and limitations of Flory-Huggins and related theories*, Journal of the Chemical Society, Faraday Transactions 89 (1993) 4339-4346.

[51] T. Lindvig, M.L. Michelsen, G.M. Kontogeorgis, *A Flory–Huggins model based on the Hansen solubility parameters*, Fluid Phase Equilibria 203 (2002) 247-260.

[52] R. Toomey, D. Freidank, J. Rühe, *Swelling Behavior of Thin, Surface-Attached Polymer Networks*, Macromolecules 37 (2004) 882-887.

[53] W. Ogieglo, H. van der Werf, K. Tempelman, H. Wormeester, M. Wessling, A. Nijmeijer, N.E. Benes, *n-Hexane induced swelling of thin PDMS films under non-equilibrium nanofiltration permeation conditions, resolved by spectroscopic ellipsometry*, Journal of Membrane Science 431 (2013) 233-243.

[54] N. Stafie, D.F. Stamatialis, M. Wessling, *Effect of PDMS cross-linking degree on the permeation performance of PAN/PDMS composite nanofiltration membranes*, Separation and Purification Technology 45 (2005) 220-231.

[55] I.F.J. Vankelecom, K. De Smet, L.E.M. Gevers, A. Livingston, D. Nair, S. Aerts, S. Kuypers, P.A. Jacobs, *Physico-chemical interpretation of the SRNF transport mechanism for solvents through dense silicone membranes*, Journal of Membrane Science 231 (2004) 99-108.

[56] Evonik Industries AG, *Membrane Properties - Products and Services*, (2008).

[57] S.J. Clarson, J.A. Semlyen, *Siloxane Polymers*, Prentice Hall 1993.

[58] F. Schneider, T. Fellner, J. Wilde, U. Wallrabe, *Mechanical properties of silicones for MEMS*, Journal of Micromechanics and Microengineering 18 (2008) 065008.

[59] M. Alm, *Impregnation and surface modification of polymers in liquid and supercritical carbon dioxide*, PhD Thesis, Roskilde University, 2007.

[60] J.A. Wesselingh, A.M. Bollen, *Multicomponent Diffusivities from the Free Volume Theory*, Chemical Engineering Research and Design 75 (1997) 590-602.

[61] D.R. Paul, *Reformulation of the solution-diffusion theory of reverse osmosis*, Journal of Membrane Science 241 (2004) 371-386.

[62] C.P. Ribeiro Jr, B.D. Freeman, D.R. Paul, *Modeling of multicomponent mass transfer across polymer films using a thermodynamically consistent formulation of the Maxwell–Stefan equations in terms of volume fractions*, Polymer 52 (2011) 3970-3983.

[63] A. Verhoef, E. De Ridder, B. Bettens, J. Degrève, B. Van der Bruggena, *Maxwell-Stefan in mass fractions for numerical simulation of the pervaporation process*, Computer Aided Chemical Engineering Volume 26 (2009) 779-784.

[64] X. Liu, T.J.H. Vlugt, A. Bardow, *Predictive Darken Equation for Maxwell-Stefan Diffusivities in Multicomponent Mixtures*, Industrial & Engineering Chemistry Research 50 (2011) 10350-10358.

[65] B.E. Poling, J.M. Prausnitz, J.P. O'Connell, *The Properties of Gases and Liquids* 5th Edition ed., McGraw-Hill 2000.

[66] A. Raisi, A. Aroujalian, T. Kaghazchi, *A predictive mass transfer model for aroma compounds recovery by pervaporation*, Journal of Food Engineering 95 (2009) 305-312.

[67] D.W. van Krevelen, K. te Nijenhuis, *Properties of Polymers: Their Correlation with Chemical Structure; their Numerical Estimation and Prediction from Additive Group Contributions*, 4th edition ed., Elsevier Science 2009.

6 Prediction of styrene oligomer rejection curve by a silicone based membrane

Organic solvent nanofiltration (OSN) has the potential to be installed in a wide range of industrial processes, where it can generate substantial energy cost savings compared to conventional separation technologies. “One limitation to a more general use of this potential emerging technology is the lack of in-depth studies of performance capabilities [1]“. The importance of determining the mass transport of multicomponent mixtures through organic solvent nanofiltration membranes still draws attention of a wide academic community [2-6].

In this chapter a systematic study of styrene oligomer/solvent mass transport through the silicone membrane ONF-2 from GMT Membrantechnik will be presented. The membrane filtration experiments were performed in an Evonik Membrane Extraction Technology (EMET) stirred cell at room temperature and different transmembrane pressures. The evaluation of the membrane rejection results was made by applying the previously obtained Sherwood correlation for the EMET stirred filtration cell (see Chapter 3).

A simple mass transfer model based on the Maxwell-Stefan equation and the Free Volume theory for predicting Maxwell-Stefan diffusion coefficients was used. The volume fraction of the components in the PDMS membrane was calculated using the previously derived Flory-Rehner/Hansen chemical potential model for a surface attached film.

6.1 Theory

6.1.1 Mass transport model

The derivation of the Maxwell-Stefan model based on volume fraction [7, 8] is given in Appendix in detail. Considering only the component friction with the stationary membrane equation 62 is obtained.

$$\frac{1}{R \cdot T}\frac{\Delta \mu_i}{z_m} = -\frac{\overline{\phi_m}}{\overline{Đ_{i,m}}}\left(\frac{J_i}{\overline{\phi_i}}\right)\frac{\overline{V_{mix}^{mol}}}{V_{m,monomer}^{mol}} \qquad 62$$

Where μ_i is the chemical potential of component i, R is the universal gas constant and T the absolute temperature of the mixture. z_m is the total membrane separation layer thickness, $\overline{\phi_m}$ and $\overline{\phi_i}$ are the average volume fraction of membrane polymer and component i, respectively, J_i is the component volumetric flux and $V_{m,monomer}^{mol}$ is the molar volume of membrane monomer and the $\overline{V_{mix}^{mol}}$ average molar volume of the mixture.

The average molar volume of the mixture was calculated using the molar volume of the monomer unit as

$$\overline{V_{mix}^{mol}} = \left(\sum_i\left(\frac{\overline{\phi_i}}{V_i^{mol}}\right) + \frac{\overline{\phi_m}}{V_{m,monomer}^{mol}}\right)^{-1}. \qquad 63$$

Where the V_i^{mol} is the molar volume of component i.

The membrane thickness in case of one-dimensional swelling of a surface attached polymer film is reversely proportional to the volume fraction of polymer in the membrane as given in equation 64.

$$z_m = \frac{z_{m,dry}}{\overline{\phi_m}} \qquad 64$$

Where $z_{m,dry}$ is the membrane separation layer thickness in the dry state taken from the SEM images of the membrane cross-section. For the component activity in the feed and permeate mixture, the Flory-Huggins/Hansen model was applied [9]. The Flory-Rehner/Hansen model for a surface attached film was used for the calculation of component volume fractions in the membrane (see equation 65). Both models and their derivation can be found in Appendix.

$$\frac{\mu_i}{R \cdot T} = \frac{\mu_i^{mix,entropy}}{R \cdot T} + \frac{\mu_i^{mix,enthalpy}}{R \cdot T} + \frac{\mu_i^{elastic}}{R \cdot T} \quad with$$

$$\frac{\mu_i^{mix,entropy}}{R \cdot T} = \ln(\phi_i) + \sum_j \phi_j \left(1 - \frac{V_i^{mol}}{V_j^{mol}}\right)$$

$$\frac{\mu_i^{mix,enthalpy}}{R \cdot T} = 2 \cdot V_i^{mol} \sum_j (\phi_j \cdot a_{i,j}) - V_i^{mol} \sum_j \sum_k (\phi_j \cdot \phi_k \cdot a_{j,k}) \qquad 65$$

$$\frac{\mu_i^{elastic}}{R \cdot T} = \frac{V_i^{mol} \cdot \rho_m}{M_c} \left(1 - \frac{2 \cdot Mw_c}{Mw_o}\right)\left(\frac{1}{\phi_m} - \frac{\phi_m}{2}\right)$$

$$a_{i,j} = \frac{0.3}{R \cdot T}\left((\delta_i^d - \delta_j^d)^2 + 0.25(\delta_i^p - \delta_j^p)^2 + 0.25(\delta_i^h - \delta_j^h)^2\right)$$

Where δ_i^d, δ_i^p and δ_i^h are dispersion, polar and hydrogen-bonding Hansen solubility parameters (HSP) of component i, respectively, $a_{i,j}$ is the symmetrical interaction parameter, Mw_c is the molecular weight of sub-chains of in the polymer network molecule between two crosslinks, Mw_o is the molar weight of oligomer before crosslinking and ρ_m is the polymer mass density.

For the definition of boundary conditions the local chemical potential equilibrium

at the membrane surface and constant feed pressure in the separation layer were assumed. The boundary conditions and average volume fraction in the membrane are given in equation 66.

$$\frac{\mu_{\alpha,i}}{R\cdot T}=\frac{\mu_{fm,i}}{R\cdot T} \qquad \text{feed side}$$

$$\frac{\mu_{\beta,i}}{R\cdot T}=\frac{\mu_{p,i}}{R\cdot T}-\frac{\Delta p\cdot V_i^{mol}}{R\cdot T} \qquad \text{permeate side} \qquad (66)$$

$$\overline{\phi_{m,i}}=\frac{\phi_{\alpha,i}-\phi_{\beta,i}}{\ln\left(\frac{\phi_{\alpha,i}}{\phi_{\beta,i}}\right)} \qquad \text{logarithmic average volume fraction}$$

The $\mu_{fm,i}$ and $\mu_{p,i}$ are chemical potentials in the feed at the membrane surface and in the permeate, respectively. Whereas $\mu_{i,\alpha}$ and $\mu_{i,\beta}$ are chemical potentials of component i in the membrane at feed and permeate side, respectively. Analogous, $\phi_{i,\alpha}$ and $\phi_{i,\beta}$ are volume fractions of component i in membrane at feed and permeate side, respectively. The Δp stands for the transmembrane pressure ($\Delta p>0$).

As evident from the Flory-Rehner/Hansen model given in equation 65, HSP for solvent, styrene oligomers, PDMS and several other membrane parameters are required within the model. As found in the previous Chapter 5, the PDMS parameters for the membrane separation layer are given in Table 10.

Table 10: Separation layer properties of ONF-2 membrane.

δ_m^d	δ_m^p	δ_m^h	Mw_c	ρ_m	$z_{m,dry}$
	[(MPa)$^{0.5}$]		[kg·mol^{-1}]	[kg·m^{-3}]	[μm]
14.8	-5.4	5.2	3.0	1.014	2.75

For all styrene oligomers a single set of HSP was assumed, which is equal to polystyrene. For polystyrene several HSP can be found in literature [10-12].

To determine the most suitable set of parameters for styrene oligomers, swelling experiments of a PDMS sheet with α-methylstyrene dimer, a component similar to styrene oligomers, were performed. The experimentally obtained volume fraction of α-methylstyrene dimer in the PDMS sheet was further compared with the predicted volume fraction of polystyrene. The Flory-Rehner/Hansen model for free standing polymer sheet (see Appendix) was used for the prediction of the polystyrene volume fraction in the PDMS sheet. For the polystyrene properties different sets of solubility parameters [10-12] and the molar volume of α-methylstyrene dimmer were used. The relative difference of measured volume fraction and predicted polystyrene volume fraction is given in Table 11. The HSP and molar volumes of the solvents can be found in literature [11].

Table 11: Relative difference of component volume fraction in a PDMS sheet: measured for α-methylstyrene dimer and predicted for polystyrene with the same molar volume.

δ_{PS}^{d}	δ_{PS}^{p}	δ_{PS}^{h}	Relative difference	Reference
	[(MPa)$^{0.5}$]		[%]	
18.1	1.9	2.8	0.07	[10]
18.34	1.0	3.3	18.53	[10]
17.6	6.1	4.1	-69.05	[10]
19.2	0.9	2.0	-38.43	[10]
18.5	4.5	2.9	-65.01	[11]
22.28	5.75	4.3	-98.23	[11]
17.9	4.2	5.0	-42.51	[12]

6.2 Experimental

6.2.1 Styrene oligomer solution

The styrene oligomer solution was made from solvent and approximately 2.1 g·L^{-1} of styrene oligomers (0.1 g·L^{-1} α-methyl styrene dimer, 1 g·L^{-1} polystyrene standard PS580, and 1 g·L^{-1}polystyrene standard PS1000) [13]. Because of limited polystyrene solubility for some solvents the concentration was reduced. The polystyrene would be weighted and stirred for one day to obtain a saturated solution. Afterwards the clear solution was decanted and diluted with the same weight of pure solvent, resulting in a concentration which is half saturated.

6.2.2 Filtration experiments

The filtration experiments were made at approximately 23 °C in the previously described stirred cell from EMET (see Chapter 3). Before and after operating with a styrene oligomer mixture the membrane was ran in pure solvent until a steady state flux was obtained and the previous solvent was completely removed from the cell. Subsequently the feed solution was replaced with approximately 250 mL of styrene oligomer solution. Permeate and retentate samples were taken after approximately 70 mL of permeate were collected. The analytic tools used for determining styrene oligomer concentration are described in Chapter 3. The membrane rejection was calculated using stagnant film concentration polarisation and the previously derived Sherwood correlation for the EMET stirred cell (see Chapter 3). The real membrane rejections of styrene oligomers are given in Figure 35 and measured solvent permeabilities in Figure 36.

6.3 Results and discussion

The Free Volume theory [7, 14] can be applied to multicomponent mixtures to predict Maxwell-Stefan diffusion coefficients. The complete set of Free Volume theory equations and the prediction accuracy of the Free Volume theory were shown in the previous Chapter 5. In this chapter, next to the solvent's Maxwell-Stefan diffusion coefficients also the diffusion coefficients of styrene oligomers will be predicted.

The free volume parameters for styrene oligomers were determined as follows: a) the minimal molar volume ($V^{\bullet}$) of the styrene oligomers was calculated using the expression of Bondi and a group contribution method for Van der Waals molar volume [15] and b) the overlap factor (λ) for styrene oligomers is assumed to be 0.7 (see Chapter 5). An overview of the assumed membrane and styrene oligomer free

volume parameters is given in Table 12.

Table 12: PDMS and styrene oligomer free volume parameters.

	λ	$V^{\bullet}$
	[-]	[$cm^3 \cdot mol^{-1}$]
Membrane monomer	0.7	60.2
Styrene oligomer	0.7	$1.3 \cdot V_{oligomer}^{VdW}$

In Figure 35 the comparison of measured (symbols) and predicted (lines) real membrane rejection of styrene oligomers at 30 bar, 20 bar and 10 bar for all used solvents is given.

Figure 36 shows the measured and predicted mixture permeabilities for 30 bar, 20 bar and 10 bar transmembrane pressure.

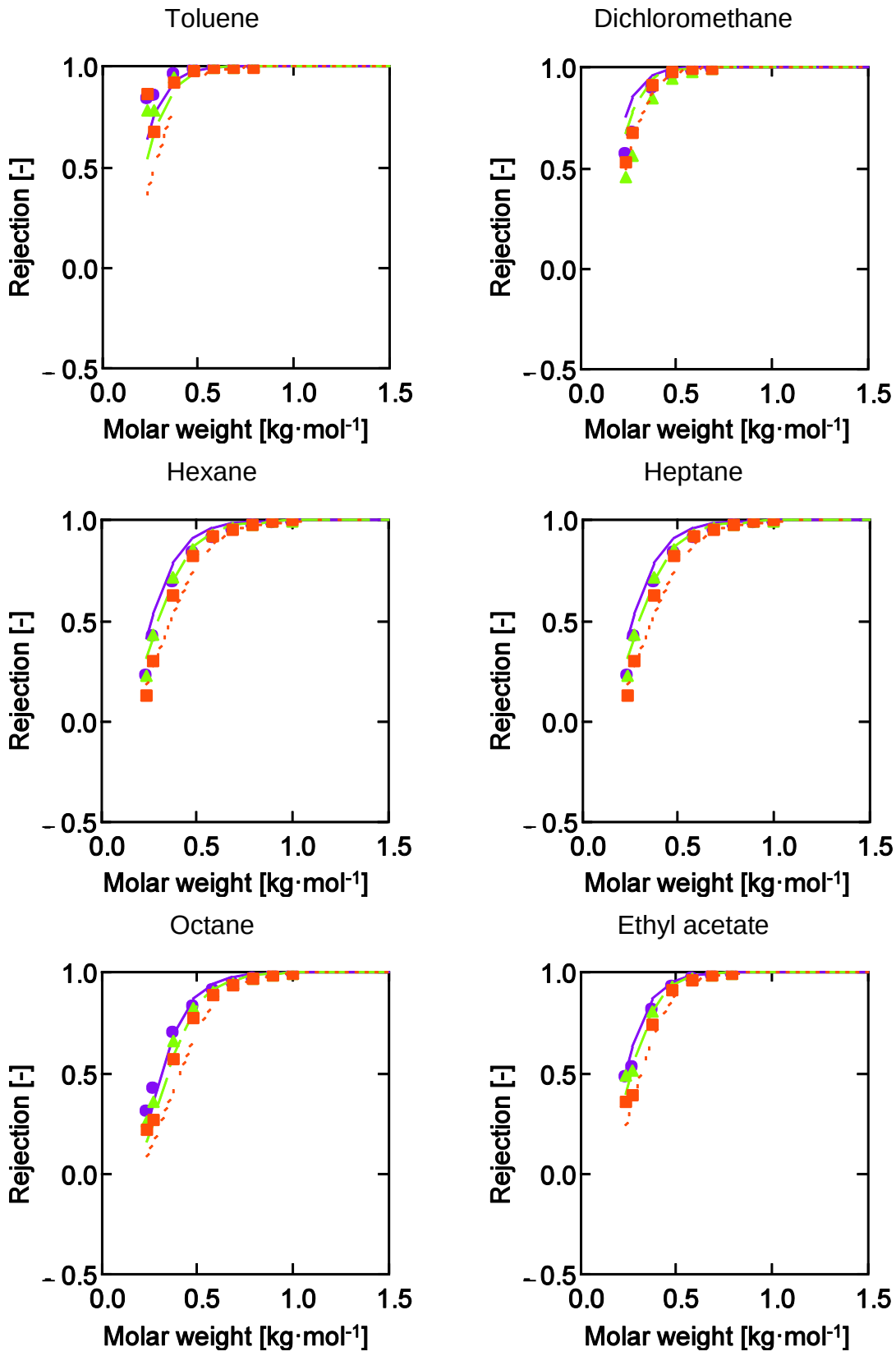
Toluene
Dichloromethane
Hexane
Heptane
Octane
Ethyl acetate
Rejection [-]
Molar weight [kg·mol-1]
1.0
0.5
0.0
-0.5
0.0
0.5
1.0
1.5

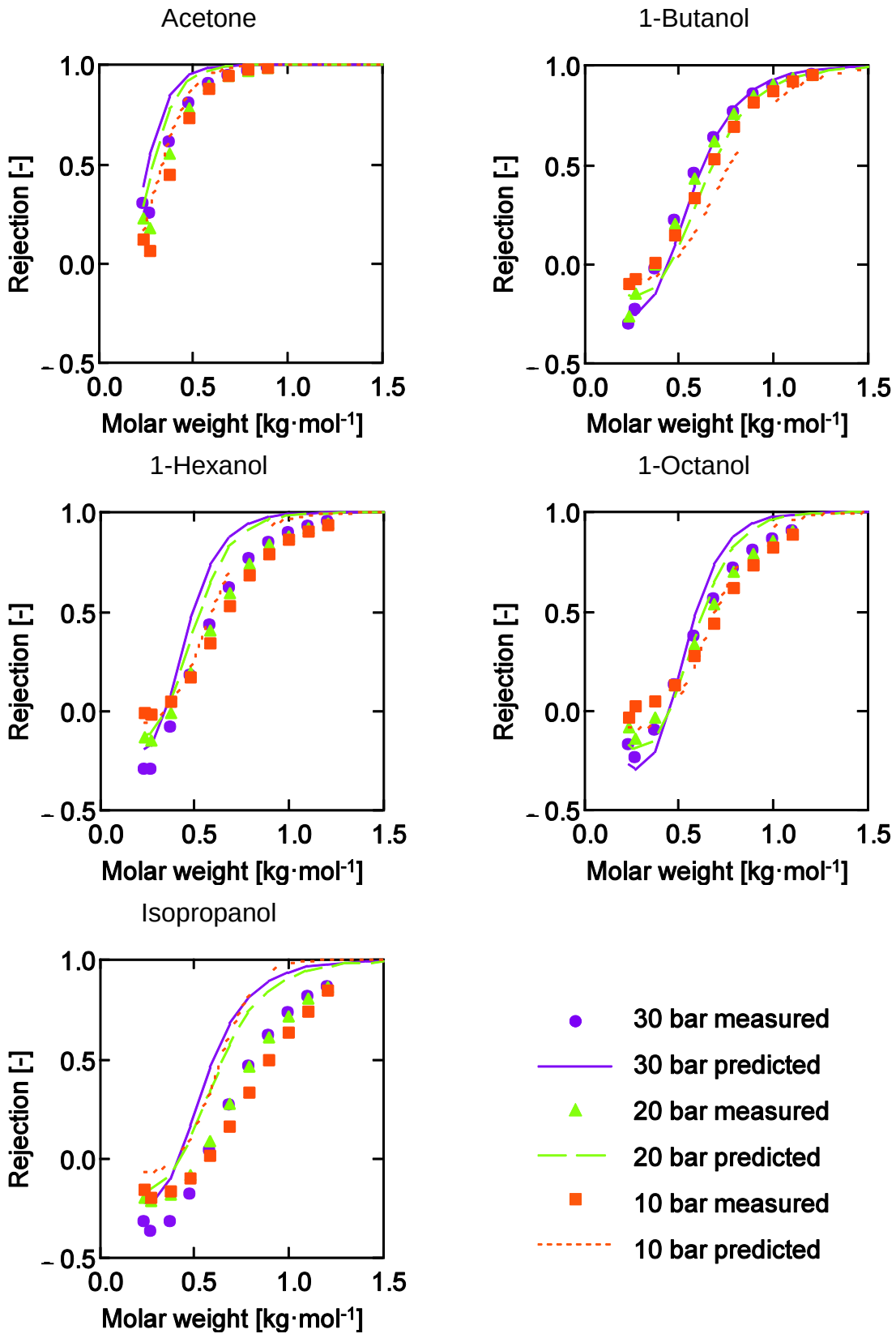

Figure 35: The measured and predicted styrene oligomer rejection of ONF-2 membrane at 23 °C and 10 bar, 20 bar and 30 bar.

Toluene

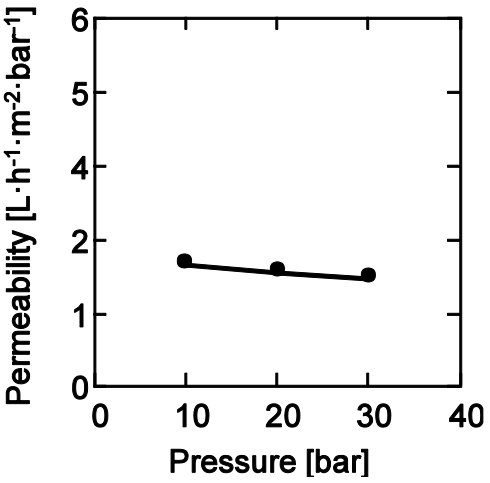

Dichloromethane

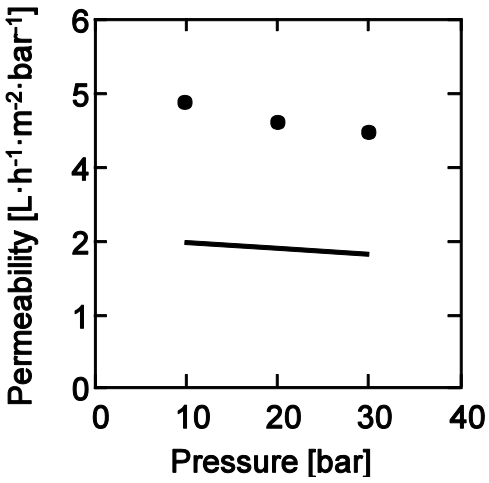

Hexane

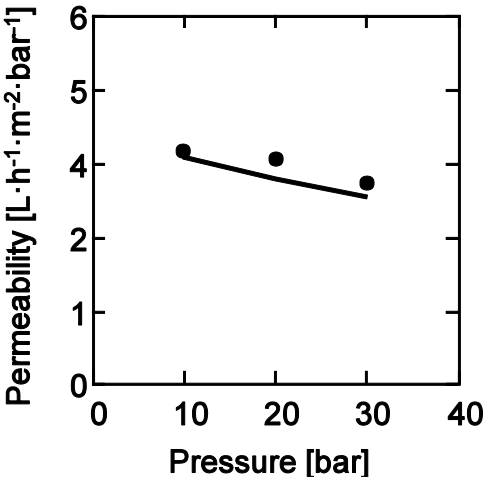

Heptane

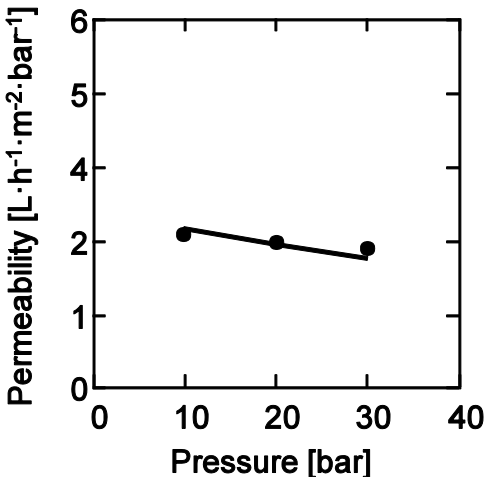

Octane

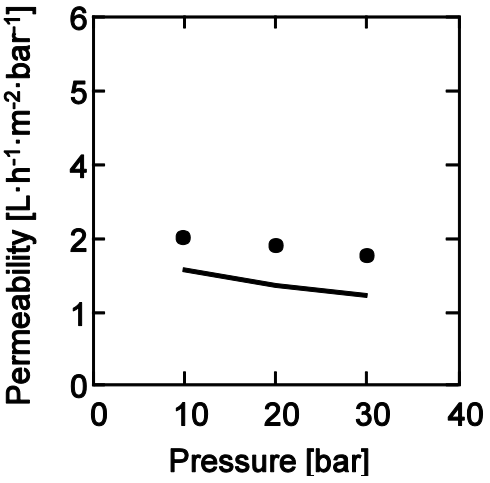

Ethyl acetate

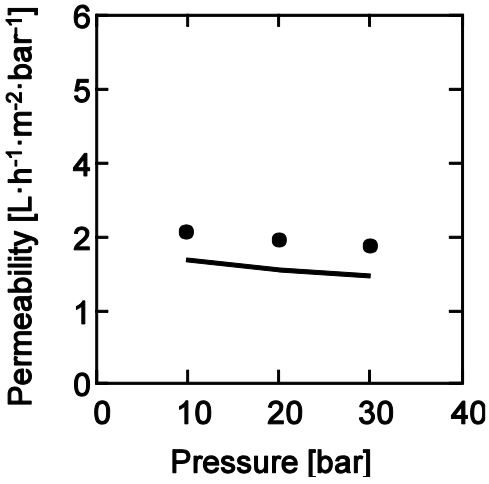

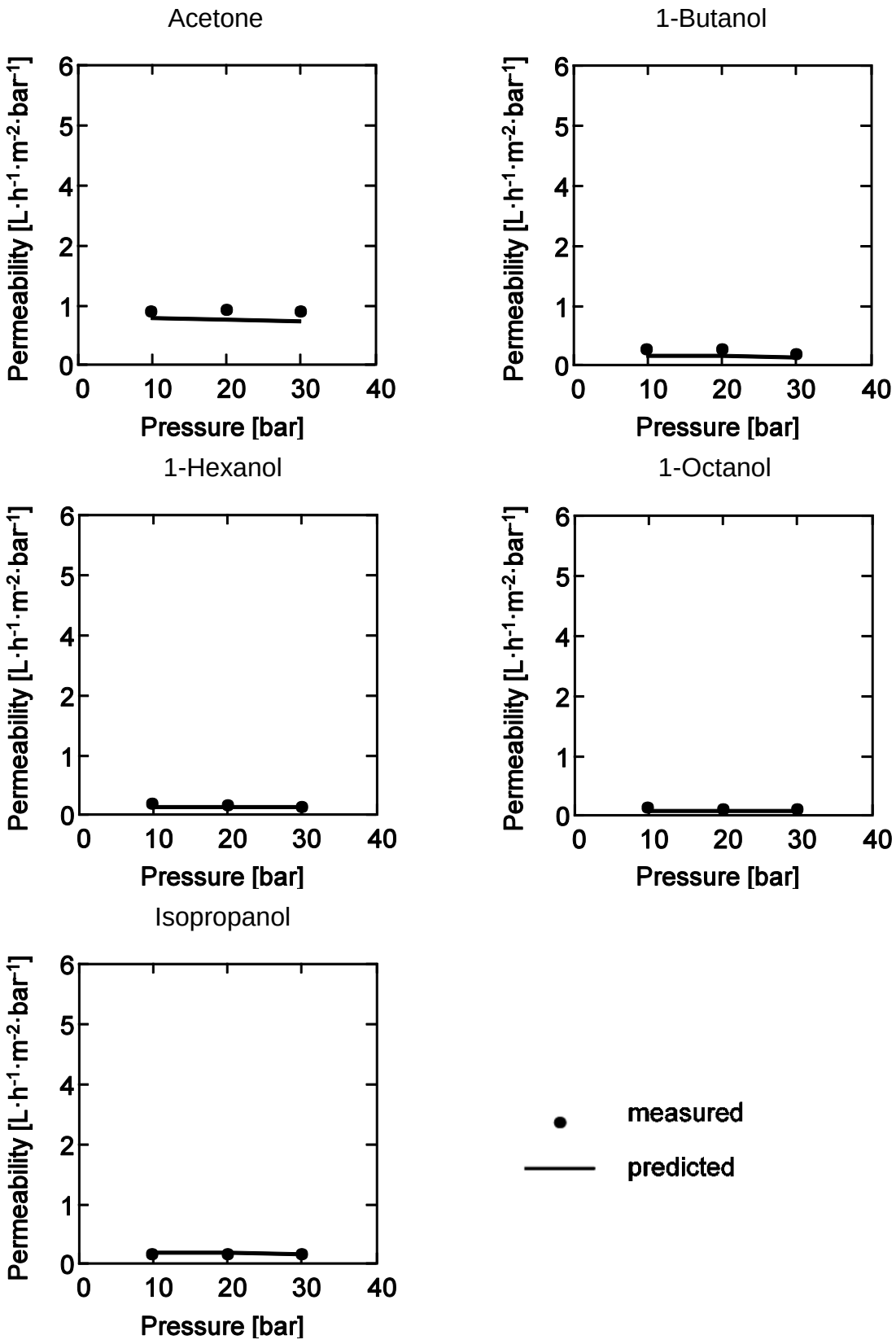

Figure 36: Measured and predicted permeabilities of ONF-2 membrane at 23 °C and 10 bar, 20 bar and 30 bar.

For most of the solvents, as given in Figure 35 and Figure 36, good prediction accuracy of the measured data was achieved. Supporting the hypothesis made that the most relevant resistance in the transport of large diluted styrene oligomers through the membrane is the membrane styrene oligomer friction. The influence of solvent on styrene oligomer transport is introduced by the increase of the total free volume of the system and the consequent increase of the Maxwell-Stefan diffusion coefficient as well as reducing the volume fraction of the polymer in the membrane.

From the rejection curves given in Figure 35, it can also be observed that the largest prediction error is made for alcohols. This discrepancy can originate from extreme mixture non-ideality, which can further lead to errors in the prediction of the partition coefficient of styrene oligomers between feed and membrane [16]. The over-prediction of styrene oligomer rejections in weak solvents, such as isopropanol, could also be a consequence of the solvent clustering in the membrane, which was not considered in the used chemical potential models [17]. Further, the correct prediction of the available free volume and hence diffusion of styrene oligomers is influenced by free volume parameters chosen for the solvent and membrane [18]. Since alcohols build hydrogen bonds, an appropriate overlap factor and minimal molar volume cannot be determined easily (see Chapter 5).

The measured rejection curves in tested alcohols (see Figure 35) show also negative values for styrene oligomers in lower molecular weight range. The negative rejections were also predicted by the applied mass transport model. Meaning, even if the concentration of the oligomer was higher in the permeate then in the feed, the applied transmembrane pressure resulted in positive values of the driving force.

Investigations of possible reasons for negative rejection calculations were made for a isopropanol mixture, in which the hydrogen bonding HSP of the isopropanol was varied. Figure 37 shows the rejection curves for isopropanol with literature value of hydrogen bonding HSP of 16.4 $(MPa)^{0.5}$, isopropanol with reduced hydrogen

bonding HSP to 14 $(MPa)^{0.5}$ and isopropanol with hydrogen bonding HSP reduced to 10 $(MPa)^{0.5}$.

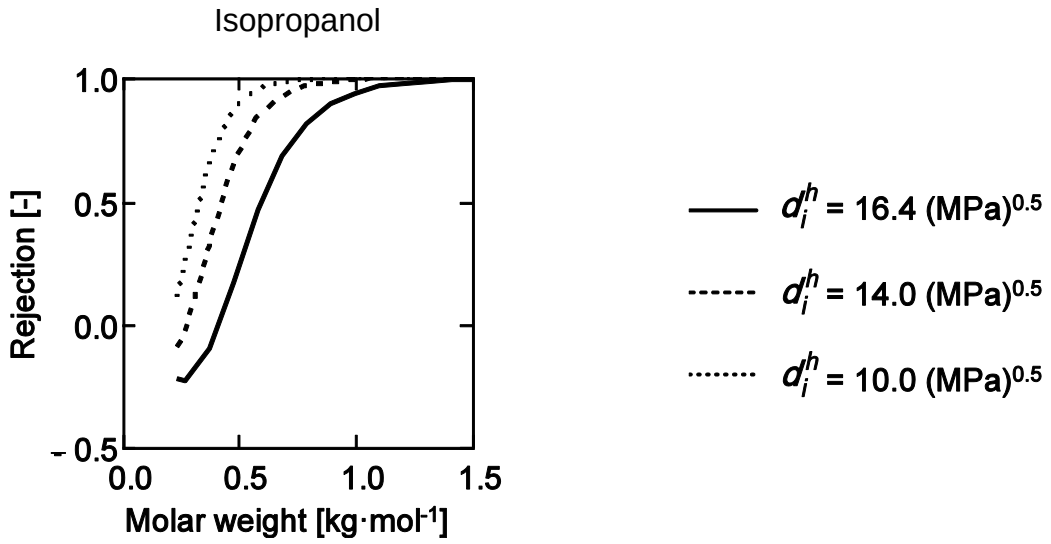

Figure 37: Predicted styrene oligomer rejection of ONF-2 membrane at 23 °C and 30 bar for isopropanol with different values of hydrogen bonding HSP.

As being observed in Figure 37, the rejection increases with reduced values of hydrogen bonding HSP, which suggests that negative rejection is caused by the low affinity of the isopropanol for styrene oligomers and silicone membrane.

6.4 Conclusion

Over all, the derived Flory-Rehner/Hansen model for surface attached polymer films combined with the Maxwell-Stefan/Free Volume theory could be used to predict the styrene oligomer rejections by a silicone membrane ONF-2 in different solvents. The assumptions made in the derived equations were proved to be valid for the used styrene oligomer solutions and cannot be generalised without further investigation of other mixtures. However, the Flory-Rehner/Hansen model combined with the Maxwell-Stefan/Free Volume theory could serve as a starting point in the development of purely predictive membrane transport models.

Future work could investigate if the derived Flory-Rehner/Hansen model can be applied on predicting PDMS swelling in solvent mixtures. Likewise, the applicability of the used simple form of the Maxwell-Stefan/Free Volume model could also be tested for predicting separation performance of solutions with higher solute concentration.

6.5 List of symbols

$a_{i,j}$	symmetrical interaction parameter between components i and j	$mol \cdot m^{-1}$
d_i	minimal molecule diameters	m
J_i	volumetric flux of component i	$m \cdot s^{-1}$
Mw_c	molar weight of subchains between two crosslinks	$kg \cdot mol^{-1}$
Mw_o	molar weight of oligomer before crosslinking	$kg \cdot mol^{-1}$
Δp	transmembrane pressure	Pa
R	the universal gas constant	$J \cdot K^{-1} \cdot mol^{-1}$
T	absolute temperature	K
V_i^{mol}	molar volume of component i	$m^3 \cdot mol^{-1}$
V_m^{mol}	molar volume of membrane polymer	$m^3 \cdot mol^{-1}$
$\overline{V_{mix}^{mol}}$	average molar volume of the mixture	$m^3 \cdot mol^{-1}$
$V_{m,monomer}^{mol}$	monomer molar volume	$m^3 \cdot mol^{-1}$
$V_{m,monomer}^{\bullet}$	minimal molar volume of monomer	$m^3 \cdot mol^{-1}$
$V_{m,monomer}^{VdW}$	Van der Waals molar volume of monomer	$m^3 \cdot mol^{-1}$

z_m	total membrane separation layer thickness	m
$z_{m,dry}$	thickness of the dry membrane separation layer	m
$\overline{Đ_{i,m}}$	average molar Maxwell-Stefan diffusion coefficients of component i and the membrane	$m^2 \cdot s^{-1}$

Greek symbols

δ_i^d	dispersion Hansen solubility parameter of component i	$(Pa)^{0.5}$
δ_i^p	dipole Hansen solubility parameter of component i	$(Pa)^{0.5}$
δ_i^h	hydrogen bonding Hansen solubility parameter of component i	$(Pa)^{0.5}$
λ_i	overlap factor	-
μ_i	total chemical potential of component i in the mixture	$J \cdot mol^{-1}$
$\mu_i^{mix,entropy}$	chemical potential contribution term of mixing entropy	$J \cdot mol^{-1}$
$\mu_i^{mix,enthalpy}$	chemical potential contribution term of mixing enthalpy	$J \cdot mol^{-1}$
$\mu_i^{elastic}$	elastic chemical potential contribution term of mixing enthalpy	$J \cdot mol^{-1}$
ρ_m	membrane mass density	$kg \cdot m^{-3}$
ϕ_i	the volume factions of component i	-
$\overline{\phi_i}$	average volume fraction of component i in the membrane	-

Indices

m	membrane polymer
α	membrane polymer near feed surface
β	membrane polymer near permeate surface

6.6 References

[1] E. Favre, P. Schaetzel, Q.T. Nguygen, R. Clément, J. Néel, *Sorption, diffusion and vapor permeation of various penetrants through dense poly(dimethylsiloxane) membranes: a transport analysis*, Journal of Membrane Science 92 (1994) 169-184.

[2] U.K. London, *3rd International Conference on Organic Solvent Nanofiltration*, 2010.

[3] G. Aachen, *4th International Conference on Organic Solvent Nanofiltration*, 2013.

[4] L. Hesse, J. Mićović, P. Schmidt, A. Górak, G. Sadowski, *Modelling of organic-solvent flux through a polyimide membrane*, Journal of Membrane Science 428 (2013) 554-561.

[5] S. Zeidler, U. Kätzel, P. Kreis, *Systematic investigation on the influence of solutes on the separation behavior of a PDMS membrane in organic solvent nanofiltration*, Journal of Membrane Science 429 (2013) 295-303.

[6] P. Schmidt, T. Köse, P. Lutze, *Characterisation of organic solvent nanofiltration membranes in multi-component mixtures: Membrane rejection maps and membrane selectivity maps for conceptual process design*, Journal of Membrane Science 429 (2013) 103-120.

[7] J.A. Wesselingh, R. Krishna, *Mass transfer in multicomponent mixtures*, Delft University Press 2000.

[8] C.P. Ribeiro Jr, B.D. Freeman, D.R. Paul, *Modeling of multicomponent mass transfer across polymer films using a thermodynamically consistent formulation of the Maxwell–Stefan equations in terms of volume fractions*, Polymer 52 (2011) 3970-3983.

[9] T. Lindvig, I.G. Economou, R.P. Danner, M.L. Michelsen, G.M. Kontogeorgis, *Modeling of multicomponent vapor–liquid equilibria for polymer–solvent systems*, Fluid Phase Equilibria 220 (2004) 11-20.

[10] R. Mieczkowski, *The determination of the solubility parameter components of polystyrene by partial specific volume measurements*, European Polymer Journal 24 (1988) 1185-1189.

[11] C.M. Hansen, *Hansen Solubility Parameters: A Users Handbook*, 2nd ed., CRC Press 2007.

[12] A. Imre, W.A. Van Hook, *Erratum: Liquid - Liquid Demixing from Solutions of Polystyrene. 1. A Review. 2. Improved Correlation with Solvent Properties*, Journal of Physical and Chemical Reference Data 25 (1996) 1277.

[13] Y.H. See Toh, X.X. Loh, K. Li, A. Bismarck, A.G. Livingston, *In search of a standard method for the characterisation of organic solvent nanofiltration membranes*, Journal of Membrane Science 291 (2007) 120-125.

[14] J.A. Wesselingh, A.M. Bollen, *Multicomponent Diffusivities from the Free Volume Theory*, Chemical Engineering Research and Design 75 (1997) 590-602.

[15] D.W. van Krevelen, K. te Nijenhuis, *Properties of Polymers: Their Correlation with Chemical Structure; their Numerical Estimation and Prediction from Additive Group Contributions*, 4th edition ed., Elsevier Science 2009.

[16] R.P. Danner, M.S. High, *Handbook of Polymer Solution Thermodynamics*, Wiley 1993.

[17] E. Favre, Q.T. Nguyen, D. Sacco, A. Moncuy, R. Clement, *Multicomponent polymer/solvents equilibria: An evaluation of Flory-Huggins theory for crosslinked PDMS networks swelled by binary mixtures*, Chemical Engineering Communications 140 (1995) 193-205.

[18] D. Fierro, N. Scharnagl, T. Emmler, A. Boschetti-de-Fierro, V. Abetz, *Experimental determination of self-diffusivities through a polymer network for single components in a mixture*, Journal of Membrane Science 384 (2011) 63-71.

7 Acrylate-functional and epoxy-functional silicone membranes

In the recent years progress in membrane production was made, making it possible to produce solvent stable membranes rejecting molecules with a molar mass of more than 500 $g \cdot mol^{-1}$ while solvents such as alcohols, ketones, aliphatic and aromatics were able to pass. With the availability of new organic solvent nanofiltration (OSN) membranes interest in this technology grows continuously. So far, organic solvent nanofiltration membranes have found use in food chemistry, petrochemistry, catalysis and pharmaceutical manufacturing [1, 2].

Silicone based composite membranes have demonstrated good thermal and chemical stability and are highly permeable. Silicone membranes have a great industrial relevance in energy and waste efficient processes [3]. The disadvantage of silicone based composite membranes is excessive swelling in some organic solvents [4-6] and the loss of separation performance as recognised by a decrease in rejection.

Evonik Industries AG provides a variety of radiation curable acrylate-functional silicone and epoxy–functional silicone resins [7]. Both, acrylate–functional silicone and epoxy–functional silicone coatings are resistant to many organic solvents [8]; therefore they could be suitable for production of organic solvent nanofiltration membranes [9].

In the research presented in this chapter composite membranes consisting of acrylate–functional silicones (SA) and epoxy–functional silicones (SE) [7] separation layers coated on commercially available ultrafiltration membrane were produced and tested. It was observed that mixing acrylate-functional resins of different

values of unmodified siloxy units or epoxy-functional resins with different values of unmodified siloxy units can be used to influence the performance of the final silicone composite membrane [9].

7.1 Experimental

7.1.1 Membrane production

A commercially available ultrafiltration membrane (L-6 from GMT Membrantechnik) based on poly(acrylonitrile) was used as supporting membrane. Acrylate–functional and epoxy–functional silicone resins and the necessary coating technology and procedure were kindly provided by and made at Evonik Industries AG in Essen [8].

A general description of acrylate–functional silicone resins produced by Evonik Industries AG, taken from patent literature [10], is given in Figure 38.

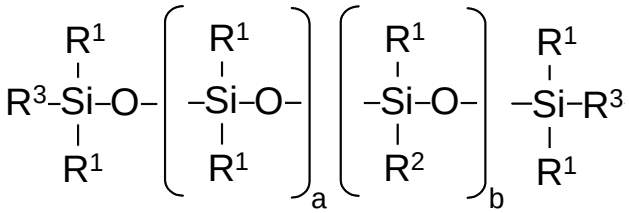

Figure 38: General molecular formula of Evonik Industries AG acrylate-functional silicone resins, taken from [10].

"R^1 is identical or different aliphatic or aromatic hydrocarbon radicals of 1 to 10 carbon atoms, R^2 is a linear, branched or aromatic hydrocarbon radical of 1 to 20 carbon atoms, with or without ether bridges, to which there are attached, by way of ester linkages, from 1 to 5 acrylic and/or methacrylic acid units and, optionally, monocarboxylic acid units of 2 to 10 carbon atoms which are free of polymerizable double bonds, R^3 is R^1 or R^2, a is 0 to 300, b is 1 to 25, and c is 5 to 50." [10].

An exemplary description of epoxy–functional silicone resins is given in Figure 39 [11].

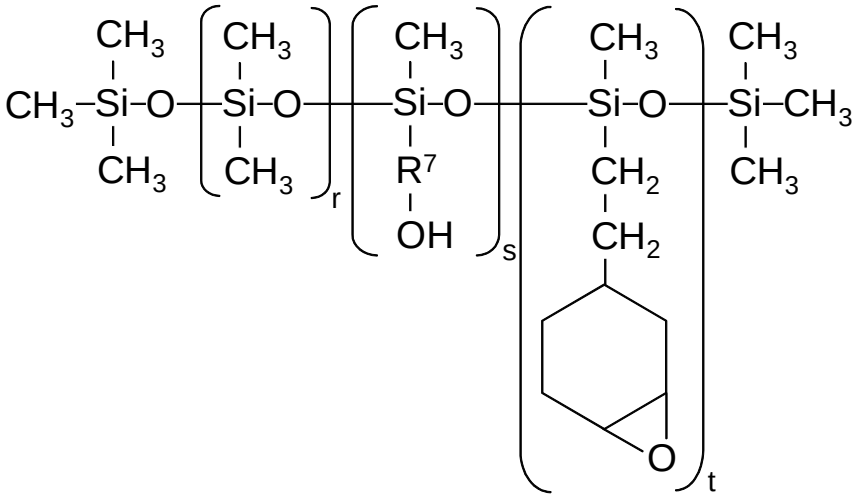

Figure 39: General molecular formula of Evonik Industries AG epoxy-functional silicone resins, taken from [11].

“In which R7 are identical or different alkenyl groups having 2 to 20 carbon atoms and my contain ether, ester, urethane or amide groups; r is 5 to 300, preferably 5 to 200; s is 0, 1 to 100, preferably 0, 1 to 10 and t is 1 to 100, preferably 2 to 40.”[11].

7.1.2 Coating procedure

For the maximal anchorage of the coated silicone, the ultrafiltration membrane was treated by corona directly before coating. The silicone resins were applied to the substrate via a five roll coating system [7].

Next to the acrylate-functional and epoxy-functional silicone oligomers the radiation cured resins contain a photoinitiator. Generally, the level of photoinitiator is approximately 2 % [7].

The crosslinking of acrylate-functional silicones is started with photoinitiator decomposition under UV light exposure, releasing a high number of radicals. The chain propagation continues until all free acrylic groups have reacted. However, the radical centre can be quenched by the presence of oxygen, therefore good inerting of the UV radiation chamber with nitrogen is necessary for coating with acrylate-functional silicones [8].

In the case of epoxy-functional silicone resins, the added photoinitiator starts a cationic polymerisation chain reaction. Hence, the chain propagation of epoxy-functional silicones is not inhibited by the presence of oxygen radicals and no nitrogen inertisation is needed. The cationic polymerisation reaction can be poisoned by the presence of Lewis bases in the substrate [8], limiting the choice of possible substrates.

The used UV lamp delivers 120 W/cm, which was sufficient for insuring complete cure of both, acrylate-functional and epoxy-functional silicone coated substrates.

For the production of acrylate-functional silicone composite membranes (SA) mixtures of two acrylate-functional silicone resins were used: One comb-like silicone with a low value of unmodified siloxy units (A) and one linear silicone with a high value of unmodified siloxy units (B).

Mixtures of two epoxy-functional silicone resins were used for production of epoxy-functional silicone membranes (SE). Both epoxy-functional silicone resins are comb-like, one having a low value of unmodified siloxy units (C) and one epoxy-functional silicone having a high value of unmodified siloxy units (D).

By mixing of silicone resins with low and high values of unmodified siloxy units, it was possible to investigate the influence of the ratio of unmodified to modified siloxy units on the membrane performance.

7.1.3 Dye stain test

The dye stain test is used to check for the uncoated areas of siliconised paper, but the test could be adapted to investigate the silicone coverage of the porous, relatively hydrophilic ultrafiltration support. The dye stain includes application of test ink for one minute onto the silicone coated surface. The test ink contains 1 weight % methylene blue in water. The applied blue ink will stain any uncoated areas of the support [8].

7.1.4 Filtration experiments

Heptane of technical purity was used as a solvent for filtration experiments. The styrene oligomer/heptane mixture containing approximately 2.1 $g \cdot L^{-1}$ of styrene oligomers (0.1 $g \cdot L^{-1}$ α-methyl styrene dimer, 1 $g \cdot L^{-1}$ polystyrene standard PS580, and 1 $g \cdot L^{-1}$polystyrene standard PS1000) was used as feed for membrane characterisation experiments. The analytical tools for determining the concentration of styrene oligomers in heptane are given in Chapter 3.

For the filtration experiments a cross flow setup was used (see Chapter 3). Filtration experiments were made at 30 bar transmembrane pressure and 30 °C temperature. The recirculation flow rate for all three membrane cells was 700 $L \cdot h^{1}$. Membrane conditioning was made with pure solvent for one day at 30 bar and 30 °C. After this step pure solvent was replaced by heptane with a styrene oligomer mixture. After 1 day of running with styrene oligomer mixtures the samples of permeate and retentate were taken. The conditioning and sampling procedure were similar for all membrane samples. The real membrane styrene oligomer rejections was evaluated using a Sherwood correlation for rectangular channels [12]. The complete set of equations is given in Chapter 3.

7.2 Results and discussion

The membranes with acrylate-functional and epoxy-functional silicone resins were produced in two successive coating steps. The minimal necessary coating weight for obtaining complete coverage of the support was determined by dye stain test on smaller substrates previous to the membrane production.

7.2.1 Acrylate-functional silicone membranes

Membrane compositions produced with comb-like acrylate-functional silicone A, with low value of unmodified siloxy units, and linear acrylate-functional silicone B, with high value of unmodified siloxy units, are given in Table 13 [9].

Table 13: Produced acrylate-functional silicone membranes and their compositions.

Membrane	SA1	SA2	SA3	SA4
Composition	100 % A	30 % A / 70 % B	20 % A / 80 % B	10 % A / 90 % B

The styrene oligomer membrane rejection curves of the produced acrylate-functional silicone membranes are analysed in comparison to the measured performance of the commercial silicone membrane ONF-2.

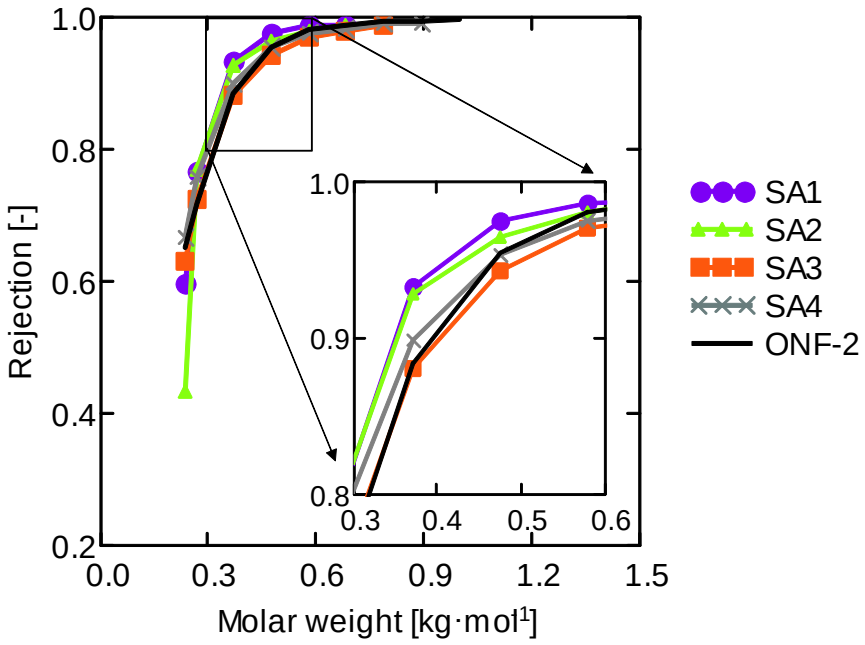

Figure 40: Styrene oligomer rejections of acrylate-functional silicone membranes and the commercial silicone membrane ONF-2.

From the rejection curves in Figure 40 it can be observed that all membranes produced with acrylate-functional silicone resins have slightly better or comparable rejection values than the commercial silicone membrane ONF-2. The measured heptane permeabilities at 30 bar and 30 °C are given in Table 14.

Table 14: Heptane permeabilities of the produced acrylate-functional silicone membranes and the commercial silicone membrane ONF-2.

Membrane	SA1	SA2	SA3	SA4	ONF-2
Permeability [$L \cdot h^{-1} \cdot m^{-2} \cdot bar^{-1}$]	0.248	0.322	1.40	3.22	4.40

The higher fraction of acrylate-functional silicone A in the membrane separation layer resulted in a higher rejection of styrene oligomers and a poor permeability (see SA1). On the other hand, the acrylate-functional silicone membrane with a high fraction of acrylate-functional silicone B had a lower rejection and a higher permeability

(see SA4). The other mixtures of these two polymers fall between the two extremes with respect to rejection and permeability. This result gives the possibility to tune the desired rejection in the range between performance of A and B acrylate-functional silicone membranes [12].

7.2.2 Epoxy-functional silicone membranes

The tested mixtures of epoxy-functional silicone C with low value of unmodified siloxy units and epoxy-functional silicone D, with high value of unmodified siloxy units are shown in Table 15.

Table 15: Produced epoxy-functional functional membranes and their compositions.

Membrane	SE1	SE2	SE3
Composition	70 % C / 30 % D	35 % C / 65 % D	100 % C

Like the produced acrylate-functional silicone membranes in Figure 40, the styrene oligomer rejection curves of the produced epoxy-functional silicone membranes are shown in comparison with the commercial silicone membrane ONF-2 in Figure 41.

From the styrene oligomer rejection curves in Figure 41 it could be observed that a higher fraction of epoxy-functional silicone C resulted in a reduced rejection of styrene oligomers.

The measured heptane permeabilities of the produced epoxy-functional silicone membranes and the commercial silicone membrane are given in Table 16.

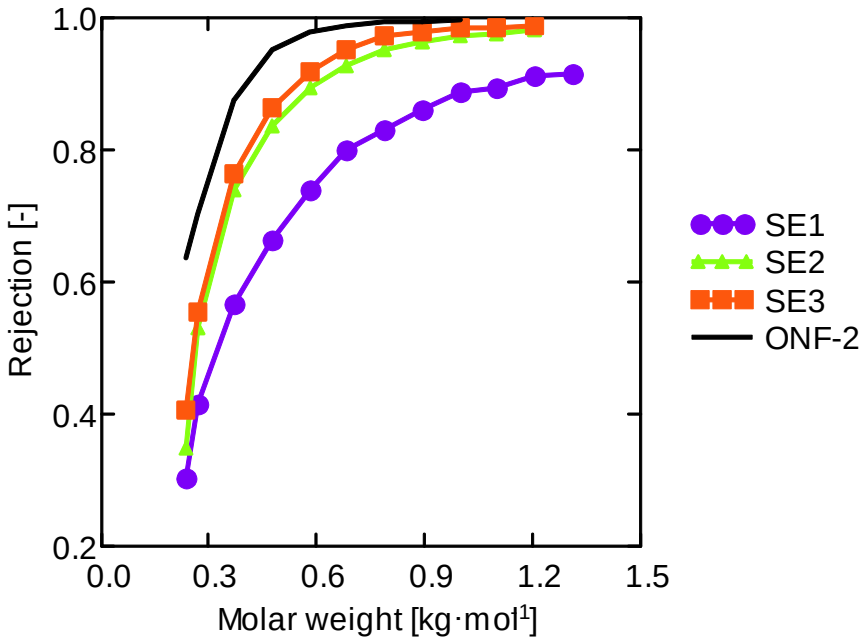

Figure 41: Styrene oligomer rejections of epoxy-functional silicone membranes and the commercial silicone membrane ONF-2.

Table 16: Heptane permeabilities of the produced epoxy-functional silicone membranes and the commercial silicone membrane ONF-2.

Membrane	SE1	SE2	SE3	ONF-2
Permeability [$L \cdot h^{-1} \cdot m^{-2} \cdot bar^{-1}$]	6.97	5.49	4.08	4.40

The produced epoxy-functional silicone membranes have generally high permeabilities as shown in Table 16. The epoxy-functional silicone membranes SE2 and SE3 have lower rejections compared to ONF-2, while the permeabilities are comparable or larger. Since the degree of modification of acrylate-functional silicone B is higher than modification of epoxy-functional silicone D, the lower rejection and higher permeability of epoxy-functional membranes compared to acrylate-functional membranes was expected.

The SE1 membrane produced with a low value of unmodified siloxy units has a significantly lower styrene oligomer rejection, which does not reach rejections higher

than 95 % for the measured molar weights of styrene oligomers. The high permeability and low rejection of SE1 could be explained by possible imperfections in the silicone epoxy separation layer, which could not be detected by the dye stain test.

7.3 Conclusion

Acrylate-functional silicone composite membranes were produced using mixtures of a comb-like structure A, with low value of unmodified siloxy units, and linear structure B, with high value of unmodified siloxy units [12]. Epoxy-functional silicone composite membranes consisting of mixtures of two comb-like structures with a low value of unmodified units (C) and a high value of unmodified units (D) were produced. The separation performance of acrylate-functional silicone and epoxy-functional silicone membranes was determined by measuring styrene oligomer rejection curves and permeabilities in heptane at 30 bar and 30 °C. Experimental results indicate that the use of acrylate-functional and epoxy-functional silicone resins composite membranes can lead to membranes with a tuneable performance. Acrylate-functional and epoxy-functional silicone membranes cover broad ranges of rejection and permeability. Compared to the commercially available silicone based membrane ONF-2, the acrylate-functional silicone membranes have a higher rejection performance and lower heptane permeability. Whereas, the epoxy-functional membranes have a lower rejection and a comparable or higher heptane permeability compared to the ONF-2 silicone membrane.

7.4 References

[1] P. Vandezande, L.E.M. Gevers, I.F.J. Vankelecom, *Solvent resistant nanofiltration: separating on a molecular level*, Chemical Society Reviews 37 (2008) 365-405.

[2] A.V. Volkov, G.A. Korneeva, F.T. Gennadii, *Organic solvent nanofiltration:*

prospects and application, Russian Chemical Reviews 77 (2008) 983.

[3] S.P. Nunes, K.-V. Peinemann, *Membrane Technology (in the Chemical Industry)*, Wiley 2006.

[4] E.S. Tarleton, J.P. Robinson, J.S. Low, *Nanofiltration: A technology for selective solute removal from fuels and solvents*, Chemical Engineering Research and Design 87 (2009) 271-279.

[5] D.F. Stamatialis, N. Stafie, K. Buadu, M. Hempenius, M. Wessling, *Observations on the permeation performance of solvent resistant nanofiltration membranes*, Journal of Membrane Science 279 (2006) 424-433.

[6] L.E.M. Gevers, G. Meyen, K. De Smet, P. Van De Velde, F. Du Prez, I.F.J. Vankelecom, P.A. Jacobs, *Physico-chemical interpretation of the SRNF transport mechanism for solutes through dense silicone membranes*, Journal of Membrane Science 274 (2006) 173-182.

[7] Evonik Industries AG, *Radiation Curable Silicones - An Overview*, 2013, Available at: www.tego-rc.com.

[8] Evonik Industries AG, *TEGO RC Silicones - Practical Guide*, 2013, Available at: www.tego-rc.com.

[9] R. Hänsel, H. Döhler, P. Schwab, P. Seidensticker, M. Ferenz, G. Baumgarten, M. Lazar, M. Ungerank, *Composite silicone membranes with high separating action*, WO2011067054 A1, Evonik Goldschmidt GmbH, 2011.

[10] H. Dohler, T. Ebbrecht, W. Hamann, P. Lersch, S. Stadtmuller, *Radiation-curable organosiloxane coating compositions*, US6268404 B1, Th. Goldschmidt AG, 2001.

[11] S. Busch, H. Döhler, M. Ferenz, S. Herrwerth, *Cationic radiation-curing controlled release coating materials*, US7893128, Evonik Goldschmidt GmbH, 2011.

[12] E. Lyster, Y. Cohen, *Numerical study of concentration polarization in a rectangular reverse osmosis membrane channel: Permeate flux variation and hydrodynamic end effects*, Journal of Membrane Science 303 (2007) 140-153.

8 Performance comparison of different silicone based membranes for OSN

The influence of epoxy and acrylate silicone chain modifications on the membrane separation performance in heptane was shown in the previous Chapter 7 [1]. Here, the influence of the introduced modifications on the sorption properties of epoxy-functional and acrylate-functional silicone membranes was investigated and compared to the measured performance of the commercial silicone based membrane, ONF-2 from GMT Membrantechnik.

The epoxy-functional silicone membrane SE3 and acrylate-functional silicone membrane SA4 were chosen for the comparison. The membranes ONF-2, SE3 and SA4 have a similar styrene oligomer rejections in heptane (see Chapter 7), indicating a similar crosslinking density of the membrane polymer.

The measured styrene oligomer rejections and permeabilities were obtained for toluene, heptane, ethyl acetate and isopropanol. From the measured solvent permeabilities several parameters of the Flory-Rehner/Hansen solubility parameter model and Free Volume theory model were estimated and used to predict the styrene oligomer rejections.

These estimated model parameters for epoxy-functional and acrylate-functional silicone membranes were compared to the model parameters of the silicone membrane to emphasise the effect of epoxy and acrylate modifications to the poly(dimethylsiloxane) chain.

8.1 Theory

The Flory-Rehner/Hansen chemical potential model for surface attached films will be used to describe sorption of components in the membrane separation layer (see Appendix).

The set of boundary equations for the membrane mass transport is given in Chapter 6. The equations of the simple Maxwell-Stefan model and the Free Volume theory as well as solvent and styrene oligomers model parameters can be also found in Chapter 6 [2, 3].

8.2 Experimental

For filtration experiments technical purity grade toluene, heptane, ethyl acetate and isopropanol were used. The preparation of styrene oligomer solutions is described in Chapter 6. The filtration tests were made in the EMET stirred cell setup, previously described in Chapter 3. For permeate and retentate samples a solvent swap was performed and the samples were analysed by a reversed phase chromatographic column. The applied analytical tools are described in Chapter 3 [4].

The measurements were made at 30 bar transmembrane pressure and room temperature. The membrane sheets were first operated with pure solvent after which the feed solution was replaced with styrene oligomer solution. Permeate and retentate samples were taken after approximately 70 mL of permeate passed through the membrane.

The membrane (real) rejection was evaluated using the previously derived Sherwood correlation for concentration polarisation (given in Chapter 3).

Previously obtained data for the silicone membrane ONF-2 and measured permeabilities and styrene oligomer rejections of epoxy-functional silicone membrane

SE3 and acrylate-functional silicone membrane SA4 are given in Figure 42 and Figure 44 together with predicted permeabilities and styrene oligomer rejections.

8.3 Results and discussion

Several assumptions were made for the estimation of the model parameters for the produced epoxy-functional and acrylate-functional membranes.

The silicone membrane ONF-2, epoxy-functional silicone resin used for the SE3 membrane and acrylate-functional silicone resin used for the SA4 membranes were assumed to consist mostly out of long poly(dimethylsiloxane) chains. The first approximation was assuming common values of Hansen solubility parameters (HSP) and a molar weight of a monomer for all three membranes based on investigations made on a crosslinked poly(dimethylsiloxane) RTV615 sheet. The estimation of dispersion, polar and hydrogen-bonding HSP of the membrane (δ_m^d, δ_m^p and δ_m^h, respectively) and molar weight between two crosslinks (Mw_c) is given in Chapter 5.

Because of strong mathematical entanglement of parameters determining free volume, only the minimal molar volume of the monomer ($V_{m,monomer}^{\bullet}$) can be estimated, while the overlap factor (λ_m) and the monomer molar volume ($V_{m,monomer}^{mol}$), defined by density and monomer molar weight, had to be assumed.

The dry membrane thickness ($z_{m,dry}$), the molar weights of the membrane oligomers before crosslinking (Mw_o) and molar weight between two crosslinks (Mw_c) determine the wet membrane thickness of the membrane. Hence, these are also highly entangled, and only the membrane thickness could be estimated, whereas the molar weight between two crosslinks and the molar weight of the oligomer were assumed.

An overview of model parameters assumed on basis of experimental data for

poly(dimethylsiloxane) RTV615 sheet is given in Table 17.

Table 17: Assumed model parameters for the ONF-2, SE3 and SA4 membranes.

δ_m^d [(MPa)$^{0.5}$]	14.8
δ_m^p [(MPa)$^{0.5}$]	-5.4
δ_m^h [(MPa)$^{0.5}$]	5.2
λ_m [-]	0.7
$V_{m,monomer}^{mol}$ [cm^3·mol^{-1}]	73.1
MW_c [kg·mol^{-1}]	3.0

The assumed molar weights of the membrane oligomers before crosslinking are given in Table 18.

Table 18: Assumed oligomer molar weight of the membranes ONF-2, SE3 and SA4.

	ONF-2	SE3	SA4
MW_o [kg·mol^{-1}]	35.5	14.8	7.4

The dry membrane thickness and the minimal molar volume of membrane monomer were further estimated from measured pure solvent flux data. The obtained parameters for the ONF-2, SE3 and SA4 membranes are given in Table 19.

Table 19: Estimated dry membrane thickness and minimal molar volume of the membrane monomer for the membranes ONF-2, SE3 and SA4.

	ONF-2	SE3	SA4
$z_{m,dry}$ [μm]	1.84	3.06	7.37
$V^{\bullet}_{m,monomer}$ [$cm^3 \cdot mol^{-1}$]	63.8	59.4	54.1

The predicted styrene oligomer rejections using the previously given model parameters and the measured membrane rejection are given in Figure 42.

The prediction accuracy for styrene oligomer rejections for the ONF-2 and SE3 membranes, given in Figure 42, are good for toluene, heptane and ethyl acetate, but the styrene oligomer rejections in isopropanol were poorly predicted. For the acrylate-functional silicone membrane SA4 the styrene oligomer rejections were underestimated for all solvents, which can be explained by low estimated value of minimal molar volume of the membrane monomer.

In Figure 43 are the measured and predicted solvent permeabilities at 23 °C for the tested silicone based membranes.

The predicted solvent permeabilities for the silicone membrane ONF-2 and the epoxy-functional silicone membrane SE3 are in good agreement with the measured values. In the case of the acrylate-functional silicone membrane SA4 the permeability of ethyl acetate is underestimated, while the heptane permeability is overestimated.

Including the estimation of the molar weight between two crosslink (Mw_c) resulted in increase of error of prediction of styrene oligomer rejections compared to results given in Figure 42.

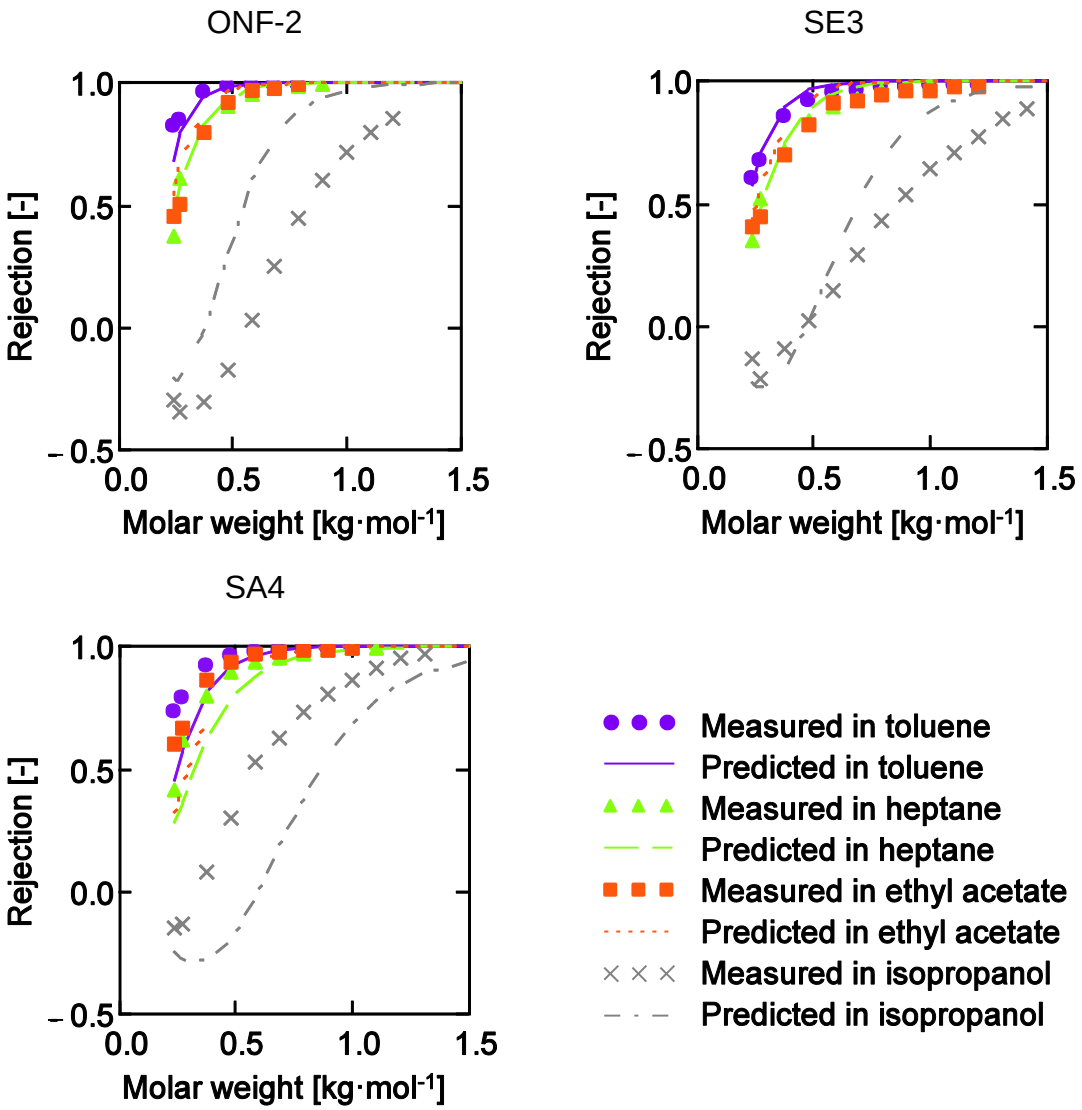

Figure 42: Measured and predicted performance of ONF-2, SE3 and SA4 membranes with estimated dry membrane thickness and minimal molar volume.

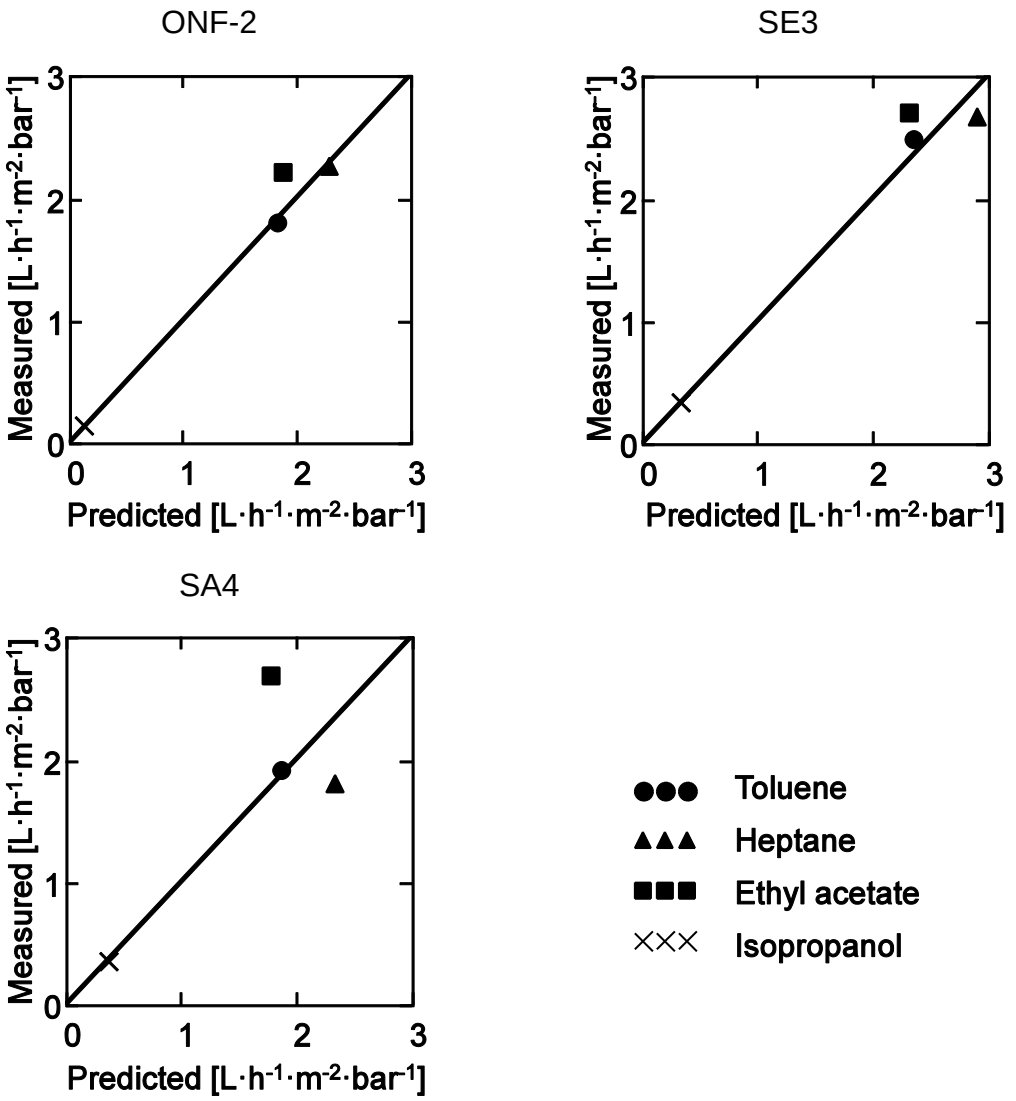

Figure 43: Measured and predicted solvent permeability of ONF-2, SE3 and SA4 membranes with estimated dry membrane thickness and minimal molar volume.

The improvement of the model prediction accuracy could be achieved by including the difference in polarity of each silicone based membrane by estimating HSP of each membrane material. The estimated dry membrane thickness ($z_{m,dry}$), minimal molar volume of membrane monomer ($V^{\bullet}_{m,monomer}$) and HSP for all three membranes are given in Table 20.

Table 20: Estimated values of dry membrane thickness, minimal molar volume of membrane monomer and HSP for the ONF-2, SE3 and SA4 membranes.

	ONF-2	SE3	SA4
$z_{m,dry}$ [µm]	1.43	2.37	2.27
$V^{\bullet}_{m,monomer}$ [$cm^3 \cdot mol^{-1}$]	64.9	61.8	63.0
δ_m^d [$(MPa)^{0.5}$]	14.6	15.3	15.0
δ_m^p [$(MPa)^{0.5}$]	-5.1	-4.7	-4.9
δ_m^h [$(MPa)^{0.5}$]	5.9	6.3	7.8

The predicted styrene oligomer rejection curves in comparison with the measured data are given in Figure 44.

By comparing Figure 42 and Figure 44 and it can be observed that the prediction of styrene oligomer rejections with additionally estimated HSP resulted in improved model prediction accuracy, especially for the SA4 membrane. The largest prediction error remains for the isopropanol/styrene oligomer mixture and the ONF-2 and SE3 membranes.

Measured and predicted volume permeabilities at 23 °C for the commercial silicone membrane ONF-2, the epoxy-functional silicone membrane SE3 and the acrylate functional silicone membrane SA4 are given in Figure 45.

As expected with the five parameters estimated from the experimental data, the solvent permeabilities are correctly represented by the used model parameters.

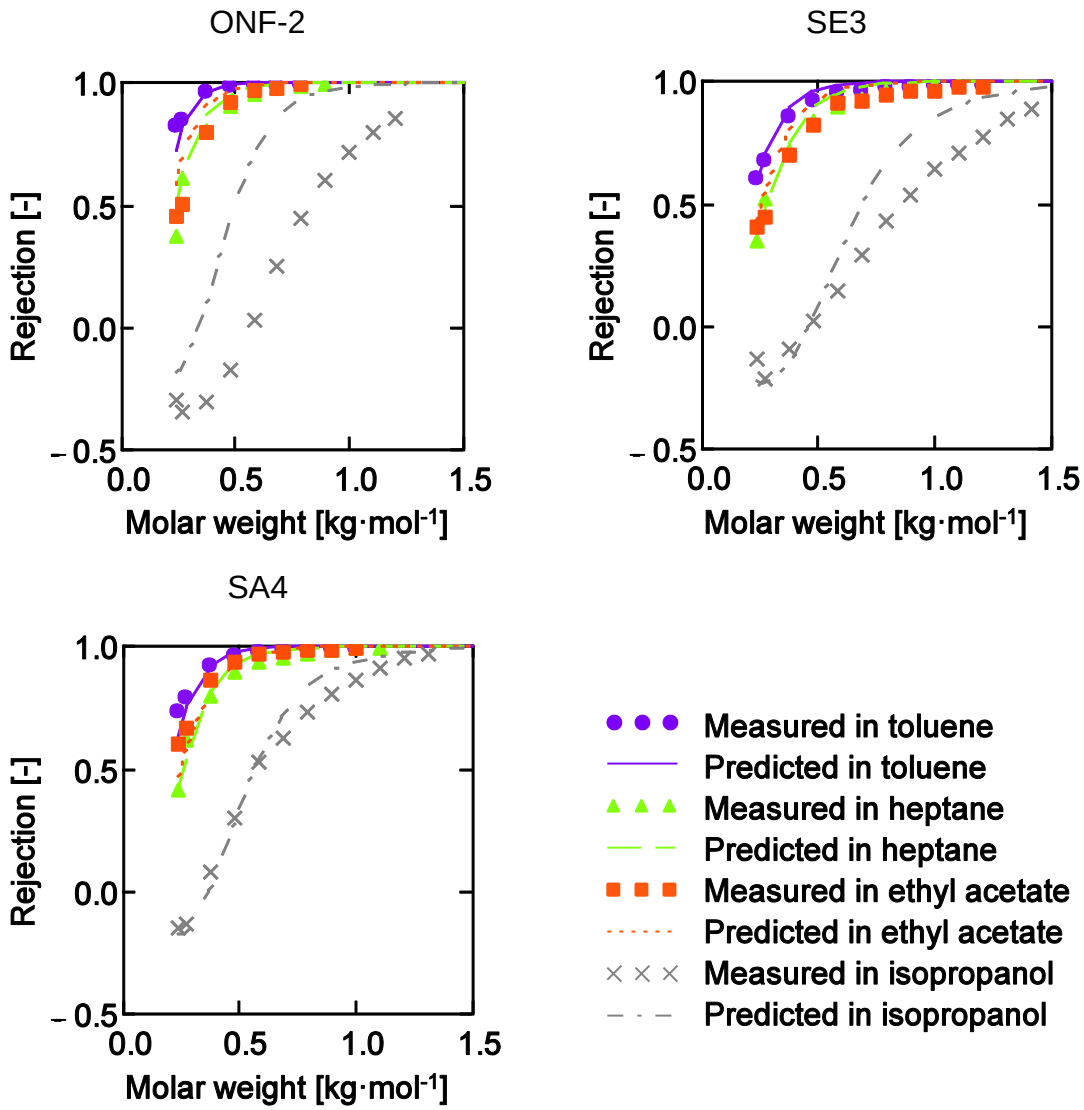

Figure 44: Measured and predicted styrene oligomer rejection of the ONF-2, SE3 and SA4 membranes with estimated dry membrane thickness, minimal molar volume and HSP.

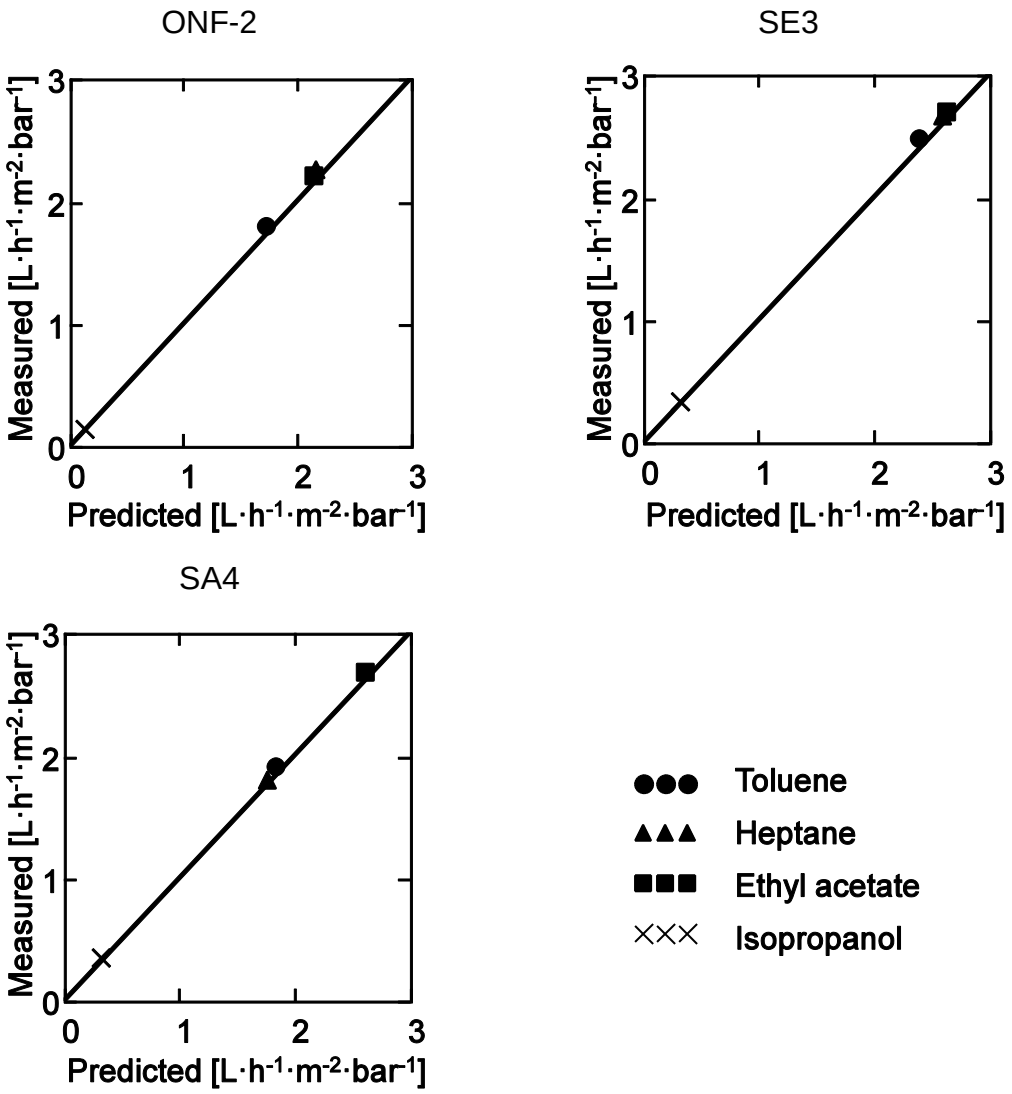

Figure 45: Measured and predicted solvent permeability of the ONF-2, SE3 and SA4 membranes with estimated dry membrane thickness, minimal molar volume and HSP.

From the estimated values of HSP (see Table 20) it can be observed that the epoxy-functional silicone membrane SE3 has a lower value of the polar Hansen solubility parameter and higher value of the hydrogen-bonding Hansen solubility parameter, overall resulting in similar polarity as ONF-2 polymer membrane. The acrylate-functional silicone membrane SA4 has a lower value of the polar and significantly higher value of the hydrogen-bonding HSP, indicating that the acrylate modifications of the used polymer for the SA3 membrane has a higher polarity compared

to both ONF-2 and SE4 membranes. Hence, the membrane separation layer has a higher affinity to moderately polar organic solvents compared to a separation layer of membranes ONF-2 and SE4.

8.4 Conclusion

By using estimated values of HSP for a PDMS sheet (see Chapter 5) and estimating the dry membrane thickness and the minimal molar volume from the permeability data, good representation of permeability and rejection was achieved for the membranes ONF-2 and SE3 (epoxy-functional membrane). For the acrylate-functional silicone membrane SA4 the solvent permeability could not be adequately represented. Hence, this discrepancy could not be attributed to the change in membrane thickness or Free Volume parameters. The improvement of the solvent permeability prediction for the acrylate-functional silicone membrane SA4 could only be achieved by estimating also the HSP from the measured solvent permeability data. The estimated HSP of silicone acrylate membrane indicate a higher polarity of the acrylate-functional silicone. Hence, making acrylate-functional silicone membranes more suitable for separation in moderately polar solvents than a purely silicone based membrane.

The Flory-Rehner/Hansen and Free Volume theory models include altogether ten parameters for predicting the solvent permeability. The basis of the measured data used for the estimation of membrane parameters included measurements of only four solvents since several parameters could be assumed with reasonable accuracy. In the case of a fully unknown polymer, estimation of the Flory-Rehner/Hansen and Free Volume model parameters on a significantly larger data set is recommended.

8.5 List of symbols

Mw_c	molar weight between two crosslinks	kg·mol^{-1}
Mw_o	molar weights of the membrane oligomer before crosslinking	kg·mol^{-1}
$V^{\bullet}_{m,monomer}$	minimal molar volume of membrane monomer	m³·mol^{-1}
$V^{mol}_{m,monomer}$	monomer molar volume	m³·mol^{-1}
$z_{m,dry}$	dry membrane thickness	m

Greek symbols

δ^d_m	membrane dispersion Hansen solubility parameter	(Pa)$^{0.5}$
δ^p_m	membrane dipole Hansen solubility	(Pa)$^{0.5}$
δ^h_m	membrane hydrogen bonding Hansen solubility parameter	(Pa)$^{0.5}$
λ_m	free volume overlap factor	-

8.6 References

[1] R. Hänsel, H. Döhler, P. Schwab, P. Seidensticker, M. Ferenz, G. Baumgarten, M. Lazar, M. Ungerank, *Composite silicone membranes with high separating action*, WO2011067054 A1, Evonik Goldschmidt GmbH, 2011.

[2] J.A. Wesselingh, R. Krishna, *Mass transfer in multicomponent mixtures*, Delft University Press 2000.

[3] J.A. Wesselingh, A.M. Bollen, *Multicomponent Diffusivities from the Free Volume Theory*, Chemical Engineering Research and Design 75 (1997) 590-602.

[4] Y.H. See Toh, X.X. Loh, K. Li, A. Bismarck, A.G. Livingston, *In search of a*

standard method for the characterisation of organic solvent nanofiltration membranes, Journal of Membrane Science 291 (2007) 120-125.

9 Conclusion and outlook

This work focuses on silicone based membranes for organic solvent nanofiltration.

This study includes a literature research on silicone membranes based on different reaction chemistry, the challenges in their production and the successful applications of already available silicone based membranes (Chapter 2). The chemical modification of the silicone separation layer combined with different membrane production technologies could lead to significant improvement of silicone based membranes compared to the currently available membranes.

Chapter 3 gives an overview of basic membrane concepts, the used filtration rigs and applied analytics. Also given in Chapter 3 are Sherwood correlations to describe the concentration polarisation phenomena for the two applied filtration cells and to calculate the real membrane rejection from the measured membrane rejection. The necessary Sherwood parameters for the EMET stirred cell setup were estimated from experiments made with docosane as solute in heptane and toluene. From the experimental data it could be observed that the concentration polarisation phenomena had significant effects on measured rejection even for systems where concentration polarisation is not expected to be relevant, as in the case of low concentrations of solute with a comparably low molar weight of 310 $g \cdot mol^{-1}$ in low viscosity solvents such as heptane at moderate membrane fluxes. Hence concentration polarisation effects should not be disregarded in evaluation of experimental results measured.

In Chapter 4 a comparison of styrene oligomer rejections by silicone membrane

ONF-2, PIM-1 and DuraMem500 (crosslinked P84) membrane in heptane and acetone are given. Even if all the membranes were developed for application in organic solvent nanofiltration significant differences were observed. For a glassy composite membrane PIM-1 high fluxes and a good performance in heptane and acetone were observed but the membrane material swells extensively and has limited stability [1]. The crosslinked P84 integrally skinned asymmetric membrane DuraMem500 (EMET) has excellent performance in acetone and is stable in several polar a-protic solvents [2], but has both low flux and low styrene oligomer rejection in heptane. The silicone based composite membrane ONF-2 (GMT Membrantechnik) combines both chemical stability and good performance in nonpolar and moderately polar organic solvents. The composite structure of a silicone based membrane also gives the possibility to develop thermodynamic models to predict the membrane separation performance and optimise the silicone separation layer. Even if silicones have been applied in membrane production since 1960s [3-5], it still remains one of the most promising materials in the development of new optimised solvent stable membranes.

In Chapter 5 a predictive model for mass transport was derived. A comparably simple Flory-Huggins/Hansen solubility parameters equation [6] was expanded for the elastic contribution term resulting in a Flory-Rehner/Hansen solubility parameters model. The swelling was differentiated as: free swelling and confined swelling when the polymer film is attached to the surface. The Hansen solubility parameters of silicone and crosslinking degree were estimated from experimental data made on crosslinked sheets of RTV615 silicone from General Electric. The derived model and the estimated parameters could describe the swelling behaviour of the produced silicone sheet for the whole range of polar to nonpolar solvents. Diffusion of a solvent through silicone membranes was investigated by a simplified Maxwell-Stefan model, where the diffusion coefficient was estimated by different diffusion

interpolation rules and the Free Volume theory. In the case of the Free Volume approach it was possible to predict the solvent permeation with no model parameters estimated from the permeability data.

The modelling approaches were used to predict permeabilities of eleven pure solvents through silicone composite membrane ONF-2 (GMT Membrantechnik). The difference and relative difference of the predicted solvent volume permeabilities by applying a modified Free Volume theory model with literature parameters and measured solvent volume permeabilities of ONF-2 (GMT Membrantechnik) membrane are given in Table 21.

The dichloromethane permeability has a considerably larger difference to its predicted permeability compared to other solvents. The predicted permeabilities of the other ten solvents have a better accuracy. The error in predicting dichloromethane permeability could be a result of excessive swelling of the supporting membrane layers which was not included in the developed model. Further research would be required to finally explain the high dichloromethane permeability. Isopropanol, the most polar solvent in the study, has the highest relative difference. Future work could focus on improving the estimation of Free Volume parameters for polar solvents, which could lead to a more accurate prediction of the permeability. The biggest advantage of the Free Volume approach is the good prediction accuracy of the permeability without parameters estimated from permeation experiments. Additionally, the derived Flory-Rehner/Hansen model and Maxwell-Stefan/Free Volume theory model can be easily applied to multicomponent mixtures.

Table 21: The difference and relative difference of the predicted permeabilities by applying a modified Free Volume theory model with literature parameters and measured permeabilities of ONF-2 (GMT Membrantechnik) membrane.

Solvent	Difference [$L \cdot h^{-1} \cdot m^{-2} \cdot bar^{--1}$]	Relative difference [-]
Toluene	-0.044	-0.021
Dichloromethane	-2.660	-0.539
Hexane	0.009	0.002
Heptane	0.169	0.067
Octane	-0.483	-0.198
Ethyl acetate	-0.265	-0.115
Acetone	0.202	0.183
1-Butanol	-0.018	-0.084
1-Hexanol	-0.025	-0.126
1-Octanol	-0.049	-0.385
Isopropanol	0.164	0.959

In Chapter 6 the prediction accuracy of the model was compared to experimental data for eleven solvents and their mixture with styrene oligomers of different molecular weights. For calculating mass transport of styrene oligomers their Hansen solubility parameters are required. Several values of polystyrene Hansen solubility parameters were found in literature. To determine which parameter set is suitable, a swelling experiment with α-methylstyrene dimer was made. Measured volume fraction of α-methylstyrene was compared with the predicted volume fraction of polystyrene with the same molar volume. The polystyrene Hansen solubility parameters set with the smallest difference in volume fractions was chosen. The predicted styrene oligomer rejection curves were in the range of the measured results and have

shown the same pressure dependence. The largest error was found in isopropanol which is partially due to overestimated solvent permeability. The good prediction accuracy of the measured styrene oligomer rejection indicates that the assumptions made in the derived equations are valid for the used styrene oligomer solutions. The model should be further investigated in more complex mixtures before the final evaluation of its prediction accuracy. However, the Flory-Rehner/Hansen model combined with the Maxwell-Stefan/Free Volume theory could serve as a starting point in the development of purely predictive membrane transport models.

In Chapter 7 production and performance of composite membranes made from acrylate-functional and epoxy-functional silicones was described. The performance of produced membranes was compared to a commercially available silicone based membrane ONF-2. Acrylate-functional and epoxy-functional silicone composite membranes were produced using mixtures of siloxanes with low and high value of unmodified units [7]. The membranes were characterised by measuring styrene oligomer rejections in heptane at 30 bar transmembrane pressure and 30 °C. Compared to the ONF-2 membrane, the acrylate-functional silicone membranes have a higher rejection performance and lower heptane permeability. Whereas, the epoxy-functional membranes have a lower rejection and an equal or higher heptane permeability compared to the ONF-2 silicone membrane. Further development of acrylate-functional and epoxy-functional silicone could both include further optimisation the chemical composition and improvement in the membrane production procedure.

In Chapter 8 a performance comparison of two developed membranes (epoxy and acrylate functional) was made in four styrene oligomer mixtures. The solvents comprise toluene, heptane, ethyl acetate and isopropanol. By estimation of the parameters of the developed Flory-Rehner/Hansen model combined with the Maxwell-Stefan/Free Volume theory model from the measured permeabilities the effect of introduced modifications was investigated. From the estimated values of Hansen

solubility parameters it can be observed that the epoxy-functional silicone membrane has a similar polarity as ONF-2. Whereas the acrylate-functional silicone membrane has higher values of the polar and hydrogen-bonding Hansen solubility parameter, indicating that small acrylate modifications have increased the polarity of the silicone polymer. Hence, the membrane separation layer has a higher affinity to moderately polar organic solvents compared to a separation layer made out of unmodified silicone. The targeted silicone modification by including polar functional groups could lead to membranes with enhanced performance in moderately polar solvents, such as acetone which is one of the large volume solvents in chemical industry.

9.1 References

[1] K. Heinrich, *Polymere mit intrinsischer Mikroporosität – Membranmaterialien mit Zukunft?*, PhD Thesis, GKSS-Forschungszentrum Geesthacht GmbH, 2009.

[2] Evonik Industries AG, *Membrane Properties - DuraMem® and PuraMem®*, (2008).

[3] K. Kammermeyer, *Separation of gases by diffusion through silicone rubber*, US2966235, Selas Corporation of America, 1960.

[4] J.E. Cadotte, *Evolution of Composite Reverse Osmosis Membranes* in: D.R. Lloyd (Ed.), *Materials Science of Synthetic Membranes*, American Chemical Society, 1985, pp. 273-294.

[5] H.K. Lonsdale, *The evolution of ultrathin synthetic membranes*, Journal of Membrane Science 33 (1987) 121-136.

[6] R. Toomey, D. Freidank, J. Rühe, *Swelling Behavior of Thin, Surface-Attached Polymer Networks*, Macromolecules 37 (2004) 882-887.

[7] R. Hänsel, H. Döhler, P. Schwab, P. Seidensticker, M. Ferenz, G. Baumgarten, M. Lazar, M. Ungerank, *Composite silicone membranes with high separating action*, WO2011067054 A1, Evonik Goldschmidt GmbH, 2011.

Appendix

A 1 Transformation of Maxwell-Stefan mass transport model

The Maxwell-Stefan model given by equation A 1, has been successfully applied to many mass transfer phenomena [1].

$$\frac{x_i}{R \cdot T} \nabla_{T,P} \mu_i = -\sum_{j=1}^{n} \left(\frac{x_i \cdot x_j \cdot (\mathbf{u}_i - \mathbf{u}_j)}{Đ_{i,j}} \right) \qquad A\ 1$$

Where x_i is the mole fraction of component i, μ_i is its chemical potential [J·mol^{-1}], $\mathbf{u}_i$ the component velocity [m·s^{-1}], and $Đ_{i,j}$ are the molar Maxwell-Stefan diffusion coefficients [m^2·s^{-1}], R is the universal gas constant and T is the absolute temperature.

For the description of the mass transfer over a polymer film it is more practical to use volume or mass fraction [1-3]. Assuming an ideal mixture and no excess volume, the average molar volume ($\overline{V^{mol}}$) is given by

$$\overline{V^{mol}} = \sum_{j=1}^{n} \left(x_j \cdot V_j^{mol} \right), \qquad A\ 2$$

where is V_j^{mol} a is the component molar volume. In equation A 3, the mole fractions are transformed into volume fractions (ϕ_i).

$$\phi_i = \frac{x_i \cdot V_i^{mol}}{\overline{V^{mol}}} = \frac{x_i \cdot V_i^{mol}}{\sum_{j=1}^{n} \left(x_j \cdot V_j^{mol} \right)} \qquad A\ 3$$

Finally, equation A 4 can be derived, which gives the Maxwell-Stefan equation in volume fractions form [2].

$$\frac{\phi_i}{V_i^{mol} \cdot R \cdot T} \nabla_{T,P} \mu_i = -\sum_{j=1}^{n} \left(\frac{\phi_i \cdot \phi_j \cdot (\mathbf{u}_i - \mathbf{u}_j)}{Đ_{i,j}} \frac{\overline{V^{mol}}}{V_i^{mol} \cdot V_j^{mol}} \right) \qquad A\ 4$$

The component velocity in the membrane can be calculated by

$$\mathbf{u}_i = \frac{J_i}{\phi_i}, \qquad A\ 5$$

where J_i is the volumetric flux of component i. Assuming one dimensional transport, equation A 6 can be obtained.

$$\frac{\phi_i}{V_i^{mol} \cdot R \cdot T}\left(\frac{d\mu_i}{dz}\right)_{T,P} = -\sum_{j=1}^{n}\left(\frac{\phi_i \cdot \phi_j}{Đ_{i,j}}\left(\frac{J_i}{\phi_i} - \frac{J_j}{\phi_j}\right)\frac{\overline{V^{mol}}}{V_i^{mol} \cdot V_j^{mol}}\right) \qquad A\ 6$$

Where z is the membrane cross-section thickness in flow direction. Assuming that only the friction of the component with the stationary membrane phase dominates the component transport, similar to a solution-diffusion model, the Maxwell-Stefan model in difference form in equation A 7 can be derived.

$$\frac{1}{R \cdot T}\frac{\Delta\mu_i}{z_m} = -\frac{\overline{\phi_m}}{\overline{Đ_{i,m}}}\left(\frac{J_i}{\overline{\phi_i}}\right)\frac{\overline{V^{mol}}}{V_m^{mol}} \qquad A\ 7$$

Where z_m is the total membrane separation layer thickness, V_m^{mol} is the molar volume of membrane polymer, $\overline{Đ_{i,m}}$ is the average molar Maxwell-Stefan diffusion coefficients between component i and the membrane, $\overline{\phi_m}$ and $\overline{\phi_i}$ are average volume fractions of membrane polymer and component i, respectively.

A 2 The Flory-Rehner/Hansen chemical potential model

There are a large number of activity coefficient models, which predict chemical potential of solvents in polymers [4-7]. For activity coefficients in the rubbery membrane a purely predictive Flory-Huggins model was chosen in which the energetic interactions between components are approximated with Hansen solubility parameters (HSP) [8-10]. Since the separation layer of the investigated membrane is a crosslinked polymer network, the elastic properties of the polymer are closely addressed.

In the Frenkel-Flory-Rehner theory it is assumed that the chemical potential can be described by two separate terms. A mixing contribution term (μ_i^{mix}), supporting the polymer dissolution, and an elastic term ($\mu_i^{elastic}$), restricting the swelling of the polymer [11-13]. The chemical potential of swelling in crosslinked networks is given by equation A 8.

$$\mu_i = \mu_i^{mix} + \mu_i^{elastic} \qquad A\ 8$$

A 2.1 Chemical potential mixing term

The mixing chemical potential of component i [eV pro molecule] in a multicomponent system can be defined by Helmholz energy (equation A 9).

$$\mu_i^{mix} = \left(\frac{\partial(\Delta F_{mix})}{\partial n_i} \right)_{T,V,n}, \qquad A\ 9$$

where n_i is the number of molecules of component i in the volume V. Considering the Flory-Huggins lattice model, the volume of molecule i (V_i) in the volume V can be defined as

$$V_i = v^* \cdot N_i \cdot n_i, \qquad A\ 10$$

where v^* is the volume of one segment, N_i is the number of segments in one molecule of component i.

In equation A 11 the volume fraction is redefined as

$$\phi_i = \frac{v^* \cdot N_i \cdot n_i}{V} \qquad \textit{resulting in} \qquad n_i = \frac{V}{v^* \cdot N_i}\phi_i . \qquad \textit{A 11}$$

The chemical potential of component i in the volume V can then be expressed by equation A 12.

$$\mu_i^{mix} = N_i \frac{v^*}{V} \frac{\partial(\Delta F_{mix})}{\partial \phi_i} \qquad \textit{A 12}$$

Victorov et. al. [14] define the Helmholz energy of mixing for a single segment by equation A 13.

$$f_{mix} = \frac{1}{k \cdot T} \frac{v^*}{V} \Delta F_{mix} \qquad \textit{A 13}$$

Further, Victorov et. al. [14] define the Helmholz energy of mixing for a segment in a multicomponent mixture by equation A 14.

$$\frac{\partial f_{mix}}{\partial \phi_i} = \frac{1}{N_i}\ln(\phi_i) + \sum_j \phi_j \left(\frac{1}{N_i} - \frac{1}{N_j} \right) + \sum_j \sum_k \left(\phi_j \phi_k \left(\chi^*_{i,j} - \frac{\chi^*_{j,k}}{2} \right) \right) \qquad \textit{A 14}$$

Where $\chi^*_{i,j}$ is an interaction parameter between segments. After transformation the expression for the mixing term of the chemical potential for a component i in eV pro molecule units becomes equation A 15.

$$\frac{\mu_i^{mix}}{k \cdot T} = \ln(\phi_i) + \sum_j \phi_j \left(1 - \frac{N_i}{N_j} \right) + N_i \sum_j \left(\phi_j \chi^*_{i,j} \right) - \frac{1}{2} N_i \sum_j \sum_k \left(\phi_j \phi_k \chi^*_{j,k} \right) \qquad \textit{A 15}$$

For solvents the volume of the whole solvent molecule is taken to be the volume

of the segment ($N_i = 1$). Hence the chemical potential of solvent i in J·mol^{-1} unit is

$$\frac{\mu_i^{mix}}{R \cdot T} = \ln(\phi_i) + \sum_j \phi_j \left(1 - \frac{V_i^{mol}}{V_j^{mol}}\right) + \sum_j \left(\phi_j \chi_{i,j}\right) - \frac{1}{2} \sum_j \sum_k \left(\phi_j \phi_k \chi_{j,k}\right) \qquad A\ 16$$

Where $\chi_{i,j}$ is the Flory-Huggins interaction parameter between component i and component j. In the Flory-Huggins model derivation, the Flory-Huggins interaction parameter contains several parameters as given by [10]

$$\chi_{i,j} = \frac{1}{Z'} \left(1 - \frac{V_i^{mol}}{V_j^{mol}}\right) + \frac{V_i^{mol}}{R \cdot T} \left(\delta_i^t - \delta_j^t\right)^2$$

$$Z' = \frac{Z_j}{\left(\frac{V_j^{mol}}{V_i^{mol}} - 1\right)(1 - f_0)} - \frac{2 \cdot f_0}{1 - f_0}, \qquad A\ 17$$

where Z_j is the component lattice coordination number and δ_i^t is the Hildebrand solubility parameter. The f_0 ($f_0 << 1$) is the probability "that the site is occupied by a component segment of a chain being placed [10]".

Gonzalez-Leon et. al. [15] approximated the Flory-Huggins interaction parameter by equation A 18.

$$\chi_{i,j} = \frac{\sqrt{V_i^{mol} \cdot V_i^{mol}}}{R \cdot T} \left(\delta_i^t - \delta_j^t\right)^2 \qquad A\ 18$$

Lindving et. al. [5] approximated the interaction parameter with HSP given by equation A 19.

$$\chi_{i,j} = 0.6 \frac{V_i^{mol}}{k \cdot T} \left(\left(\delta_i^d - \delta_j^d\right)^2 + 0.25\left(\delta_i^p - \delta_j^p\right)^2 + 0.25\left(\delta_i^h - \delta_j^h\right)^2\right) \qquad A\ 19$$

Where δ_i^d , δ_i^p and δ_i^h are dispersion, polar and hydrogen-bonding Hansen solubility parameters (HSP) of component i , respectively.

A 2.2 Rubber elasticity theory

In the literature, the elastic contributions in membrane swelling are mostly defined for one solvent [16, 17]. Only a few articles address the applicability of the Flory-Rehner equations to ternary mixtures of two solvents and a PDMS network [18-20]. Since a multicomponent mixture is considered here, the Flory-Rehner [21] approach was adapted to a multicomponent mixture. In this derivation the reduced number of possible configurations of penetrates in the swollen polymer network is not included. The statistical thermodynamic theory defines the elastic Gibbs energy through deformation α of the polymer network and is given by equation A 20 [11].

$$\frac{\Delta G_{elastic}}{k \cdot T} = \frac{\dim}{2} \vartheta_e \left(\alpha^2 - 1 - \ln \alpha \right) \qquad A\ 20$$

Where ϑ_e is the effective number of crosslinks in the polymer network molecule and $\dim$ is the number of dimensions in which the network can swell. The chemical potential in eV unit is defined by equation A 21.

$$\mu_i^{elastic} = \left(\frac{\partial \left(\Delta G_{elastic} \right)}{\partial n_i} \right)_{T,P,n} = \left(\frac{\partial \left(\Delta G_{elastic} \right)}{\partial \alpha} \right)_{T,P,n} \left(\frac{\partial \alpha}{\partial n_i} \right)_{T,P,n} \qquad A\ 21$$

By substituting equation A 20 into equation A 21, equation A 22 is obtained.

$$\frac{\mu_i^{elastic}}{k \cdot T} = \frac{\dim}{2} \vartheta_e \left(2\alpha - \frac{1}{\alpha} \right) \left(\frac{\partial \alpha}{\partial n_i} \right)_{T,P,n} \qquad A\ 22$$

The effective number of crosslinks can be expressed as total number of crosslinks in the polymer network molecule (ϑ), given by equation A 23.

$$\vartheta_e = \vartheta\left(1 - \frac{2 \cdot Mw_c}{Mw_o}\right) \qquad A\ 23$$

Where Mw_c is the molar weight of subchains (between two crosslinks) of the polymer network molecule and Mw_o is the molar weight of oligomer before crosslinking. The total number of crosslinks in one polymer network molecule is shown in equation A 24.

$$\vartheta = \frac{N_m \cdot \mathrm{v}^* \cdot N_A \cdot \rho_m}{Mw_c} \qquad A\ 24$$

Where N_m is the number of lattice places occupied by one polymer molecule, ρ_m is the polymer mass density and N_A is the Avogadro constant.

After substitution of equations A 23 and A 24 into equation A 22, the chemical potential equation has been derived as a function of deformation variable according to

$$\frac{\mu_i^{elastic}}{k \cdot T} = \frac{\dim}{2} \frac{N_m \cdot \mathrm{v}^* \cdot N_A \cdot \rho_m}{Mw_c}\left(1 - \frac{2 \cdot Mw_c}{Mw_o}\right)\left(2\alpha - \frac{1}{\alpha}\right)\left(\frac{\partial \alpha}{\partial n_i}\right)_{T,P,n}. \qquad A\ 25$$

The polymer network deformation can be expressed using polymer volume fraction in the polymer/solvent mixture. Observing one molecule of the polymer network ($n_m = 1$) in swollen and dry state and combining this with the Flory-Huggins lattice theory, the following expression can be obtained for the membrane volume fraction.

$$\frac{1}{\phi_m} = \frac{\mathrm{v}^* \cdot N_m + \mathrm{v}^* \sum_i (n_i \cdot N_i)}{\mathrm{v}^* \cdot N_m + V_F} \qquad A\ 26$$

Where V_F is the polymer free volume in dry state. Further assuming that the free

volume in dry state is negligible, equation A 26 can be transformed to equation A 27.

$$\frac{1}{\phi_m} = \frac{N_m + \sum_i (n_i \cdot N_i)}{N_m} \qquad A\ 27$$

A 2.3 Elastic term for one-dimensional swelling

Since the membrane separation layer is attached to the substrate, one-dimensional swelling is assumed ($\dim = 1$). Hence, one-dimensional deformation α is inversely proportional to the volume fraction of polymer as given by

$$\alpha = \frac{1}{\phi_m} = \frac{N_m + \sum_i (n_i \cdot N_i)}{N_m} \; . \qquad A\ 28$$

Substituting previous equation and differentiating equation A 25 the chemical potential contribution for one-dimensional swelling is derived (see equation A 29).

$$\frac{\mu_i^{elastic}}{k \cdot T} = \frac{1}{2} \frac{N_m \cdot \mathrm{v}^* \cdot N_A \cdot \rho_m}{Mw_c} \left(1 - \frac{2 \cdot Mw_c}{Mw_o}\right)\left(\frac{2}{\phi_m} - \phi_m\right)\frac{N_i}{N_m} . \qquad A\ 29$$

Considering that the component molar volume is $V_i^{mol} = N_i \cdot v^* \cdot N_A$, equation A 30 is derived.

$$\frac{\mu_i^{elastic}}{k \cdot T} = \frac{V_i^{mol} \cdot \rho_m}{Mw_c} \left(1 - \frac{2 \cdot Mw_c}{Mw_o}\right)\left(\frac{1}{\phi_m} - \frac{\phi_m}{2}\right) \qquad A\ 30$$

The total chemical potential of a component i in J·mol^{-1} is given by equation A 31.

$$\frac{\mu_i}{R\cdot T} = \frac{\mu_i^{mix,entropy}}{R\cdot T} + \frac{\mu_i^{mix,enthalpy}}{R\cdot T} + \frac{\mu_i^{elastic}}{R\cdot T} \quad with$$

$$\frac{\mu_i^{mix,entropy}}{R\cdot T} = \ln(\phi_i) + \sum_j \phi_j \left(1 - \frac{V_i^{mol}}{V_j^{mol}}\right)$$

$$\frac{\mu_i^{mix,enthalpy}}{R\cdot T} = 2\cdot V_i^{mol} \sum_j (\phi_j \cdot a_{i,j}) - V_i^{mol} \sum_j \sum_k (\phi_j \cdot \phi_k \cdot a_{j,k}) \qquad A\ 31$$

$$\frac{\mu_i^{elastic}}{R\cdot T} = \frac{V_i^{mol}\cdot \rho_m}{Mw_c}\left(1 - \frac{2\cdot Mw_c}{Mw_o}\right)\left(\frac{1}{\phi_m} - \frac{\phi_m}{2}\right)$$

$$a_{i,j} = \frac{0.3}{R\cdot T}\left(\left(\delta_i^d - \delta_j^d\right)^2 + 0.25\left(\delta_i^p - \delta_j^p\right)^2 + 0.25\left(\delta_i^h - \delta_j^h\right)^2\right)$$

Where $a_{i,j}$ is the symmetrical interaction parameter between two components.

The mass molar volume of the monomer unit is defined as

$$V_{m,monomer}^{mol} = \frac{Mw_{monomer}}{\rho_m}. \qquad A\ 32$$

By substitution of equation A 32 into equation A 31 the total chemical potential of a component for one-dimensional swelling of the surfaced attached polymer film is obtained

$$\frac{\mu_i}{R\cdot T} = \frac{\mu_i^{mix,entropy}}{R\cdot T} + \frac{\mu_i^{mix,enthalpy}}{R\cdot T} + \frac{\mu_i^{elastic}}{R\cdot T} \quad with$$

$$\frac{\mu_i^{mix,entropy}}{R\cdot T} = \ln(\phi_i) + \sum_j \phi_j \left(1 - \frac{V_i^{mol}}{V_j^{mol}}\right) \qquad A\ 33$$

$$\frac{\mu_i^{mix,enthalpy}}{R\cdot T} = 2\cdot V_i^{mol} \sum_j (\phi_j \cdot a_{i,j}) - V_i^{mol} \sum_j \sum_k (\phi_j \cdot \phi_k \cdot a_{j,k})$$

$$\frac{\mu_i^{elastic}}{R \cdot T} = \frac{V_i^{mol}}{V_{m,monomer}^{mol}} \frac{Mw_{monomer}}{Mw_c} \left(1 - \frac{2 \cdot Mw_c}{Mw_o}\right)\left(\frac{1}{\phi_m} - \frac{\phi_m}{2}\right)$$

$$a_{i,j} = \frac{0.3}{R \cdot T}\left(\left(\delta_i^d - \delta_j^d\right)^2 + 0.25\left(\delta_i^p - \delta_j^p\right)^2 + 0.25\left(\delta_i^h - \delta_j^h\right)^2\right) .$$

A 2.4 Elastic term for three-dimensional swelling

The tree-dimensional isotropic swelling ($\dim = 3$) of a free standing film assumes relation between the polymer network deformation and membrane polymer volume fraction as

$$\alpha_x \cdot \alpha_y \cdot \alpha_z = \alpha^3 = \frac{1}{\phi_m} . \qquad A\ 34$$

Considering one molecule of membrane polymer and neglecting the free volume of dry polymer network, expression A 35 is derived.

$$\alpha^3 = \frac{N_m + \sum_i \left(n_i \cdot N_i\right)}{N_m} \qquad A\ 35$$

By substituting equation A 35 into equation A 25 and consecutive differentiation, equation A 36 obtained.

$$\frac{\mu_i}{R\cdot T}=\frac{\mu_i^{mix,entropy}}{R\cdot T}+\frac{\mu_i^{mix,enthalpy}}{R\cdot T}+\frac{\mu_i^{elastic}}{R\cdot T} \quad with$$

$$\frac{\mu_i^{mix,entropy}}{R\cdot T}=\ln(\phi_i)+\sum_j \phi_j\left(1-\frac{V_i^{mol}}{V_j^{mol}}\right)$$

$$\frac{\mu_i^{mix,enthalpy}}{R\cdot T}=2\cdot V_i^{mol}\sum_j\left(\phi_j\cdot a_{i,j}\right)-V_i^{mol}\sum_j\sum_k\left(\phi_j\cdot\phi_k\cdot a_{j,k}\right) \qquad A\ 36$$

$$\frac{\mu_i^{elastic}}{R\cdot T}=\frac{V_i^{mol}\cdot\rho_m}{Mw_c}\left(1-\frac{2\cdot Mw_c}{Mw_o}\right)\left(\phi_m^{1/3}-\frac{\phi_m}{2}\right)$$

$$a_{i,j}=\frac{0.3}{R\cdot T}\left(\left(\delta_i^d-\delta_j^d\right)^2+0.25\left(\delta_i^p-\delta_j^p\right)^2+0.25\left(\delta_i^h-\delta_j^h\right)^2\right)$$

Substituting expression for mass density of the membrane (equation A 32) into equation A 36, the following model for the total chemical potential of a component for three-dimensional swelling of the free standing polymer film is derived.

$$\frac{\mu_i}{R\cdot T}=\frac{\mu_i^{mix,entropy}}{R\cdot T}+\frac{\mu_i^{mix,enthalpy}}{R\cdot T}+\frac{\mu_i^{elastic}}{R\cdot T} \quad with$$

$$\frac{\mu_i^{mix,entropy}}{R\cdot T}=\ln(\phi_i)+\sum_j \phi_j\left(1-\frac{V_i^{mol}}{V_j^{mol}}\right)$$

$$\frac{\mu_i^{mix,enthalpy}}{R\cdot T}=2\cdot V_i^{mol}\sum_j\left(\phi_j\cdot a_{i,j}\right)-V_i^{mol}\sum_j\sum_k\left(\phi_j\cdot\phi_k\cdot a_{j,k}\right) \qquad A\ 37$$

$$\frac{\mu_i^{elastic}}{R\cdot T}=\frac{V_i^{mol}}{V_{m,monomer}^{mol}}\frac{Mw_{monomer}}{Mw_c}\left(1-\frac{2\cdot Mw_c}{Mw_o}\right)\left(\phi_m^{1/3}-\frac{\phi_m}{2}\right)$$

$$a_{i,j}=\frac{0.3}{R\cdot T}\left(\left(\delta_i^d-\delta_j^d\right)^2+0.25\left(\delta_i^p-\delta_j^p\right)^2+0.25\left(\delta_i^h-\delta_j^h\right)^2\right)$$

Applying equation A 36 to a single solvent i the known Flory-Rehner chemical

potential model is derived (see equation A 38), where the interaction parameter is defined according to Lindvig et. al. [8, 13, 21].

$$\frac{\mu_i}{R\cdot T} = \frac{\mu_i^{mix,entropy}}{R\cdot T} + \frac{\mu_i^{mix,enthalpy}}{R\cdot T} + \frac{\mu_i^{elastic}}{R\cdot T} \quad \textit{with}$$

$$\frac{\mu_i^{mix,entropy}}{R\cdot T} = \ln(\phi_i) + \phi_m\left(1-\frac{V_i^{mol}}{V_m^{mol}}\right)$$

$$\frac{\mu_i^{mix,enthalpy}}{R\cdot T} = \phi_m^2\cdot\chi_{i,m} \qquad \textit{A 38}$$

$$\frac{\mu_i^{elastic}}{R\cdot T} = \frac{V_i^{mol}\cdot\rho_m}{Mw_c}\left(1-\frac{2\cdot Mw_c}{Mw_o}\right)\left(\phi_m^{1/3}-\frac{\phi_m}{2}\right)$$

$$\chi_{i,m} = 0.6\frac{V_i^{mol}}{RT}\left(\left(\delta_i^d-\delta_m^d\right)^2+0.25\left(\delta_i^p-\delta_m^p\right)^2+0.25\left(\delta_i^h-\delta_m^h\right)^2\right)$$

A 3 Sensitivity analysis of the developed Flory-Hugging/Hansen and Maxwell-Stefan/Free Volume theory model

An overview of membrane model parameters for predicting mass transport through the silicone membrane ONF-2 by the developed Flory-Hugging/Hansen model and Maxwell-Stefan/Free Volume theory model is given in Table A 1. The parameters were estimated from performed swelling experiments with PDMS sheets of RTV615 provided by General Electrics.

Table A 1: Overview of membrane model parameters for predicting mass transport through the silicone membrane ONF-2.

1	$z_{m,dry}$ [µm]	dry membrane thickness	2.75
2	$V_{m,monomer}^{mol}$ [$cm^3 \cdot mol^{-1}$]	molar volume of monomer	73.1
3	λ_m [-]	free volume overlap factor	0.7
4	$V_{m,monomer}^{\bullet}$ [$cm^3 \cdot mol^{-1}$]	minimal molar volume of monomer	63.9
5	$\frac{Mw_{monomer}}{Mw_c}\left(1-\frac{2 \cdot Mw_c}{M_o}\right)$	non-dimensional crosslinking parameter	0.021
	δ_m^d [$(MPa)^{0.5}$]		14.8
6	δ_m^p [$(MPa)^{0.5}$]	Hansen solubility parameters	-5.4
	δ_m^h [$(MPa)^{0.5}$]		5.2

The parameters given in Table A 1 could be also estimated from experimentally determined pure solvent permeability for ONF-2 membrane.

The estimated values and averaged absolute and averaged relative deviation of predicted permeabilities for the reported Free Volume approach [22] are given in

Table A 2.

Table A 2: The estimated values and averaged absolute and averaged relative deviation of predicted permeabilities for the reported Free Volume approach [22].

Reported Free Volume theory (see Eq. 51) Estimated parameter	value	*AAD* [L·h^{-1}·m^{-2} ·bar^{-1}]	*ARD* [-]
-	-	0.372	0.246
$z_{m,dry}$ [μm]	2.71	0.372	0.246
$V_{m,monomer}^{mol}$ [cm^3·mol^{-1}]	73.2	0.372	0.244
λ_m [-]	0.689	0.370	0.244
$V_{m,monomer}^{\bullet}$ [cm^3·mol^{-1}]	61.9	0.370	0.243
$\frac{Mw_{monomer}}{Mw_c}\left(1-\frac{2\cdot Mw_c}{M_o}\right)$	0.021	0.372	0.246
δ_m^d [(MPa)$^{0.5}$]	14.9		
δ_m^p [(MPa)$^{0.5}$]	-5.4	0.362	0.242
δ_m^h [(MPa)$^{0.5}$]	5.3		

From the comparison of deviations in Table A 2 a slight improvement of model prediction accuracy of the reported Free Volume model could only be achieved by the estimation of Hansen solubility parameters.

A 4 List of symbols

$a_{i,j}$	symmetrical interaction parameter	$mol \cdot m^{-3}$
dim	number of dimensions in which the network can swell	-
F_{mix}	Helmholz energy	eV
f_0	probability “that the site is occupied by a component segment of a chain being placed [10]”	-
f_{mix}	Helmholz energy of mixing for segment	-
$G_{elastic}$	Gibbs energy	eV
J_i	volumetric flux of component i	$m \cdot s^{-1}$
k	Boltzmann constant	$J \cdot K^{-1}$
Mw_c	molar weight of subchains between two crosslinks	$kg \cdot mol^{-1}$
Mw_o	molar weight of oligomer	$kg \cdot mol^{-1}$
N_A	Avogadro constant	mol^{-1}
N_i	number of segments in one molecule of component i	-
N_m	number of lattice places occupied by one polymer molecule	-
n_i	number of molecules of component i in the volume V	-
n_m	number of the polymer network of molecules	-
R	the universal gas constant	$J \cdot mol^{-1} \cdot K^{-1}$
T	absolute temperature	K

$\mathbf{u}_i$	velocity of component i	$m \cdot s^{-1}$
V	volume	m^3
V_F	polymer free volume in dry state	m^3
V_i	volume of molecule i	m^3
V_j^{mol}	molar volume of component j	$m^3 \cdot mol^{-1}$
V_m^{mol}	molar volume of membrane polymer,	$m^3 \cdot mol^{-1}$
$V_{m,monomer}^{mol}$	monomer molar volume	$m^3 \cdot mol^{-1}$
$V_{m,monomer}^{\bullet}$	minimal molar volume of monomer	$m^3 \cdot mol^{-1}$
$\overline{V^{mol}}$	average molar volume	$m^3 \cdot mol^{-1}$
v^*	segment volume	m^3
x_i	mole fraction of component i	-
Z_j	component lattice coordination number	-
z	membrane cross-section thickness in flow direction	m
z_m	total membrane separation layer thickness	m
$z_{m,dry}$	dry membrane thickness	m
$Đ_{i,j}$	molar Maxwell-Stefan diffusion coefficient	$m^2 \cdot s^{-1}$
$\overline{Đ_{i,m}}$	is the average molar Maxwell-Stefan diffusion coefficients between component i and the membrane	$m^2 \cdot s^{-1}$

Greek symbols

α	deformation of polymer network	-
δ_i^t	Hildebrand solubility parameter of component i	$(Pa)^{0.5}$
δ_i^d	dispersion Hansen solubility parameter of component i	$(Pa)^{0.5}$
δ_i^p	dipole Hansen solubility parameter of component i	$(Pa)^{0.5}$
δ_i^h	hydrogen bonding Hansen solubility parameter of component i	$(Pa)^{0.5}$
ϑ	total number of crosslinks in the polymer network molecule	-
ϑ_e	is the effective number of crosslinks in the polymer network molecule	-
λ_m	membrane free volume overlap factor	-
μ_i	chemical potential of component i	$J \cdot mol^{-1}$
μ_i^{mix}	mixing contribution term of chemical potential of component i	$J \cdot mol^{-1}$
$\mu_i^{elastic}$	elastic contribution term of chemical potential of component i	$J \cdot mol^{-1}$
ρ_m	polymer mass density	$kg \cdot m^{-3}$
ϕ_i	volume fraction of component i	-
$\overline{\phi_i}$	average volume fraction of component i	-
$\chi_{i,j}$	Flory-Huggins interaction parameter	-
$\chi_{i,j}^*$	interaction parameter between segments	-

A 5 References

[1] J.A. Wesselingh, R. Krishna, *Mass transfer in multicomponent mixtures*, Delft University Press 2000.

[2] C.P. Ribeiro Jr, B.D. Freeman, D.R. Paul, *Modeling of multicomponent mass transfer across polymer films using a thermodynamically consistent formulation of the Maxwell–Stefan equations in terms of volume fractions*, Polymer 52 (2011) 3970-3983.

[3] A. Verhoef, E. De Ridder, B. Bettens, J. Degrève, B. Van der Bruggena, *Maxwell-Stefan in mass fractions for numerical simulation of the pervaporation process*, Computer Aided Chemical Engineering Volume 26 (2009) 779-784.

[4] G.M. Kontogeorgis, G.K. Folas, *Thermodynamic Models for Industrial Applications: From Classical and Advanced Mixing Rules to Association Theories*, Wiley 2010.

[5] T. Lindvig, I.G. Economou, R.P. Danner, M.L. Michelsen, G.M. Kontogeorgis, *Modeling of multicomponent vapor–liquid equilibria for polymer–solvent systems*, Fluid Phase Equilibria 220 (2004) 11-20.

[6] R.P. Danner, M.S. High, *Handbook of Polymer Solution Thermodynamics*, Wiley 1993.

[7] E. Favre, Q.T. Nguyen, R. Clément, J. Néel, *The engaged species induced clustering (ENSIC) model: A unified mechanistic approach of sorption phenomena in polymers*, Journal of Membrane Science 117 (1996) 227-236.

[8] T. Lindvig, M.L. Michelsen, G.M. Kontogeorgis, *A Flory–Huggins model based on the Hansen solubility parameters*, Fluid Phase Equilibria 203 (2002) 247-260.

[9] C.M. Hansen, *Hansen Solubility Parameters: A Users Handbook*, 2nd ed., CRC Press 2007.

[10] J.G. Bitter, *Transport mechanisms in membrane separation processes*, Plenum Press 1991.

[11] R. Toomey, D. Freidank, J. Rühe, *Swelling Behavior of Thin, Surface-Attached Polymer Networks*, Macromolecules 37 (2004) 882-887.

[12] J.E. Mark, *Physical Properties of Polymers Handbook*, 2nd ed., Springer 2007.

[13] P.J. Flory, J.J. Rehner, *Statistical Mechanics of Cross-Linked Polymer Networks II. Swelling*, The Journal of Chemical Physics 11 (1943) 521-526.

[14] A.I. Victorov, C.J. Radke, J.M. Prausnitz, *Molecular thermodynamics for swelling of a bicontinuous gel*, Molecular Physics 100 (2002) 2277-2297.

[15] J.A. Gonzalez-Leon, A.M. Mayes, *Phase Behavior Prediction of Ternary Polymer Mixtures*, Macromolecules 36 (2003) 2508-2515.

[16] L.R.G. Treloar, *The Physics of Rubber Elasticity* 3rd ed., Oxford University Press 2005.

[17] X.-M. Li, Z. Shen, T. He, M. Wessling, *Modeling on swelling behavior of a confined polymer network*, Journal of Polymer Science Part B: Polymer Physics 46 (2008) 1589-1593.

[18] E. Favre, Q.T. Nguyen, D. Sacco, A. Moncuy, R. Clement, *Multicomponent polymer/solvents equilibria: An evaluation of Flory-Huggins theory for crosslinked PDMS networks swelled by binary mixtures*, Chemical Engineering Communications 140 (1995) 193-205.

[19] J.S. Yoo, S.J. Kim, J.S. Choi, *Swelling equilibria of mixed solvent/poly(dimethylsiloxane) systems*, Journal of Chemical & Engineering Data 44 (1998) 16-22.

[20] W. Ogieglo, H. van der Werf, K. Tempelman, H. Wormeester, M. Wessling, A. Nijmeijer, N.E. Benes, *n-Hexane induced swelling of thin PDMS films under non-equilibrium nanofiltration permeation conditions, resolved by spectroscopic ellipsometry*, Journal of Membrane Science 431 (2013) 233-243.

[21] P.J. Flory, J. John Rehner, *Statistical Mechanics of Cross-Linked Polymer Networks I. Rubberlike Elasticity*, The Journal of Chemical Physics 11 (1943) 512-520.

[22] J.A. Wesselingh, A.M. Bollen, *Multicomponent Diffusivities from the Free Volume Theory*, Chemical Engineering Research and Design 75 (1997) 590-602.